AFM investigations of critical interactions in the *Bacillus* primosome
and
Cryogenic AFM a new tool for structural biology

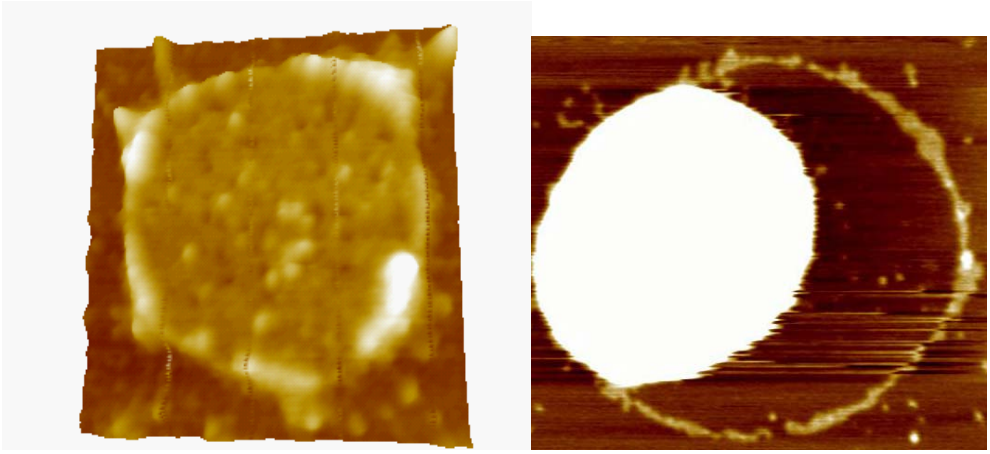

Ian James Turner BSc (Hons), MSc

Thesis submitted to The University of Nottingham

for the degree of Doctor of Philosophy

September 2005

This thesis is dedicated to my mum and dad; I know what you have been through to get me here.

Abstract

In this thesis for the first AFM has been employed for the high resolution imaging of a protein assembly. The DnaB-DnaG Helicase-Primase interaction in *Bacillus* is the key reaction that causes the switch from primase mode to polymerisation mode. This assembly was imaged using the AFM to a sub-molecular resolution revealing structural detail of the interaction. It is shown that the binding of the primase causes the structure of the helicase to switch from a hexamer to a trimer of dimers with one primase molecule bound to each dimer; also the existance of sub-populations with one and two primases bound suggests a sequential mode of binding. Recently crystallography data has been published that confirms the structural observations generated by AFM here. This is the first time that AFM and crystallography data have been used concurrently to solve the molecular structure of a protein assembly and it shows the potential application of AFM for sub-molecular resolution imaging of other protein assemblies.

The role of DnaD in the *Bacillus* primosome is well established, however, its exact function was unknown. In this thesis AFM was applied to help solve this biomolecular problem, it revealed that DnaD has a pivotal role in early primosome assembly, 'opening up' the DNA allowing other components of the cascade to bind. DnaD was shown to cause supercoiled DNA to adopt an open circular formation; this reaction was shown to be both reversible and universally applicable to all sequences of DNA. Comparisons are made between the role of DnaD and the roles of the histone-like proteins H-NS and HU. These experiments show that AFM can be applied to the imaging of proteins and their interactions with DNA and used to solve biomolecular problems that other techniques cannot solve.

The design and implementation of a novel cryogenic AFM system for the imaging of biomolecules at subzero temperatures was executed. Preliminary results show that such a system has the potential to reduce the two main intrinsic effects limiting current AFM imaging; sample softness and thermal motion.

The application of AFM in this thesis shows its strength as a tool in molecular biology not only for the high resolution imaging of proteins and protein assemblies but also as a technique that can be uniquely applied to solve biomolecular problems. This thesis also shows for the first time that AFM can be applied to generate sub-molecular resolution of protein assemblies. The strength of the AFM data when combined with crystallography data shows that AFM is a very powerful tool for the imaging of protein assemblies; it could even become the technique of choice.

Table of Contents

Abstract….....3

Contents….....5

List of Figures….....11

List of Tables….....17

List of Abbreviations……..18

1. Introduction….....19

1.1 Background….....19

1.2 Modes of operation….....21

1.3 Additional signals….....24

1.4 Limitations….....24

2. Bacillus….....26

2.1General….....26

2.1.1 Endospore….....27

2.1.2 Species….....29

2.2. Replication Overview….....30

2.3. Replication Initiation….....32

2.3.1 Initiation regulation….....33

2.3.2 The primosomal cascade….....35

3. Methods….....39

3.1 AFM Imaging….....39

3.1.1 Air Imaging….....39

3.1.2 Liquid Imaging….....40

3.2 DNA preparation….....40

3.2.1 Harvesting bacteria susceptible for transfection. ….....40
3.2.2. Transforming the bacteria….....40
3.2.3. Removing non-transformed bacteria….....41
3.2.4. Purifying plasmid….....41
3.2.5 Check for plasmid DNA….....41
3.2.6 Restriction digest….....43

4. The interaction of the bacterial helicase (DnaB) and primase (DnaG)

4.1. Introduction….....43
4.1.1 General….....43
4.1.2 Helicases….....43
4.1.3 DnaB Helicase….....47
4.1.4 DnaG Primase….....49
4.1.5 DnaBG Complex….....50
4.2. Method ….....52
4.2.1 Atomic Force Microscopy….....52
4.2.2 Protein Purification….....52
4.2.3 BG Complex….....52
4.2.4 Complementary Techniques….....53
Site-directed mutagenesis ….....53
Analytical gel filtration….....53
ATPase assays….....53
Helicase assays….....54
Yeast two-hybrid (Y2H) experiments….....54
Limited proteolysis….....55
4.3. Results….....56
4.3.1 DnaB Helicase….....56
4.3.2 DnaG primase….....58

4.3.3 DnaBG……59
4.3.4 Subpopulations……61
4.4. Complementary Work……63
4.4.1 Mutations in the N-Domain and n linker region of DnaB……64
4.4.2 Mutations in the C-domain of DnaB……65
4.4.3 The N- & C-domains of DnaB do not interact with DnaG……65
4.4.4 Primase-mediated protection of the linker region……65
4.5. Discussion……67
4.6. Recent Advances……70

5.What is the role of DnaD in the Bacillus subtilis Primosome?

5.1. Introduction……73
5.2. Method……79
5.2.1 Atomic Force Microscopy……79
5.2.2 DnaD and pBR322 preparation……79
5.2.3 Complementary techniques……79
5.2.3.1 Protein purifications……80
5.2.3.2 Sedimentation velocity experiments……81
5.2.3.3 Gel shift assays……81
5.2.3.4 Analytical gel filtration……82
5.3. Results……83
5.3.1 Imaging of DnaD Protein……83
5.3.2 Imaging of supercoiled pBR322……87
5.3.3 Imaging of DNA and DnaD Protein complexes……88
5.3.4 DnaD-DNA Complexes in Liquid……91
5.4. Complementary Data……95
5.4.1 DnaD Oligomeric State……95
5.4.2 DnaD Mediated Nucleoprotein Complexes……97
5.5. Discussion……99

5.6. Model….105

6. Is DnaD a global regulator of DNA architecture?

6.1. Introduction….107
6.1.1General….107
6.1.2 H-NS….107
6.1.3 HU….110
6.1.4 H-NS and HU….112
6.2. Method….114
6.2.1 Atomic Force Microscopy….114
6.2.2 DnaD preparation….114
6.2.3 DNA Preparation….114
6.2.4 Complex Preparation….115
6.3. Results….116
6.3.1 Linear Plasmid….116
6.3.2 Protease Experiments….121
6.3.3 Lambda DNA….125
6.4. Discussion….128
6.4.1 Linear Plasmid….128
6.4.2 Protease experiments….130
6.4.3 Lambda DNA….131
6.4.4 Summary….132
6.4.5 DnaD as a global regulator….134

7. Cryogenic Atomic Force Microscopy: A New Tool for Structural Biology

7.1. Introduction….136
7.1.1 General….136

7.1.2 Freezing Process.....139
7.1.2.1 Cryogens.....139
7.1.2.2 Freezing Methods.....140
7.1.3 The Cryogenic Microscope.....142
7.1.4 Post-Freezing.....143
7.1.5 The Structure of Ice.....144
7.2. The Cryogenic AFM.....148
7.2.1 General.....148
7.2.2 Operation Overview.....148
7.2.3 The AFM.....150
7.2.4 Sample Freezing.....153
7.2.5 The cryogenic chamber.....154
7.2.6 Operation.....155
7.2.6.1 Aligning the laser.....155
7.2.6.2 Preparing the cryogenic chamber.....160
7.2.6.3 Freezing the sample.....160
7.3. Methodology.....161
7.3.1 Atomic Force Microscopy.....161
DI Multimode.....161
Cryogenic-AFM.....161
7.3.2 Polystyrene spheres.....161
Air Imaging.....161
Cryogenic imaging.....161
7.4. Results.....162
7.4.1 Air imaging.....162
7.4.1.1 Cryogenic-AFM.....162
7.4.1.2 DI Multimode.....164
7.4.2 Cryogenic Imaging.....166
7.4.2.1 Vacuum.....166

7.4.2.2 Initial freezing……167
7.4.2.3 Gradual warming……168
7.4.2.4 Cryogenic imaging……168
7.5. Discussion……171

8. Conclusion……174

9. Future Perspective……177

References……178

Acknowledgments……191

Appendix – Scientific publications……192

List of Figures

Figure 1.1: The basic operating principles of the AFM.….....20

Figure 1.2: Scanning Electron Microscopy Images of AFM cantilevers…....21

Figure 1.3: The convolution effect. ….....25

Figure 2.1: Electron micrograph of a bacterial endospore. ….....28

Figure 2.2: Electron micrograph of Gram-stained Bacillus. ….....28

Figure 2.3: Bacterial chromosome replication. ….....32

Figure 2.3: The initiation of replication sequences. ….....34

Figure 2.4: The primosomal cascade. ….....38

Figure 4.1: Electron microscopy of hexameric helicases. ….....44

Figure 4.2: Models of helicase loading. ….....46

Figure 4.3: AFM image of DnaB. ….....47

Figure 4.4: The main domains in the DnaG primase protein. ….....49

Figure 4.5: The primosomal cascade. ….....50

Figure 4.6: AFM images DnaB protein. ….....57

Figure 4.7: AFM image of DnaG primase protein….....58

Figure 4.8: AFM images of DnaB-DnaG complex….....60

Figure 4.9: DnaB-DnaG subpopulations. ….....61

Figure 4.10: DnaB interaction domain….....63

Figure 4.11: DnaB-DnaG model….....68

Figure 4.12: DnaB-DnaG 3D model….....69

Figure 4.13: Advanced DnaB-DnaG model….....71

Figure 4.14: Evolution of DnaB and DnaG….....72

Figure 5.1: Replication start points….....75

Figure 5.2: The structure of the DnaD protein ….....76

Figure 5.3: AFM image of the DnaD protein at 0.49nM….....83

Figure 5.4: A histogram of 0.49nM DnaD population….....87

Figure 5.5: AFM image of the DnaD protein at 4.9nM….....85

Figure 5.6: A histogram of 4.9nM DnaD population….....85

Figure 5.7 AFM image of the DnaD protein at 49nM….....86

Figure 5.8: A histogram of 4.9nM DnaD population….....87

Figure 5.9: AFM images of DNA. ….....88

Figure 5.10: AFM images of DnaD-DNA complexes. ….....89

Figure 5.11: Features of an DnaD-DNA complex….....90

Figure 5.12: AFM images in liquid of DnaD-DNA complexes. ….....91

Figure 5.13: Graph of DnaD-DNA contour length size. ….....94

Figure 5.14: sedimentation velocity ultracentrifugation data….....95

Figure 5.15: Table of frictional coefficients. ….....96

Figure 5.16: Gel shift analysis of DnaD binding ….....97

Figure 5.17: Behaviour of DnaD proteins….....100

Figure 5.18: model of DnaD binding to DNA. ….....100

Figure 5.19: AT rich sequence in the pBR322 genome…..... 102

Figure 5.20: AFM image in air of a DnaD-DNA complex….....103

Figure 5.21: The effect of HU and H-NS on DNA….....104

Figure 5.22: Speculative model for nucleoid remodelling ….....106

Figure 6.1: The binding domains of the H-NS protein ….....108

Figure 6.2: The repression of transcription by H-NS. ….....109

Figure 6.3: Molecular model of HU protein ….....110

Figure 6.4: Effect of H-NS and HU in DNA compaction….....113

Figure 6.5: AFM images in air of plasmid-DnaD complexes ….....116

Figure 6.6 AFM image of liner plasmid DNA-DnaD complexes ….....118

Figure 6.7: Linear DNA-DnaD complex ….....119

Figure 6.8: Graph of DnaD-DNA size effect….....120

Figure 6.9: AFM image of DnaD-DNA complexes at 0 hours….....121

Figure 6.10: Graph of DnaD-DNA size effect….....122

Figure 6.11: AFM image of DnaD-DNA complexes at 24 hours….....124

Figure 6.12: AFM image of DnaD-DNA complexes at 48 hours….....124

Figure 6.13: AFM image of DnaD-DNA complexes at 72 hours….....125

Figure 6.14: Lambda DNA-DnaD interaction. ….....126

Figure 6.15: Action of DnaD on digested plasmid DNA….....129

Figure 6.16: Reversibility of DnaD effect….....130

Figure 6.17: Action of DnaD on Lambda DNA…..132

Figure 6.18: Summary of DnaD DNA induced effect…..133

Figure 6.19: Model for interaction of DnaD and DnaB …..135

Figure 7.1: Deformation of biomolecules by AFM tip. …..137

Figure 7.2: Previous AFM system. …..137

Figure 7.3: Hexagonal ice …..146

Figure 7.4: Cubic ice …..147

Figure 7.5: The AFM…..149

Figure 7.6: The AFM setup…..149

Figure 7.7: AFM in chamber…..151

Figure 7.8: Photo of cold stage…..152

Figure 7.9: Photo of heater modules…..152

Figure 7.10: The CF100 system…..153

Figure 7.11: Photo of cryogenic chamber …..154

Figure 7.12: Photo of inside the cryogenic chamber …..154

Figure 7.13: AFM control interface. …..155

Figure 7.14: AFM control by the interface…..156

Figure 7.15: A vertical scan of the cantilever ….157

Figure 7.16: A second vertical scan of the cantilever ….158

Figure 7.17: A vertical and parallel scan of the cantilever….158

Figure 7.18: Photo of the sample in its holder ….159

Figure 7.19: Images of 404nm spheres in air on the cryogenic-AFM…….163

Figure 7.20: Cross section of spheres…….164

Figure 7.21: Images of 404nm spheres in air on the DI multimode…….164

Figure 7.22: Cross section of spheres…….165

Figure 7.23: Images of 404nm spheres in vacuum on the cryogenic-AFM…166

Figure 7.24: Images of 404nm spheres at -176°C the cryogenic-AFM…….167

Figure 7.25: Images of 404nm spheres at 176°C to –134°C ….168

Figure 7.26: Images of 404nm spheres at –134°C on the cryogenic-AFM …169

Figure 7.27: Cross section of spheres…….170

Figure 7.28: AFM generated tip profiles…….172

List of Tables

Table 2.1: Important Bacillus species and there properties. ….....26

Table 2.2: The key components of bacterial replication ….....36

Table 3.1: The components of the gel electrophoresis wells….....41

Table 5.1: Size comparison of unbound DNA and DNA- DnaD complexes….93

Table 7.1: The properties of cryogens used in cryomicroscopy….....139

Table 7.2: The conditions of ice formation in cryomicroscopy ….....145

List of Abbreviations

AFM	- atomic force microscopy
bp	- base pair
Da, kDa	- Dalton, kilo Dalton
DDT	- dithiothreitol
DNA	- deoxyribonucleic acid
EDTA	- ethylenediaminetetraacetic acid
kbp	- kilo base pairs
khz	- kilo hertz
LB buffer	- laria bertani buffer
PAGE	- polyacrimalide gel electrophoresis
PBS	- phosphate buffered saline
RNA	- ribonucleic acid
SEM	- scanning electron microscopy
SPM	- scanning probe microscopy
SSB	- single stranded binding protein
STM	- scanning tunnelling microscopy
TEM	- transmission electron microscopy
UV	- unltraviolet light
Y2H	- yeast 2 hybrid assay

1. Introduction

1.1 Background

The first scanning tunnelling microscope was developed in 1981 by Binnig and Roher (Binnig *et al,* 1982). This can be seen to have grown from principles developed in an instrument called the topographiner developed by Russell Young in 1971, a technique that exploited the fact that the electron field emission current between a sharp metal probe and a electrically conductive sample is dependent on the distance separating them. Binnig and Roher applied this principle to develop the scanning tunnel microscope which monitored instead the quantum tunnelling of electrons from a sample surface to a probe. This is much more sensitive than electron field emission and yields an increased resolution of the image; however the probe must be in much closer proximity to the sample. Binnig and Roher used their STM to image individual silicon atoms on a surface by spatially measuring localised charge densities.

In 1986 the AFM or scanning force microscope (SFM) was invented by Binnig *et al* this microscope, the most widely used and versatile modification of the STM microscope, has undergone much advancement since its initial development. The first AFM operated in contact mode (Binnig *et al,* 1986; Ruger *et al*, 1990) non-contact mode was introduced in 1987 (Martin *et al*, 1987), Microfabricated AFM tips where developed in 1991 (Prater *et al*, 1991) which lead to the development of tapping mode (Zhong *et al*, 1993) and tapping mode in liquid (Hansma *et al* 1994). The first commercial production of an AFM was in 1990 (Park Scientific, Northampton, UK).

Since AFM has been widely available rapid advancements have allowed high resolution image of a wide range of biomolecules in a variety of media. AFM has been successful in imaging DNA, where the helical pitch of DNA has been shown to be 3.4 nm (Hansma *et al*, 1993; Hamsma *et al* 1995; Mou *et al*, 1995), RNA polymerases transcribing a ssDNA circular template (Kasas *et al*,

1997, Hansma 1996) polysaccachrides such as scleroglucan (Brant *et al*, 1996), cellulose in plant cell walls (Kirby *et al* 1996, Round *et al* 1996), a wide range of proteins including globular proteins such as chaperonin proteins (Mou *et al* 1996) and helicases (Haroniti *et al*, 2004) antibodies (Yang *et al,* 1996) and muscle protein such as myosin and titin (Hallet *et al*, 1996), lipid bilayers (Hui *et al*, 1995; Mou *et al*, 1994; Grandbois *et al*, 1998), membrane protein crystals such as purple membrane (Muller *et al*, 1995; Muller *et al*, 1996), whole cells such as bacteria (Gunning *et al* 1996), red blood cells (Zachee *et al*, 1994) and platelets (Radmacher *et al*, 1996) and many other systems.

The basic operating principle of the AFM is simple in theory (figure 1.1); a sharp probe mounted at the end of a flexible cantilever (figure 1.2) raster-scans over the sample surface in a series of horizontal movements. Deflections of this cantilever caused by interactions between the probe and the sample are monitored by an optical detector which measures the signal from a laser beam that is positioned on the cantilever surface above the probe. This signal is then used by a feedback system to alter the force applied to the sample by the tip by controlling the movements of a piezo crystal. A so called topographic image can then be created from the vertical movements of this crystal.

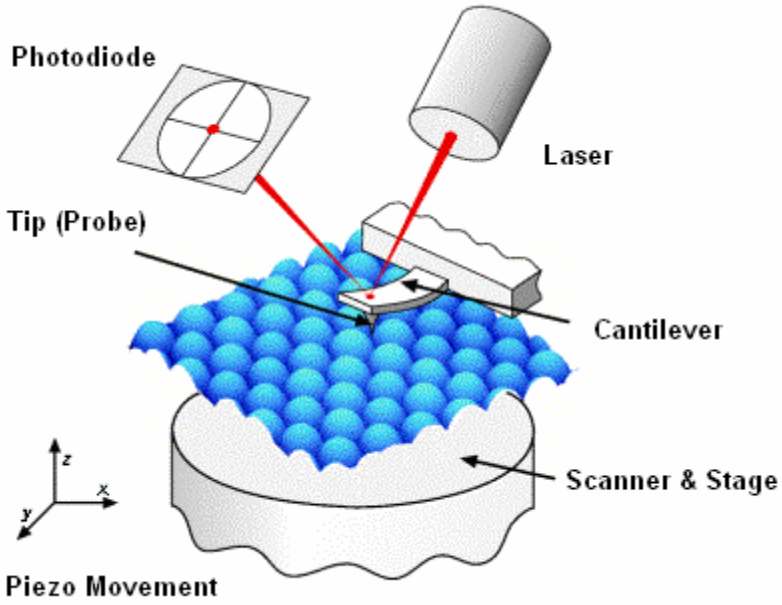

Figure 1.1: A General scheme showing the basic operating principles of the AFM

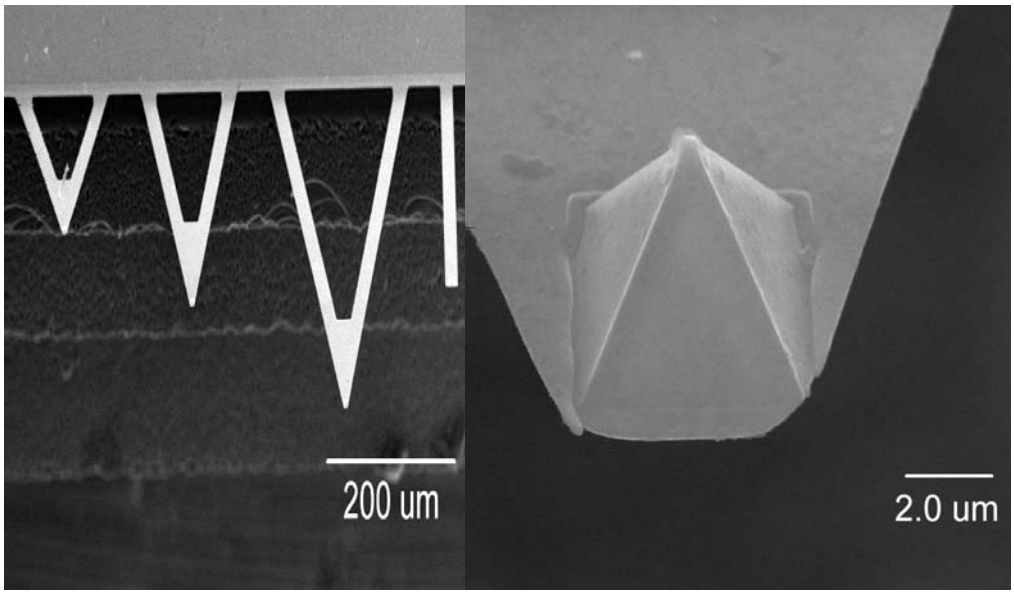

Figure 1.2: Scanning Electron Microscopy Images of (left) A selection of cantilevers used in AFM biomolecule investigation (right) a close up of the probe on the underside of the cantilever (Gunning, 2000)

1.2 Modes of operation

AFM can operate in a number of modes;

1) Contact mode is when the tip scans the sample in close proximity to the surface; the deflection of the cantilever is measured by the detector and compared in a feedback loop to a desired value of deflection. If the measured deflection is different from the desired value the feedback amplifier applies a voltage to the piezo to raise or lower the sample relative to the cantilever to restore the desired value of deflection. The voltage that the feedback amplifier applies to the piezo is a measure of the height of features on the sample surface.

2) Non-contact mode is used in situations where tip contact might alter the sample in subtle ways. In this mode the cantilever is vibrated at its resonant frequency and the tip hovers 50 - 150 Ångströms above the sample surface. Long range attractive van der Waals forces acting between the tip and the sample are detected, and topographic images are constructed by scanning the tip above the surface, whereby the amplitude or phase of the oscillating lever

is kept at a constant pre-set value. Unfortunately the attractive forces from the sample are substantially weaker than the forces used by contact mode. Therefore the tip must be given a small oscillation so that AC detection methods can be used to detect the small forces between the tip and the sample by measuring the change in amplitude, phase, or frequency of the oscillating cantilever in response to force gradients from the sample. For highest resolution, it is necessary to measure force gradients from Van der Waals forces which may extend only a nanometre or so from the sample surface.

3) Tapping mode is a key technique in AFM; it allows high resolution topographic imaging of sample surfaces that are easily damaged by the lateral forces in contact mode or loosely held to their substrate, such as many biomolecules. Tapping mode imaging is implemented by oscillating the cantilever assembly at or near the cantilever's resonant frequency using a piezoelectric crystal. The piezo motion causes the cantilever to oscillate with a high amplitude (typically greater than 20 nm) when the tip is not in contact with the surface. The oscillating tip is then moved toward the surface until it begins to lightly touch, or tap the surface. During scanning, the vertically oscillating tip alternately contacts the surface and lifts off, generally at a frequency of 50,000 to 500,000 cycles per second (50k - 500k Hz). As the oscillating cantilever begins to intermittently contact the surface, the cantilever oscillation is necessarily reduced due to energy loss caused by the tip contacting the surface. The reduction in oscillation amplitude is used to identify and measure surface features.

During tapping mode operation, the cantilever oscillation amplitude is maintained constant by a feedback loop. Selection of the optimal oscillation frequency is software-assisted and the average force on the sample is automatically set and maintained at the lowest possible level. When the tip passes over a bump in the surface, the cantilevers amplitude of oscillation decreases. Conversely, when the tip passes over a depression, the cantilever amplitude of oscillation increases (approaching the maximum free air amplitude). The oscillation amplitude of the tip is measured by the detector and input to the AFM controller electronics. The digital feedback loop then

adjusts the tip-sample separation to maintain a constant amplitude and force on the sample.

AFM has three main advantages over other high resolution microscopic techniques. Firstly it is generally non-destructive, for example the sample preparation does not involve any negative staining or metal coating like in electron microscopy, and secondly the microscope can be operated in liquid, mimicking the *in vivo* situation as close as possible. Thirdly the AFM has a high signal to noise ratio that allows single proteins to be imaged at a resolution better than 1nm.

Under ambient conditions, sample surfaces are covered by a layer of adsorbed gases consisting primarily of water vapour and nitrogen which is 10-30 monolayers thick. When the probe touches this contaminant layer, a meniscus forms and the cantilever is pulled by surface tension toward the sample surface. The magnitude of the force depends on the details of the probe geometry, but is typically on the order of 100 nN. This capaillary force can be removed by operating contact mode under a liquid. As well as elimination of capillary forces, the reduction of van der Waals forces and the ability to study technologically or biologically important processes at liquid solid interfaces make liquid AFM imaging a valuable biological tool.

Tapping mode operation in fluid has the same advantages as in air or vacuum; however imaging in a fluid medium dampens the cantilever's normal resonant frequency. In tapping mode, the entire fluid cell can be oscillated to drive the cantilever into oscillation compared to operation in air or vacuum where the cantilever itself is oscillating. Very soft cantilevers are used due to the decreased resonant frequency in liquid. The spring constant is typically 0.1 N/m in liquid compared to tapping mode in air where the cantilever may be in the range of 1-100 N/m.

1.3 Additional Signals

As well as topographic information the AFM can generate a phase signal when operated in tapping mode, in this mode the feedback loop measures the drop of amplitude of the oscillating cantilever to determine the vertical movement of the piezoelectric tube. This differs from the topographic signal because when the tip strikes the sample its phase of oscillation is disturbed and no longer precisely in step with the phase of the electrical oscillator that is driving it, because each time the tip touches the sample a small amount of energy is transferred to it. This is useful in determining for example, the differing elastic properties of a sample.

Other signals measured by the AFM (but not employed in this thesis) are frictional force, elastic and adhesion properties of the surface and non-imaging applications, this is a large and exciting area of AFM where the AFM probe, often modified is used to measure intra and intermolecular forces of biomolecules, for example the unbinding forces of DNA oligonucleotides were calculated by covalently attaching the DNA to both the tip and substrate (Lee *et al* 1994) and the binding energy was calculated for a single biotin-avidin complex (Allen *et al* 1996).

1.4 Limitations

The AFM is susceptible, as are all high resolution microscopic techniques to temperature variation and vibration. Temperature drift caused by the AFM is reduced by careful selection of the material that compose components of the AFM and temperature control around the instrument. Building vibrations (15-20Hz) that may affect imaging can be reduced by isolation of the AFM on a mechanical anti vibration air table or active piezo isolation platforms.

There are also some limitations of AFM related to its imaging capabilities. Thermal drift, especially apparent when imaging under liquid is caused by temperature difference between the liquid and the liquid cell, causing the cantilever to bend, this can be reduced by allowing the AFM to equilibrate.

Tip convolution is an imaging artifact that occurs because of the large nature of the AFM probe in relation to the samples imaged. In many cases the sides of the AFM probe will interact with the sample leading to a broadening of the image (see figure 1.3). This can be reduced by tight packing on the surface of the sample to be imaged and the use of sharper probes. AFM samples have a limited range of roughness that cannot be too high or the sample will touch the underside of the cantilever severely reducing image quality. A typical AFM tip is 3µm tall, though rougher samples can be imaged by using higher aspect ratio tips (though the z direction piezo range is normally about one micron) or imbedding the rough sample in a matrix. Other intrinsic factors that inhibit imaging are discussed in chapter 7.

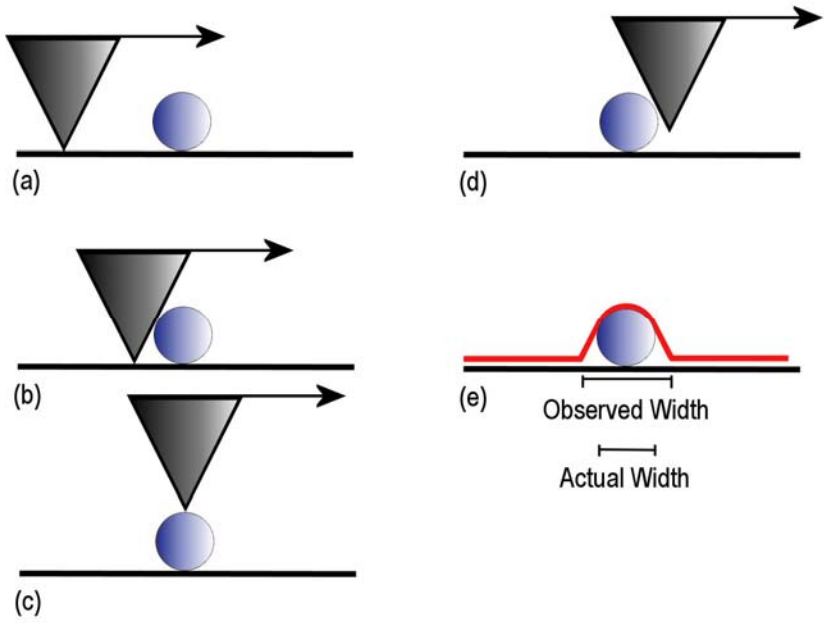

Figure 1.3: As the tip approaches the obstruction, the side of the tip hits first, causing the premature raising of the cantilever. The difference between observed width and actual width can be seen (Image used with permission of James Moody).

2. *Bacillus*

2.1 General

The genus *Bacillus* was recognized and named by Ferdinand Cohn (a student of Robert Koch) in 1872. The bacteria are grouped in the family *Bacillaceae* whose distinguishing feature is the production of endospores. These are highly refractile quiescent structures formed within the bacterial cells during aerobic growth. Grouping *Bacillus* species together based on spore production has resulted in many different bacteria with a wide range of physiological aspects being grouped together. The genus *Bacillus* is comprised of over 40 recognized species, more than 200 which have been inadequately described; a list of some of the common features and important species in this genus are shown below (table 3.1) (Bergey, 2001)

Classification	Important Species	Common Features
Kingdom – Bacteria	***B.subtilis***	**Endospores**
Phylum – *Firmicates*	***B.anthracis***	**Antibiotic**
Class – *Bacilli*	***B.Thuringenisis***	**Autotrophy**
Order – *Bacillales*	***B.cereus***	**Acidophily**
Family – *Bacillaceae*	***B.stereothermophilus***	**Alkaliphily**
Genus – *Bacillus*	***B.larvae***	**Thermophily**
Species – *subtilis*	***B.popilliae***	**Parasitism**

Table 2.1: The classification, important species and common features of members of the genus *Bacillus*.

Bacillus species are gram positive (gram-positive bacteria are those that stain dark blue by gram staining, the stain reacts with the high amount of peptidoglycan which is found in the cell wall, which in gram-positive bacteria lacks the secondary membrane and lipopolysaccharide layer, that is present in gram-negative bacteria) and have a G+C content ranging from 32% to 69%. Not only is there variation between species but within species, for example the bacteria *B.megaterium* can have a G+C content ranging from 36% to 45% (Todars, 2001)

2.1.1 Endospore

The distinguishing feature of *Bacillus* species is their ability to form endospores, the primary function of *Bacillus* endospores are to ensure the survival of a colony through periods of environmental stress. Endospores which are different from vegative cells are the most resilient cells found in nature and can remain viable for extremely long periods of time, up to millions of years. Endospores are highly resistant to disinfectants, temperature, acids, radiation and lysozyme and normally form when a vegative cell passes out of the exponential phase of growth, as a result of nutrient depletion, at a rate of one endospore per vegative cell.

Spore position in the mother cell or sporangium differs among species and is useful in identification. The spore itself is often surrounded by a thin covering called exosporium. A spore coat lies under the exosporium (see figure 2.1). This spore coat is impermeable to many toxic molecules and also contains enzymes that are involved in germination. Beneath the spore coat is a cortex that consists of peptidoglycan (that stains with the gram stain) and surrounds the spore cell wall (core wall) which itself surrounds the protoplast or core. The core has normal cell structures but is metabolically inactive.

Up to 15% of the spore's dry weight may consist of dipicolinic acid complexed with calcium ions; dipicolinic acid is thought to be responsible for the heat resistance of the spore, whilst calcium acts as resistance to oxidising agents as well as heat resistance. It is also thought that the combination of calcium ions and the dipicolinic acid may stabilize the endospore nucleic acids.

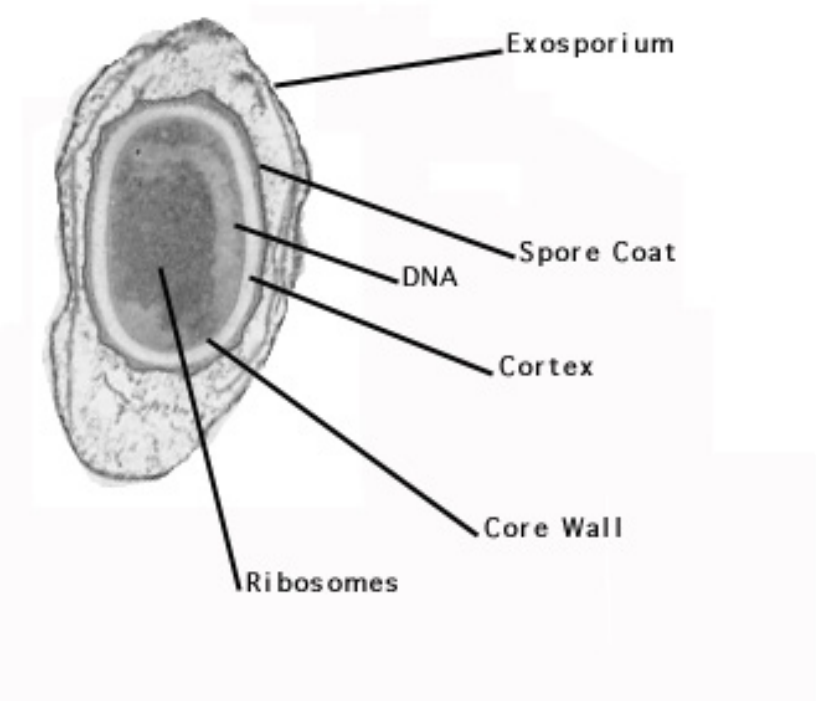

Figure 2.1: Electron micrograph of a bacterial endospore. The spore has a core wall of unique peptidoglycan surrounded by several layers, including the cortex, the spore coat and the exosporium. The dehydrated core contains the bacterial chromosome and a few ribosomes and enzymes to jump-start protein synthesis and metabolism during germination (Todars, 2001).

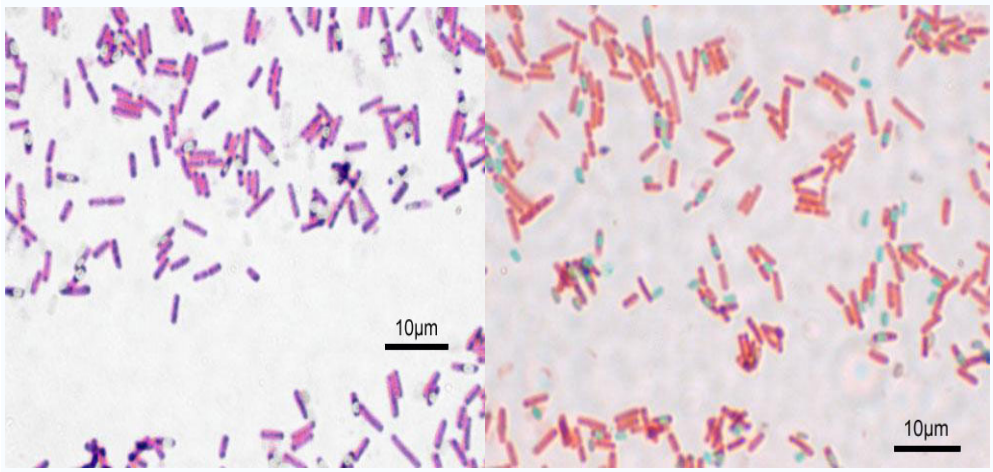

Figure 2.2; (Left) electron micrograph of Gram-stained *Bacillus*. (Right) electron micrograph of spore stained *Bacillus* subtilis, red (vegatives) green (spores)

2.1.2 Species

There are many medically and environmentally important *Bacillus* species, (table 1) *B.anthracis* is the causative agent of anthrax a potentially fatal disease that infects wild animals and occasionaly humans. *B.cereus* causes two types of food poisoning; *B.thuringinesis* also causes food poising and is a pathogen of *Lepidoptera* insects. *B.larvae* and *B.popilliae* are major insect pathogens (bees and beetles respectively). Many *Bacillus* species also produce antibiotics such as *B.cereus* (cerexin and zwittermicin) and *B.subtilis* (difficidin and subtilin).

Bacillus subtilis is the most widely studied *Bacillus* species (fig 3.2), it grows as a unicellular rod and very rarely forms chains. It is an obligate anerobe bacterium and is commonly found in soil and plant rhizobium, and like other *Bacillus* species, it has the ability to form tough protective endospores. *B.subtilis* is not considered a human pathogen, but it can contaminate food and in rare cases causes food poisoning . Its spores can survive the extreme heating that is used to cook food, and can be responsible for causing ropiness in bread (bacterial spoliage through production of extracellular slimy polysaccahrides) (Bergy, 2001).

B. subtilis ability to grow on minimal defined medium with no added growth factors and the fact that it is highly amenable to genetic manipulation, has led to it becoming a model organism for laboratory studies. This is especially so for sporulation, which is a simplified example of cellular differentiation. In terms of use as a laboratory model *B. subtilis* can be considered the Gram-positive equivalent of *Escherichia coli*, the most extensively studied Gram-negative bacteria.

The *B.subtilis* genome was completely sequenced in 1997, this was the first complete sequence for a single living bacterium. It has a single, circular chromosome, which is 4.2 mega basepairs long with a 4,100 base pair protein coding region and has a single origin from which bidirectional DNA replication initiates. Newly replicated sister chromosomal regions move apart from each other soon after duplication, thus a semi duplicated chromosome is

partially segregated before the bulk of DNA is even replicated. *B.subtilis* can also often have self replicating conjugative plasmids.

In this thesis the bacteria *Bacillus subtilis* is studied as model organism for bacterial replication initiation, though in several experiments, equivalent proteins (due to there more stable nature) where isolated from *B.stearothermophilus* which grows at 65°C and has tolerance to acid. It occurs naturally in soil, hotsprings, desert sand, artic waters, ocean sediments, food and compost.

2.2. Replication Overview

The DNA molecules of bacteria that encode the genes are essential for survival and are enclosed in a structure called a chromosome (in analogy to chromosomes of higher order organisms) This is different from plasmid DNA, which is present in some bacteria and can be of equal size to the chromosome but carries genes that may not be required for growth of the organism (such as antibiotic resistance or virulence factors). Bacterial chromosomes are unique (only one copy per cell) and normally circular with a circumference of ~1mm. This allows bacterial DNA to replicate in its entirety with out using telomeres as eukaryotes do. Bacterial chromosomes are usually wrapped around histone like proteins such as HU and H-NS as they need to be compacted ~100 fold to fit inside the bacterial cell (Lewis *et al*, 2004).

The replication of the circular bacterial chromosome initiates at a unique site in the DNA called the origin of chromosomal replication (*oriC*) and proceeds in both directions around the circle forming two replication forks as new DNA is sequenced. The two replication forks continue until they meet and terminate chromosomal replication (figure 2.3). Once DNA replication has started it proceeds at an apparent constant rate (at 37 °C), therefore the regulation of chromosome replication is carried out at the initiation stage

An initiative event occurs once per cell division cycle in response to a signal that is coupled to cell mass. Initiation requires the origin initiation protein

DnaA which initiates melting of the ds DNA at *oriC* and recruits the replisome to that site. The replication helicase (DnaC in *Bacillus*) and other components of the replisome are probably added onto DNA at a AT rich sequence initially with in the *oriC* in a sequence of events called the primosomal cascade. In the penultimate step of the cascade, hexameric helicases are loaded onto the DnaA unwound origin by helicase loading proteins forming the primosome, the primosome is a multi-enzyme complex that travels along the lagging strand template and acts to both unwind the template DNA and synthesize the primers for initiation of Okazaki fragments. The primosome then expands the single stranded DNA bubble by unwinding DNA strands in an ATP dependent manner, with the aid of single stranded binding proteins. Finally primase is able to synthesize the RNA primers required for DNA polymerase to begin DNA replication. This completed complex is termed the replisome, it encompasses all enzymatic activity at the replication fork including the primosome, SSB and DNA polymerase.

Bacterial DNA polymerases are highly processive, multisubunit protein complexes that synthesise DNA at a high speed, replication of the 4.6Mb chromosome of *E.coli* takes ~40 mins. Therefore, each replication fork formed at the *oriC* proceeds at nearly 1000 nucleotides a second (Helmstetter *et al*, 1987). As DNA unwinds, DNA polymerse III moves along and synthesises new DNA continuously on the leading strand (5' to 3') but in a series of fragments called Okazaki fragments on the lagging strand (3' to 5'). These fragments require the exonuclease activity of DNA polymerase I and the activity of DNA ligase to join them into a continuous strand of DNA.

Replication termination usually occurs within a defined region not a specific site. This termination region called *ter* contains a cluster of sites called *ter* sequences, which are only 22bp long. These sequences allow the replication fork through in one direction but not in the other. The sequence on its own is not sufficient to stop the replication fork, proteins are also required at *ter* sites. These proteins, called terminus utilization substance (tus) in *E.coli* and replication terminator proteins (RTP) in *Bacillus* and are thought to bind to the *ter* sites and stop the replicating helicase that is separating the strands of DNA

ahead of the replication fork. These proteins also have a role in separating the daughter DNA and stopping replication proceeding on any free ends. Deletion of *ter* sequences in *Bacillus* still allows replication to continue but more slowly than in the wild type (Lemon *et al*, 2001).

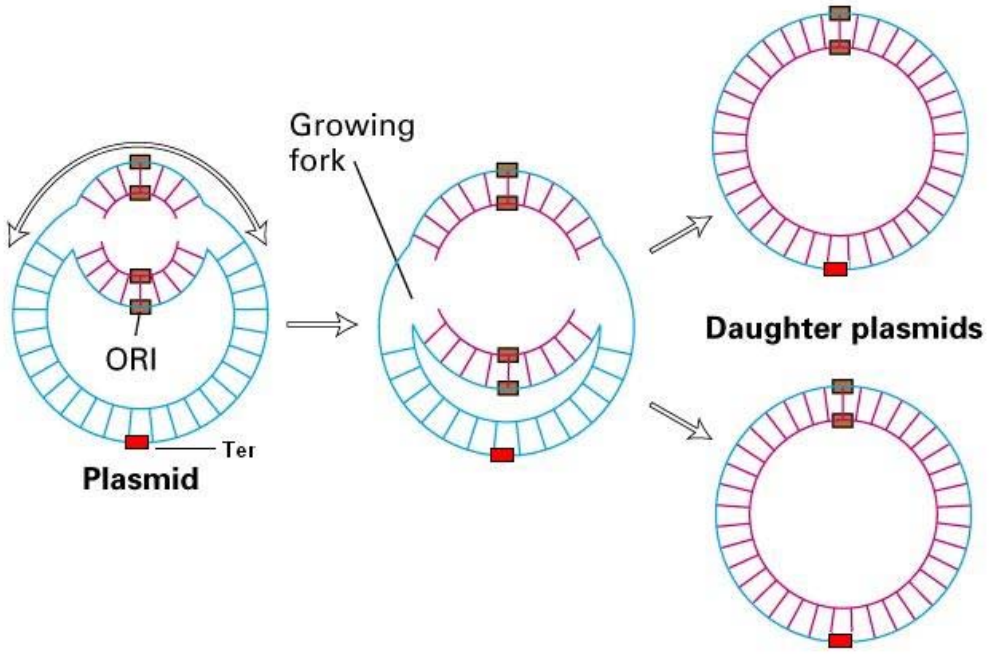

Figure 2.3: A schematic diagram showing bacterial chromosome replication. A replisome forms at the *oriC* and two replication forks move away in opposite directions. Untill they reach the ter sequence causing replication to terminate and two daughter plasmids to form.

2.3. Replication Initiation

The initiation of replication has already been shown to be the key step in the regulation of bacterial chromosomal replication. Extensive studies have been carried out on the factors involved in the initiation and elongation of replication in *E.coli*, many of the proteins identified have subsequently been shown to be conserved in *B.subtilis*. However, a few of these proteins have not been found by homology searches of the *B.subtilis* genome. Additional factors have been identified that are not present in *E.coli*, showing that these

bacteria may use distinct mechanisms for basic processes such as DNA replication.

2.3.1 Initiation regulation

Bacterial replication origins (*oriC*) have been isolated as autonomously replicating segments in seven species of bacteria. These have been found to contain multiple binding sequences (9 base pairs in length) for the DnaA protein called DnaA Boxes as well as 13bp long sequences with a higher than average AT base pair frequency (Moriya *et al*, 1999). The DnaA protein is also largely conserved in eubacteria. It is widely accepted that DnaA is the initiator for chromosome replication in *E.coli*, which binds to DnaA boxes within the *oriC* and causes local unwinding of DNA within it (Herrick et al, 1996). DnaA has also been shown to bind to DnaA boxes within the *oriC* of *B.subtilis* (Fukouka et al 1990) to be required specifically for the initiation of chromosome replication (Moriya *et al* 1990), and shown to cause unwinding of dsDNA within the *oriC* (Krause *et al*, 1997).

The DnaA protein appears to have a common function in bacteria as the initiator of replication, there is however some variation between species. In gram positive bacteria, DnaA boxes exist in two noncoding regions upstream and downstream of the dnaA gene. Replication initiates within the downstream box (Moriya et al, 1992) whilst in gram-negative bacteria there is no DnaA box cluster downstream of the dnaA gene and the *oriC* location has changed relative to the dnaA gene (figure 2.3).

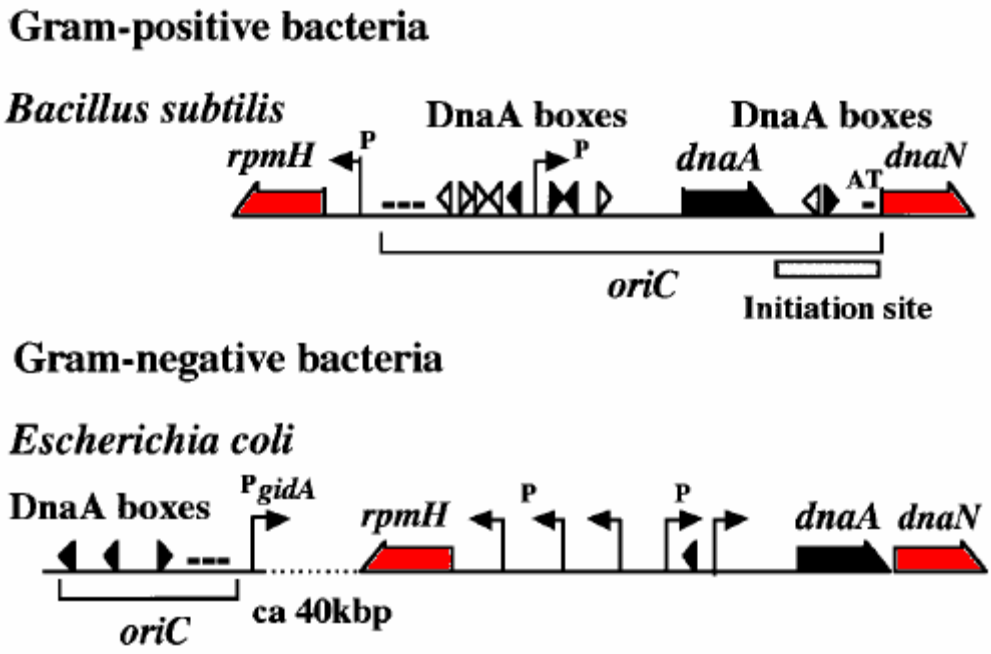

Figure 2.3: The initiation of replicaton sequences in a typical gram-positive (top) and gram-negative (bottom) bacteria. DnaA gene is shown in black, other genes in red DnaA boxes are white triangles located in the *oriC*. AT rich regions and gene promoters are highlighted (adapted from Moriya *et al*, 1999).

B.subtilis is slightly different from most gram negative bacteria in that the DnaA boxes both upstream and downstream are required for initiation of replication, suggesting a loop forms between these two boxes. This loop has been proven to form in the precence of DnaA *in vitro* (Krause *et al* 1997, Moriya *et al* 1992)

The expression of the *B.subtilis dnaA* gene is regulated by itself. The DnaA protein level in a temperature sensitive *dnaA* mutant decreased upon the temperature shift up, due to rapid degredation of inactive DnaA, but it rapidly recovered and increased to an elevated level by enhanced expression. In addition Northen blot analysis has revealed that the amount of protein from the *dnaA-dnaN* operon increased in a *dnaA* null mutant and decreased in a *dnaA* overproducing strain (Moriya *et al*, 1992)

At least two major regulatory mechanisms contribute to the control of replication initiation (the translation of DnaA), a positive mechanism triggers initiation in response to the initiation mass, and a negative one suppresses

extra initiations. In *E.coli* the balance between the DnaA protein level and the number of DnaA binding sites within the cell is thought to correlate with the initiation mass in *E.coli* because overproduction of DnaA and deletion of datA (a locus containing high affinity DnaA binding sites) both promote initiation (Lobner-olesen *et al*, 1989) as does the production of extra DnaA boxes (Christensen *et al*, 1999) In *B.subtilis*, overproduction of DnaA decreases the initiation mass slightly suggesting that DnaA concentration to be important for determining the timing of initation. However transcription of *dnaA* seems to occur after replication initiation and the DnaA level may reach a constant level at an early stage of the replication cycle. Detailed analysis of the flucuations of DnaA levels within the cell divison cycle is needed before conclusions can be reached.

2.3.2 The primosomal cascade

In *E.coli,* binding events in the *oriC* cause local unwinding of AT rich sequences in the *oriC* and opening up of dsDNA triggering a series of events called the primosomal cascade, both ATP bound DNA and a high concentration of ATP are required for this initial step (Sekimizu *et al.,* 1987). Then DnaB helicase is transferred to the open site with the aid of DnaC from a stable hexameric complex of these proteins. Then the completed primosome complex forms the replisome by the helicases interacting with the DnaG primase and DNA polymerase III holoenzyme, which are necessary for priming and DNA synthesis respectively as well as single stranded binding protein (Baker and Wickner, 1992; Baker and Bell, 1998).

In *B. subtilis,* at least four other proteins, DnaB, DnaC, DnaD, and DnaI, are genetically shown to be required in the initiation of chromosome replication (Ogasawara *et al.,* 1986; Sakamoto *et al.,* 1995; Bruand *et al.,* 1995a; Bruand and Ehrlich, 1995; Moriya, S., unpublished result). It should be noted that the nomenclature of *dna* genes in *B. subtilis* is different from that in *E. coli.* DnaC was genetically identified to be the major DNA helicase of chromosome replication, the counterpart of *E.coli* DnaB (Sakamoto *et al.,* 1995) also used

in this thesis are *B.stererothermophilus* which has similar nomenclature to *E.coli* (DnaB is the helicase).

Protein	*E.coli*	*B.Subtilis*	*B.stereothermophilus*
Initiator	***dnaA***	***dnaA***	***dnaA***
Replicative DNA helicase	***dnaB***	***dnaC***	***dnaB***
Helicase loader	***dnaC***	***dnaI***	***dnaI***
Primosomal protein n	***priA***	***priA***	***priA***
DNA pol. III α subunit	***dnaE***	***dnaE + polC***	***dnaE + polC***
DNA pol. III β subunit	***dnaN***	***dnaN***	***dnaN***
Primase	***dnaG***	***dnaG***	***dnaG***
SSB	***ssb***	***ssb***	***ssb***
DNA pol. I	***polA***	***polA***	***polA***
DNA ligase	***lig***	***yerG***	***yerG***
Unknown		***DnaD, DnaB, DnaI***	

Table 2.2: The key components of bacterial replication and there nomenclature in different bacterial species (adapted from lemon *et al* 2002)

DnaB, DnaD, and DnaI, are proteins which (among others) were isolated from efforts to reconstitute bacteriophage φX174-type complementary strand DNA replication *in vivo* (Bruand *et al.,* 1995b, Marring 2000, Wickner *et al* 1977). However, as components of the *Bacillus* primosome (except for the DnaC helicase) are not required for *oriC* plasmid replication in *E. coli* (Messer and Weigel, 1996) and homologues of the three *B. subtilis* Dna proteins are not

found in *E. coli,* their roles in initiation of chromosome replication remain speculative.

Using the yeast two-hybrid system, it has been found that DnaI interacts with the DnaC helicase (Imai *et al.,* submitted for publication). As its interaction is strong and as there is a weak but significant homology between DnaI and the *E. coli* DnaC helicase loader (Koonin,1992), DnaI appears to be the helicase loader in *B. subtilis.* The DnaD protein has been shown to interact with DnaA by the yeast two-hybrid assay (Ishigo-oka *et al.,* unpublished). As this protein is known to be a component of the primosome (Bruand *et al.,* 1995b), it might be involved in activation of DnaA and/or loading of DnaC helicase. DnaB appears to be required for association of the *oriC* with the cell membrane and exhibits a strong single stranded DNA binding ability. In *E.coli* the helicase loader has such an activity when it forms a stable complex with the helicase, it could be that DnaI and DnaB both have the different functions of the *E.coli* helicase loader DnaC (figure 3.4).

Replication forks once formed proceed around the chromosome making two daughter DNAs, however when the fork encounters either damaged DNA, a nick in the template strand or a 'frozen' protein-DNA complex the replication machinery is dissambled while the damage is repaired by recombination, there is a problem because there is no *oriC* site to reinitiate primosome assembly and DNA synthesis. Instead the bacteria utilises another pathway dependent on the priA protein and involving other proteins such as PriB, PriC and DnaT which reassemble the replication apparatus, using the ss 3' OH end of DNA that invades the ds DNA to form a "D-loop" recombination intermediate as the primer to initiate new synthesis, this primosome is called the replication restart primosome (Marians 2000).

Both primosomes have been identified in *E.coli*, a DnaA-dependent primosome is assembled at *oriC* the chromosomal origin as well as at the A site, a single stranded DNA hairpin containing a dnaA box sequence in its stem. In contrast PriA recognises a hairpin n-primosomal activation sequence and intiaties assembly of a priA dependent primosome in conjuction with

other prepriming proteins. PriA inactivation blocks recombination formation (Kogoma *et al*, 1996). *E.coli* possess two distinct, mutually exclusive primosomes which are differentially utilized by the chromosome as well as by the plasmids (Masai *et al*, 1996).

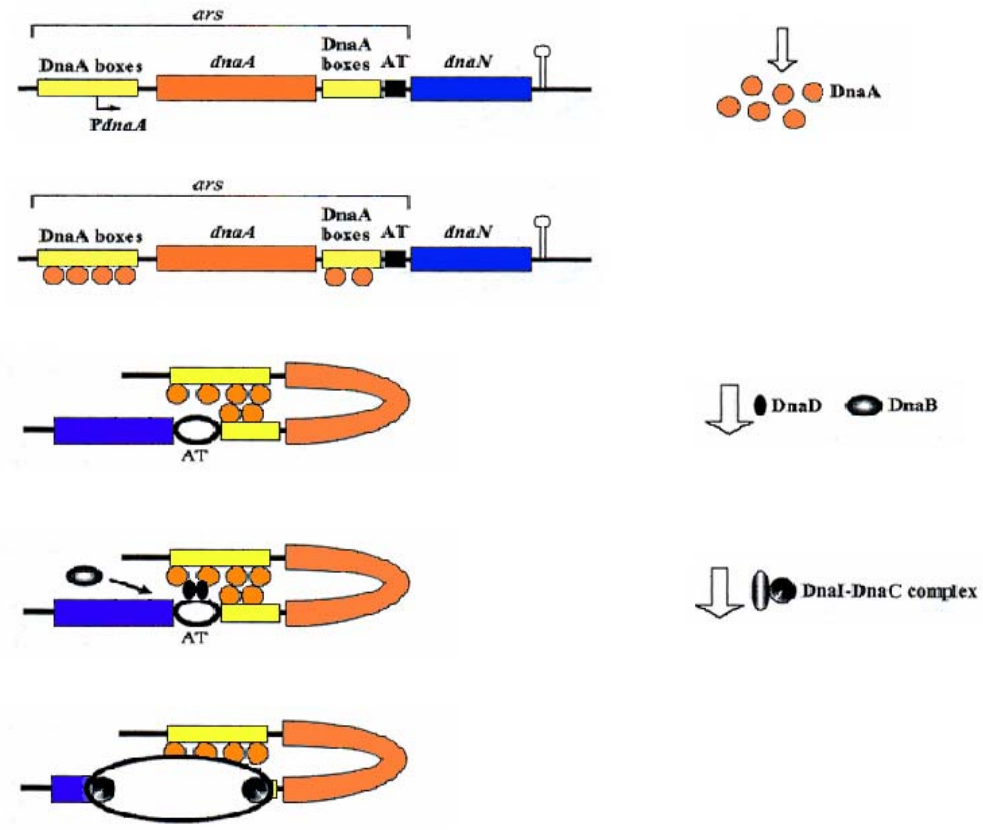

Figure 2.4: The primosomal cascade is sequential in the DnaA (or PriA)–DnaD–DnaB order to set up an initial complex that then recruits DnaC helicase. DnaC exists in a complex with DnaI, whilst the role of DnaB is still unclear. It may act together with DnaI forming a pair of helicase loaders or alternatively as a membrane attachment protein to regulate initiation of DNA replication by regulating the recruitment of DnaD to the membrane. The role of the cell membrane in the initiation of DNA replication in B. subtilis is well documented, but the precise molecular mechanisms that underpin this function have just started to be unraveled.

3. Methods

All materials, unless otherwise stated were purchased from Sigma-Aldrich (Poole, UK) and used without further purification. All water used was obtained from an ELGA purification system (resistivity ca 18.2 MΩ.cm, Maxima USF ELGA, High Wycombe, UK). Water and buffers were filtered through a 0.2 μm pore size filter, (Sartorius, Göttingen, Germany) prior to use. Specific experimental conditions are described in chapters 4-7.

3.1 AFM Imaging

All AFM imaging was carried out on a Nanoscope IIIa with a type E Scanner (Veeco, Bicester, UK) AFM was conducted at room temperature and humidity, with a scanning rate typically between 1 – 3 Hz using tapping mode in either air or liquid. The tapping set-point was adjusted to minimise probe-sample interactions. Images were recorded in both topography and phase modes with a pixel size of 512 x 512, flattened and analysed with WSXM software 3.0 beta 2.3 (Nanotec Electronica S.L., Spain).

3.1.1 Air Imaging

Samples were prepared (as described in experimental chapters) then 5 -10 μl was placed onto freshly cleaved muscovite mica (Agar Scientific, Stanstead, UK). Mica is an anatomically flat substrate that has been shown to be good for the immobilisation and imaging of DNA (Hansma *et al*, 1992, Wagner, 1998) attached to a magnetic metallic disc. Samples were then washed 3 – 5 times with ultra pure water and dried under a gentle stream of Nitrogen gas before being transferred to the AFM for imaging. The cantilevers used for air imaging were 'spring board' cantilevers with a resonant frequency of 200-300 kHz and a spring constant of 34.4 – 74.2 N/m (Olympus, OMCL-AC160TS)

3.1.2 Liquid Imaging

Samples were prepared (as described in experimental chapters) and 30-50 µl were placed on the underside of the liquid cell before being placed on freshly cleaved muscovite mica present in the AFM head. The sample was then imaged using silicon nitride sharpened, triangular cantilevers with a resonant frequency of 8-10 kHz and a spring constant of approximately 0.32 N/m (Olympus, OMCL-AC160TS)

3.2 DNA preparation

3.2.1 Harvesting bacteria susceptible for transfection.

500 µl of an overnight culture of XL1-Blue *E.coli* was transferred to 300ml of Laria Bertani (LB) buffer and allowed to grow for 2.5 hours at 37°C in a shaker. After incubation the cells are transferred from the medium into two large plastic centrifuge tubes and spun for 12mins at 6,000rpm. The supernatant was then disposed of and the pellet resuspended in LB before being spun for 12mins at 6,000rpm and 4°C This step was repeated several times, gradually purifying the pellet. When the pellet was free of debris it was resuspend into a small volume of dH_2O and snap frozen in liquid Nitrogen and stored at -80°C.

3.2.2. Transforming the bacteria

0.5µl of the plasmid, pBR322 at a concentration of 1000µl/ml was added to a electroporation cuvette of bacteria grown in section 3.2.1. The electroporation cuvette was micropulsed then added to 1ml of LB buffer, and left to grow for approx 2hrs at 37°C in a rotating shaker. After 50µl of the bacteria were plated on a ampicillin resistant agar plate. The culture was grow overnight at 37°C before 4 single colonies where picked and placed in LB buffer and grow at 37°C for 12 hours.

3.2.3. Removing non-transformed bacteria

The bacteria were inoculated in 200ml of LB with 50 µg/ml of ampicillin and tetracycline, then grown for 4hrs at 37°C in a shaker before being centrifuged for 12mins at 6,000rpm.

3.2.4. Purifying plasmid

Plasmid was purified from the bacteria using the Miniprep kit (Qiagen Ltd, West Sussex, UK) as in the operating instructions.

3.2.5 Check for plasmid DNA

A 1 % agrose gel was made by adding 0.35g of agrose gold powder to 35ml of TAE XX Buffer and microwaving for 1min to dissolve. The solution was allowed to cool then 0.75µl of Ethidium Bromide was added before the gel was poured. Two samples where added (table 3.1) and the gel allowed to run for 30 minutes at 65 volts

After the gel has run, it was viewed under a UV lamp to reveal the 3 bands for supercoiled, circular and linear forms of the plasmid confirming the presence of pBR322.

Component	Sample One	Sample Two
Plasmid DNA	1 µl	0.5 µl
Loading Buffer	1 µl	1 µl
Distilled Water	4 µl	4.5 µl

Table 3.1: The components of the gel electrophoresis wells

3.2.6 Restriction digest

A sample was made containing 2µl of the restriction enzyme PstI, 5µl of 10xNEB 2 buffer and 43µl of pBR322. The sample was left for 4 hours at 37°C in hot plate then placed at 75°C for 20mins to deactivate the restriction enzyme. 5µl of Potassium Acetate and 165µl of cold 100% ethanol were added and the sample stored at -20°C for one hour. The sample was then centrifuged for 12 minutes, the supernatant was removed and the pellet allowed to air dry for 45 mins before being redissolved in 50µl EB buffer and snap frozen.

4. The interaction of the bacterial helicase (DnaB) and primase (DnaG)

4.1. Introduction

4.1.1 General

Helicases are motor proteins that are integral members of the protein complexes that catalyse the reactions of nucleic acid metabolism. The basic reaction catalyzed is the unwinding of a DNA or RNA duplex coupled to the hydrolysis of nucleotide triphosphates (NTPs) (Soultanas *et al*, 2000). This unwinding activity is crucial in all aspects of nucleic acid metabolism, including DNA replication and repair. The most important bacterial helicase is DnaB which recruits the primase, DnaG and signals the end of the primosome cascade and the switch to polymerisation mode. Currently little is known about the molecular and structural details of the helicase-primase interaction.

4.1.2 Helicases

Helicases are universal proteins found in almost all organisms, it is estimated that about 1% of both the prokaryotic and eukaryotic genome codes for helicases. In the well studied yeast *Saccharomyces cerevisiae* 134 helicases have been identified, suggesting nearly 2% of its open reading frame encodes helicases (Gorbalenya *et al*, 1993).

Helicase is an essential protein in humans, to the extent that disorders and diseases such as xeroderma pigmentosum, Cockayne's syndrome and trichothiodystrophy all of which cause cancer, immunodeficiency, mental retardation and premature aging, are caused by mutation in six proteins that are predicted to be helicases from there primary sequences (Ellis *et al*, 1995, 1997, Shen *et al* 1998).

A wide variety of helicases from different organisms have been studied by electron microscopy and shown to form a hexameric ring structure (figure 4.1), these hexameric rings are similar in size and structure. It is thought that this hexameric structure helps the helicase to increase its processivity, because by encircling the DNA, the ring protein is topologically linked to the DNA, and therefore able to interact with the DNA longer. In many cases hexamer formation was shown to be dependent on Mg^{2+} (as is the case for DnaB in *E.coli*, Bujawoski *et al*, 1998) or NTP/NDP binding or both.

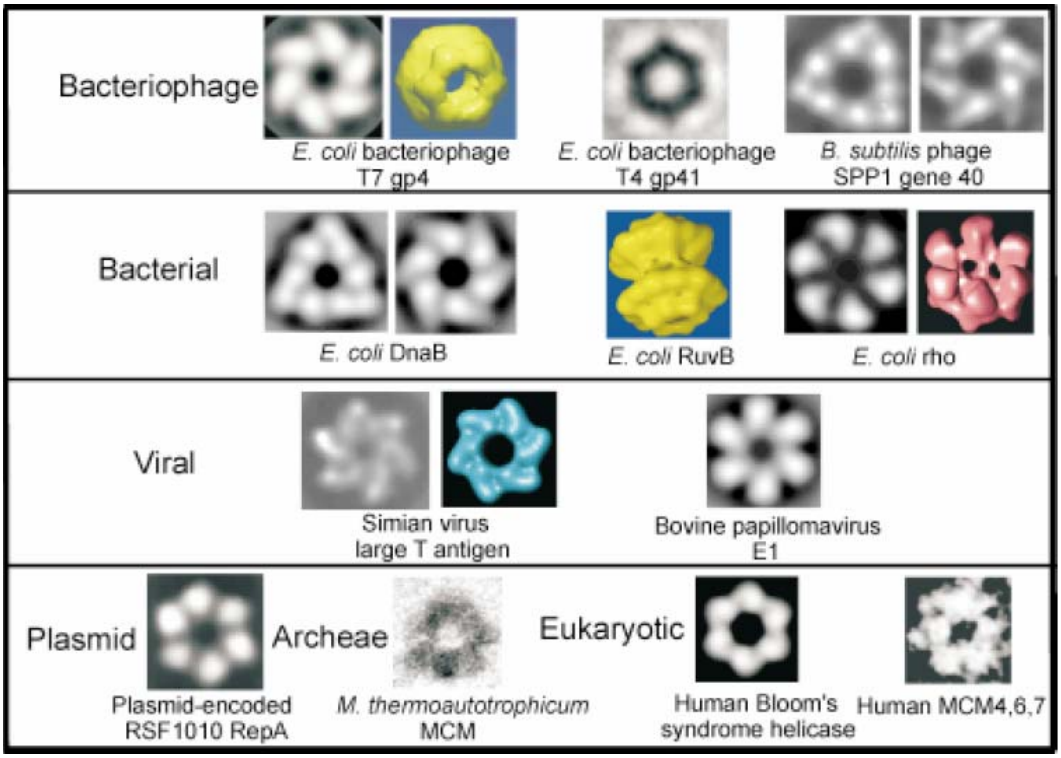

Figure 4.1: Electron microscopy images and reconstruction of hexameric helicases from a range of organisms (Patel *et al*, 2000)

All six hexameric subunits in the ring are essential for helicase activity, studies using a modified subunit of the helicase protein rho, show that modifying one rho protein subunit with 8-azido-ATP was enough to inactivate its ATPase activity (Stitt *et al*, 1994), however it maybe that not all subunits interact with DNA directly.

The hexameric ring structure of the helicase presents several possibilities for DNA binding. The DNA could in theory bind in the centre channel, on the outside of the ring or both. It is thought, primarily through FRET, crystal structure and EM work on the helicase T7gp4, that most DNA helicases bind DNA in the centre channel (Yu *et al*, 1996).

The mechanism by which DNA enters the central channel is not currently well understood, there are three proposed general models; (figure 4.2)

i) Ring opening model – In this model one of the subunit interfaces is disrupted, which allows the DNA to bind in the central channel of the open ring, before the subunit rejoins.

ii) Threading model – In this model one end of the linear DNA is threaded into the central channel.

iii) Disassembly model – In this model two or more subunit interfaces are disrupted, and the disassembled subunits reassemble around the DNA.

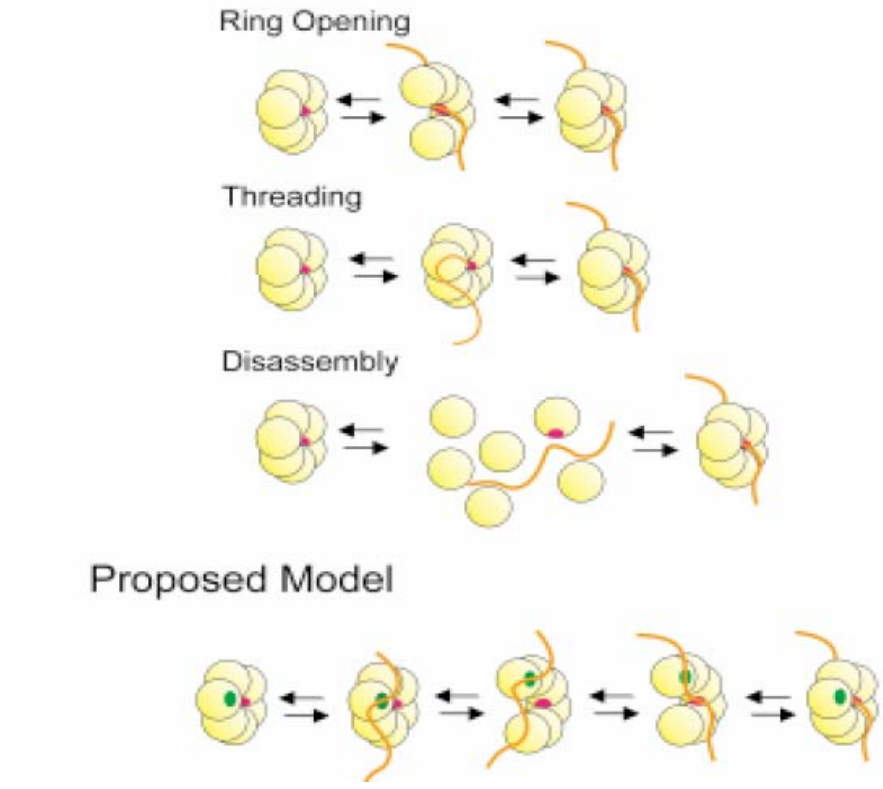

Figure 4.2: Three general models of helicase binging to DNA and a proposed model based on studies of T7 gp4 and rho protein helicase (Adapted from Patel *et al*, 2000)

There may be variation between helicases, but a facilitated model based on experimental evidence from the rho protein and T7 gp4 suggests the real situation is a combination of all these models in which, the DNA binds to the outside of the helicase causing the helicase to open up, DNA then threads into the hole before the ring closes. This interaction may require an assisting helper protein, as is the case with *E.coli* DnaB, which uses DnaC and DnaT to facilitate loading, and *Bacillus stearothermophilus* DnaB which is proposed to use DnaI as a helicase loader (Soultanas *et al*, 2002).

Sequence comparison between a wide range of helicases reveals the majority have a conserved sequence motif located on the RecA-like nucleotide-binding core, suggesting all helicases have this same core (Bird *et al*, 1998). Other than this region helicases have a highly varied structure with many non-homologous domains bound to the core. For example, the N-terminal domains of two *E.coli* helicases, DnaB and rho transcription termination factor have no sequence or structural homology, and the bacteriophage T7 gp4 protein contains a helicase domain and a primase domain within the same protein, whilst in *E.coli* this is performed by two different proteins, DnaB and DnaG respectively.

4.1.3 DnaB Helicase

The DnaB protein has been identified as the most important bacterial helicase, it is the main helicase associated with the replisome during bacterial DNA replication. *E.coli* DnaB protein is 52kDa in size and has been shown to be essential for both the initiation and elongation of DNA replication (Patal *et al*, 2000).

The DnaB protein can unwind duplex DNA without any accessory proteins, however it needs the addition of the DnaG primase protein to stimulate this

helicase activity (in some cases the helicase and primase role are carried out by the same protein). DnaB like most helicase is a hexameric ring, though in the absence of Mg^{2+} or nucleotides it has been shown to form trimers, with the hexameric structure returning upon addition of the salt (Bujalowski *et al*, 1998).

EM and AFM images have visualised both the hexameric and trimeric forms of DnaB, using a variety of NTP co-factors it was shown that the two different forms of the DnaB ring, one with a 3-fold symmetry and one with a 6-fold symmetry are both hexamers (figure 4.3). There were also rings identified in an intermediate state between these two, this suggests the transition between theses two states could be co-operative and that they may exist in equilibrium (Yu *et al*, 1996, Haroniti *et al,* 2004).

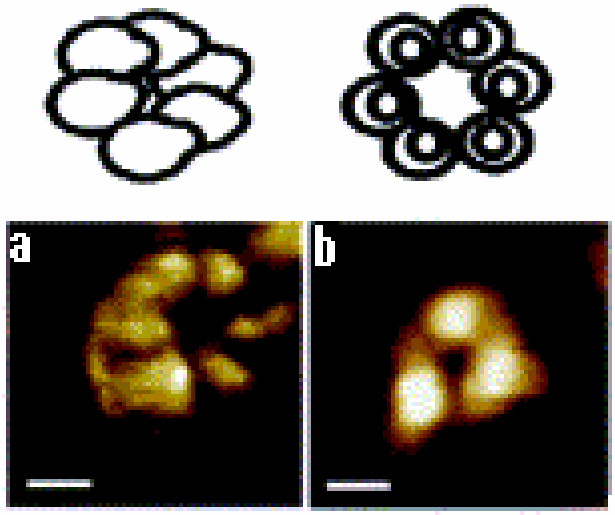

Figure 4.3: Topographical AFM image in air using carbon nanotube tips reveal 6-fold symmetric ring (left) and 3-fold symmetric rings (right) forms of DnaB. Schematic diagrams show positions of individual DnaB subunits. Scale bars represent 10nm. Adapted from Haroniti *et al,* 2004

Many of the mechanistic details of DnaB coupling the hydrolysis of ATP to the opening of dsDNA remain unclear, it has been shown ssDNA binds through the central channel and only one subunit of the hexamer efficiently cross-links with the ssDNA (Yu *et al*, 1996). FRET analysis has show that the DnaB helicase domain (C-terminus) faces dsDNA at a replication fork, while

the primase domain (N-terminal) would face away from this fork. The subunits in DnaB can exist in two very different conformations, giving rise to either symmetrical hexamers or a trimer of dimers. The difference between these two states involves both a major conformational change of the helicase domain and a large movement of the N-terminal domain. It is possible that such conformational changes are important in helicase activity and that they also play a role in the loading of DnaB on DNA (Yang *et al*, 2002).

Using chemical quenching techniques the kinetic step size of the DnaB helicase (the number of base-pairs unwound in a single catalytic step) was calculated as 1.4 base pairs. This low value indicates that the helicase unwinds a single base pair in a single catalytic step. Generally however the protein is a fast helicase that at 25ºC unwinds at approximately 150bp/s, this rate could increase at higher temperatures. However the ATP-enzyme has an increased dissociation rate, resulting in moderate unwinding processivity suggesting there are many binding and unbinding events of the helicase during DNA replication (Galleto *et al*, 2004).

4.1.4 DnaG Primase

The DnaG primase has been isolated in *Bacillus stearothermophilus* and *E.coli*; it is a 597 long amino acid protein with a molecular mass of 67 kDa. The primase is a single stranded DNA dependent RNA polymerase; it is responsible for synthesis of RNA primers on ssDNA templates. DnaG primase is composed of three domains; (figure 4.4) a small N-terminal DNA binding domain (that is 12kDa and has been crystallised), a larger central domain responsible for RNA synthesis, and a C-terminal domain that interacts with DnaB helicase (Loscha *et al*, 2004, Pan *et al,* 1999)

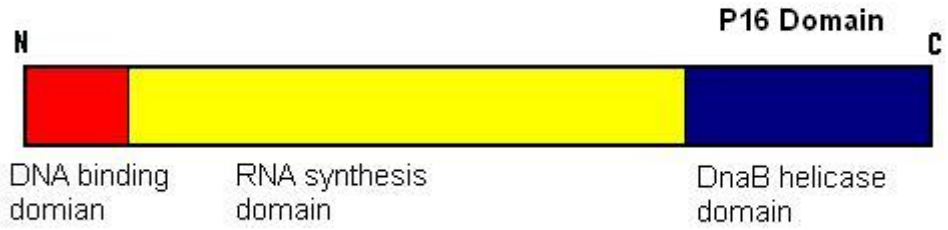

Figure 4.4: The main domains in the DnaG primase protein.

4.1.5 DnaBG Complex

DnaB, DnaG and DNA polymerase III form a dynamic protein complex at the replication fork so that the functions of all three enzymes are co-ordinated properly (Figure 4.5). DnaG interacts with DnaB which introduces it to the replication fork and activates its priming activity, DnaB is known to interact with the π subunit of DNA polymerase III (Haroniti *et al*, 2004, Pan *et al*,

1999). The interaction between the DnaB helicase and DnaG primase is needed repeatedly to regulate the cyclic synthesis of Okazaki fragments during lagging strand synthesis as well as continual synthesis on the leading strand (Tougu *et al*, 1996).

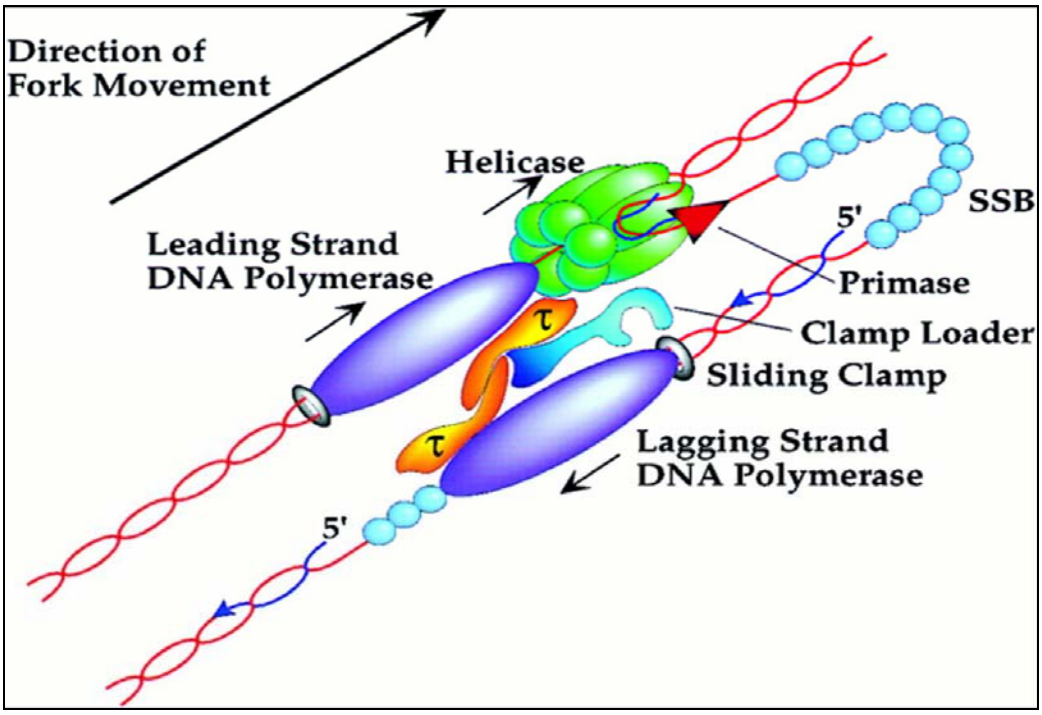

Figure 4.5: A schematic representation of the proposed end point of the primosomal cascade where the helicase-primase complex triggers the switch to polymerisation mode. The helicase and primase have formed a complex with DNA threaded though the central pore; the helicase is interacting with subunits of DNA polymerase III.

There are homologues of the *E.coli* DnaB and DnaG genes in *Bacillus stereothermophilius* in which, the enzymes form a tighter more stable complex that have been isolated by gel filtration and dissected using a range of biochemical techniques. A 16kDa C-terminal domain of DnaG (P16) has been identified as the region (see figure 4.4) that interacts with the interface of both the N- and C-terminal domains of DnaB. This interaction involves two or three primase molecules per helicase hexamer. The result of this interaction is

the stimulation of the ATPase and helicase activities of the helicase (Bird *et al*, 2000).

The DnaG interaction site on DnaB has been reported to reside on the surfaces of the N-teriminal (Chang *et al*, 2000) and C-terminal (Lu *et al*, 1996) as well as the flexible linker region that connects the two domains in *Salmonella typhmuirium* and *B.stearothermophilus* (Stordal *et al*, 1996).

Mutagenesis studies in *E.coli* and S*almonella typhmurium* have linked five key residues in the N-terminal domain to this interaction. The equivalent residues are conserved in *Bacillus stearothermophilus* DnaB (E15, Y88, I119, I125 and L138) (Bird *et al*, 1999). Another study proposes different distant residues on the C-terminal that may be involved, as two double DnaB mutants (D212A-D213A and K216A-K217A) where deficient in DnaG binding (Yu *et al*, 1996) the equivalent residues are not conserved in *B.stereothermophilus*. These results suggest that different regions residing on the N- and C- domains of DnaB are involved with its interaction with the primase.

In this chapter (based on the publication - DnaG interacts with a linker region that joins the N- and C-domains of DnaB and induces the formation of 3-fold symmetric rings. Jenny Thirlway, Ian J. Turner, Christopher T. Gibson, Laurence Gardiner, Kevin Brady, Stephanie Allen, Clive J. Roberts and Panos Soultanas. *Nucleic Acid Research,* 2004, Vol. 32, No.10 2977-2986) the interaction between the helicase and primase will be studied by AFM and classical biochemical techniques to investigate in detail the structural relationship between the helicase (DnaB) and primase (DnaG).

4.2. Method

4.2.1 Atomic Force Microscopy

AFM images were carried out in an air and liquid environment as described in section 2.1.1 and 2.1.2

All images were flattened and analysed as described in section 2.1

4.2.2 Protein Purification

Work carried out by Jenny Thirlway, Laurence Gardiner, Kevin Brady and Panos Soultanas, Centre of Biomolecular Sciences, University of Nottingham, University Park, Nottingham, NG7 2RD. Brief experimental details are given below.

DnaB and DnaG where overexpressed in BL21 *E.coli* and purified by a combination of Sepharose, MonoQ, Hi-Trap heparin and Superdex S-200 gel filtration chromatography as previously described (Bird *et al*, 2000). Proteins were >98% pure as assessed by SDS-PAGE and concentrations were determined spectrophotometrically.

4.2.3 BG Complex

The DnaB-DnaG complex was formed by mixing DnaB with a 6M excess of DnaG and separating unbound DnaG from the complexes by gel filtration through a superdex S200 gel filtration column (Amersham Pharmacia Biotech, Buckinghamshire, UK) in 50nM Tris pH 7.4 and 1mM EDTA.

Protein samples were diluted between 10 and 85 µg/ml to the values described in individual experiments in 50nM Tris pH 7.4, 1mM EDTA 2 mM of MgCl. Before being imaged by AFM (Section 2.1)

4.2.4 Complementary Techniques

Work carried out by Jenny Thirlway, Laurence Gardiner, Kevin Brady and Panos Soultanas, Centre of Biomolecular Sciences, University of Nottingham, University Park, Nottingham, NG7 2RD. Brief details of the experimental

conditions are given below. Further details can be found in Jenny Thirlways Docterate thesis, University of Nottingham

Site-directed mutagenesis

Site-directed mutagenesis was carried out by PCR, as described elsewhere (Soultanas *et al*, 2000), using appropriate mutagenic oligonucleotides, together with the forward (5'-GCAAGGAATGGTGCATGCAAGGAG-3') and reverse (5'-CTCGAGTGCGGCCGCAAGCTTGTC-3') cloning primers. All mutant genes were cloned as NdeI-HindIII fragments in pET22b (Novagen, North Ryde, Australia). All mutations as well as the absence of other spurious mutations were verified by sequencing.

Analytical gel filtration

Wild-type or mutant DnaB was mixed with DnaG in 0.5 ml TED [50 mM Tris pH 7.4, 1 mM EDTA, 1 mM dithiothreitol (DTT)] including 100, 250 or 500 mM NaCl and in a molar ratio of 0.5 mM DnaB (referring to hexamer) to 3 mM DnaG (referring to monomer). The mixtures were equilibrated on ice for 15 min prior to loading onto a Superdex S-200 10/30 (Amersham Pharmacia Biotech) gel filtration column, equilibrated in the same buffer (TED plus 100, 250 or 500 mM NaCl, as appropriate). Gel filtration was carried out at 0.5 ml/min and 0.5 ml fractions were collected. Samples from the peaks were analysed by SDS±PAGE and gels were stained by silver staining or a Coomassie BioSafe stain (Bio-Rad, Hercules, CA).

ATPase assays

The DNA-independent ATPase activity of wild-type and mutant DnaB proteins was assayed by monitoring NADH oxidation, as described before. Briefly, reactions were carried out in 20 mM Tris pH 7.5, 50 mM NaCl, 10 mM $MgCl_2$, 5 mM DTT and 100 nM DnaB (referring to hexamer), in the presence or absence of 400 nM DnaG, at varying ATP concentrations in a total volume of 1 ml. The reaction was initiated by addition of the helicase (or helicase-primase mixture). All the ATPase reaction profiles shown represent the averages of three independent experiments. The *B.stearothermophilus*

DnaB protein does not exhibit first order Michaelis-Menten kinetics. Instead, the ATPase profile exhibits a characteristic curve attributed to cooperative allosteric effects within the hexame. No quantitative parameters can be derived and our comparisons of ATPase activities are merely qualitative.

Helicase assays

Helicase assays were carried out as described elsewhere (Soultanas *et al*, 2000).

Yeast two-hybrid (Y2H) experiments

Y2H experiments were carried out using the MATCHMAKER Two-Hybrid system 2 (Clontech, Mountain View, CA). The dnaG gene was cloned as an NcoI±XhoI fragment into pACT2, while DnaB, P17 (N-terminal domain of DnaB) and P33 (C-terminal domain of DnaB) were cloned as NcoI-XhoI fragments into the NcoI-SalI sites of pAS2-1. The positive control is based upon the p53-SV40 T antigen interaction. It has the pVA3-1 plasmid carrying the GAL4 DNA binding domain fused to murine p53 and a trp nutritional selection marker, together with the pTD1 plasmid carrying the GAL4 activation domain fused to the SV40 large T antigen and a leu nutritional selection marker. The negative control shows that there is no interaction between DnaB and SV40 large T antigen, using the pAS2-1-DnaB and pTD1 plasmids described above. All plasmids were transformed into yeast by electroporation and the detection of positive interactions was carried out by the agarose overlay method.

Limited proteolysis

Limited proteolysis was carried out in 50 mM Tris pH 7.4, 2 mM EDTA, 100 mM NaCl, 10% (v/v) glycerol and 1 mM DTT, using a molar ratio of 1:5000 for papain:DnaB and 1:100 for trypsin:DnaB, in the presence or absence of a large excess of P16 for 25 min at 37°C. DnaB and P16 mixtures were incubated for 15 min on ice prior to the addition of the protease. Samples were

removed at 5 min intervals and quenched by addition of gel loading buffer [50 mM Tris pH 6.8, 100 mM DTT, 2% (w/v) SDS, 10% glycerol, 0.1% bromophenol blue] and heating at 94°C for 5 min. Protein fragments were resolved by SDS-PAGE through a 15% polyacrylamide gel and visualized by Coomassie staining.

4.3. Results

4.3.1 DnaB Helicase

Previous work imaging the DnaB protein on the EM and the AFM using a combination of standard and carbon nanotube coated tips revealed DnaB forms a population of polymorphic rings with a mixture of 3-fold, 6-fold and open-ring structures, as well as smaller non-circular structures representing various oligomeric forms of dissociated DnaB monomers (Haroniti *et al*, 2004).

In this experiment DnaB was imaged in air at a concentration of 30 μg/ml in the presence of $MgCl_2$ and showed a similar population distribution to the previous study (figure 4.6). The field view reveals a diversity of the population with 3-fold, 6-fold symmetrical rings and other circular structures present, zoomed in highlights show detailed representative examples of the 3-fold and 6-fold symmetrical rings.

The population is a mixture of 3-fold, 6-fold and intermediate structures many of which are difficult to identify possibly due to the way they are orientated onto the mica surface, the 6-fold symmetric rings are the most abundant of the different species present (12:1 ratio of 6-fold to 3-fold symmetric rings). The DnaB dimers that make up the 3-fold structures were measured and show dimensions of 14.5 ± 2.5 nm in the X axis and 14.5 ± 2.8nm in the Y axis. The subunits of the 6-fold rings where not imaged to a high enough resolution for the dimensions of individual subunits to be measured accurately.

This is consistent with a previously recorded diameter of approximately 15nm observed by electron microscopy of negatively stained DnaB (Yu *et al*, 1996, Yang *et al*, 2002) and an improvement on the value of 22nm obtained through previous AFM images of DnaB (Haroniti *et al*, 2004). This difference could be explained by the use of prototype carbon nanotubes tips in the previous study or difference in the lateral force applied by the tips causing the proteins to become deformed.

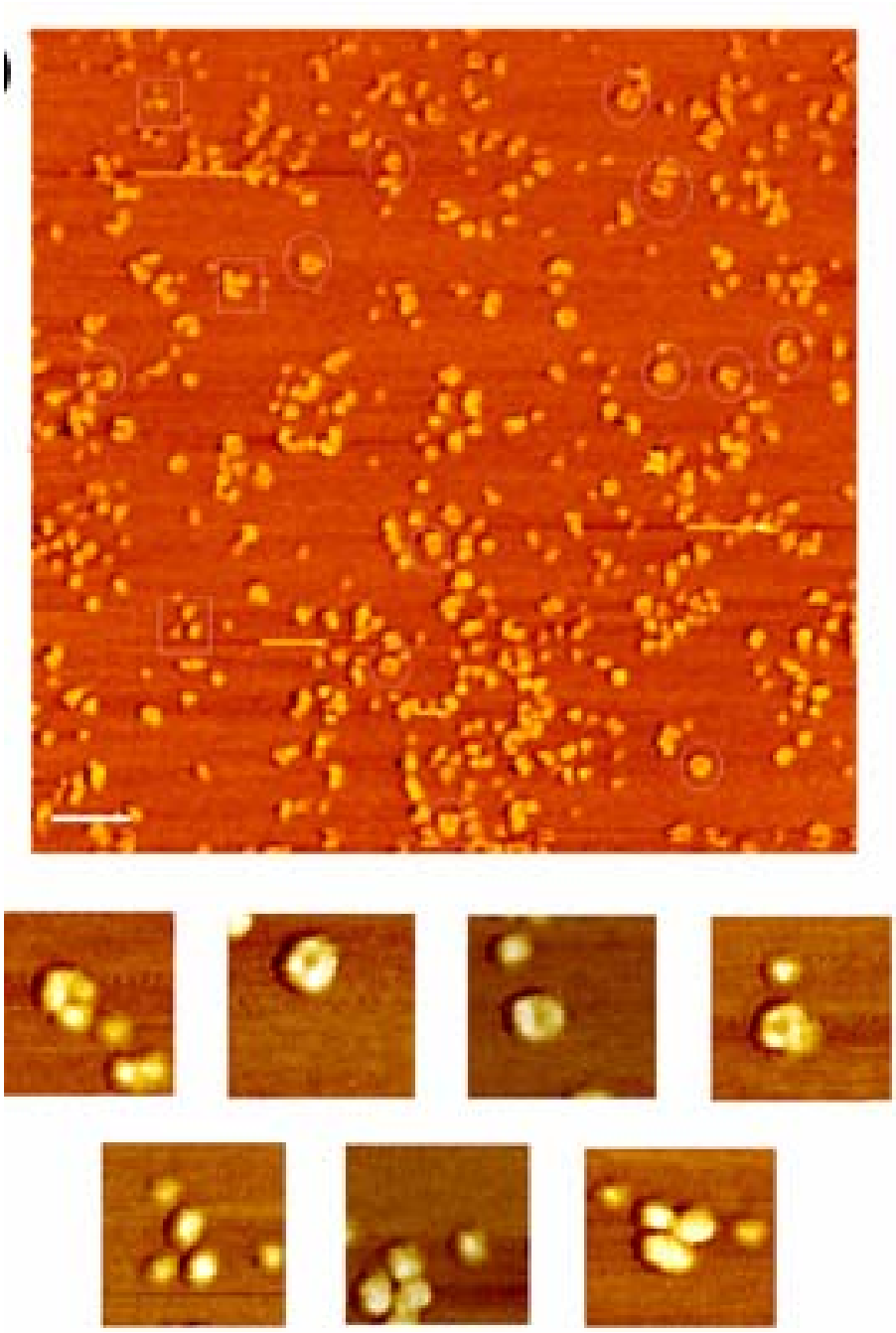

Figure 4.6: Topographical AFM image in air of *Bacillus stearothermophilus* DnaB protein. A representative field view showing the complete population, with 6-fold structures (circles) and 3-fold symmetric rings (squares) highlighted. Scale bar represent 100nm. Zoomed in highlights (50nm) show the detail of 3-fold and 6-fold symmetric rings.

4.3.2 DnaG primase

AFM images of DnaG at a concentration of 60 µg/ml show it exists as a monomeric population (figure 4.7) the resolution of the images is not enough to identify the domains of DnaG, especially the P16 domain which has been shown to be critical in DnaB binding. The protein appears to be oblong in shape with average dimensions of 10.6 ± 3.0nm in the X dimension and 15.8 ± 2.9nm in the Y dimension of 20 proteins, because of the variable orientations of the protein on the surface, the longest dimension was taking to be the Y in all cases.

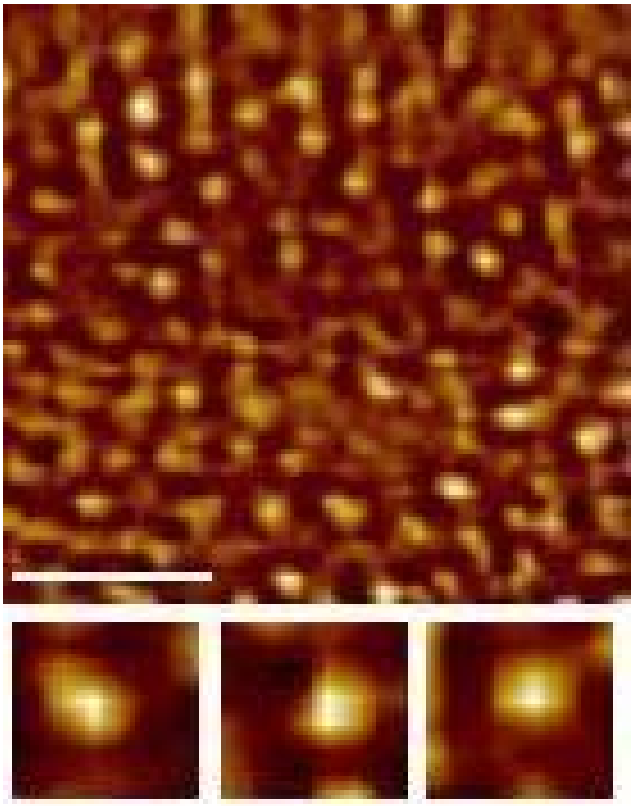

Figure 4.7: A topographical field view in air of *Bacillus stearothermophilus* DnaG primase protein. A field view reveals a largely monomeric population. Scale bar represents 100nm. Zoomed in highlights (30nm) show the detail of individual monomers

4.3.3 DnaBG

AFM images of DnaB-DnaG complexes at a concentration of 30 µg/ml (the complexes are not simple mixes of the DnaB and DnaG proteins but complexes purified by gel filtration experiments) show that the complex has adopted the 3-fold symmetric rings structure (figure 4.8). Although there are other structures evident (which may be dissociated DnaB and DnaG) there is no evidence of any 6-fold symmetric rings in the sample. This suggests that the DnaG causes some structural change from 6-fold to 3-fold symmetric rings when it binds.

Size analysis shows that the dimensions of the globular sub units of the rings are 26.1 ± 5.0 nm in the X dimension and 25.1 ± 5.0nm in the Y axis. Although the spatial resolution is not high enough to resolve individual subunits within the complex, this data indicates that the dimensions of the complex are approximately equal to the dimensions of the DnaB dimer alone plus the dimensions of the globular DnaG monomer (figure 4.9).

Collectively size data suggests that the DnaB-DnaG complex adopts a 3-fold symmetric structure (almost 100%), whilst DnaB alone adopts a variety of ring conformations with the 6-fold symmetrical rings clearly over-represented in this mixed population of structures (~75%). Whether DnaG binds only to 3-fold symmetric DnaB rings or also to 6-fold rings, converting them to 3-fold rings, is not known. However, if DnaG were to only bind to 3-fold symmetric rings some 6-fold rings would be expected to be visualised in the population.

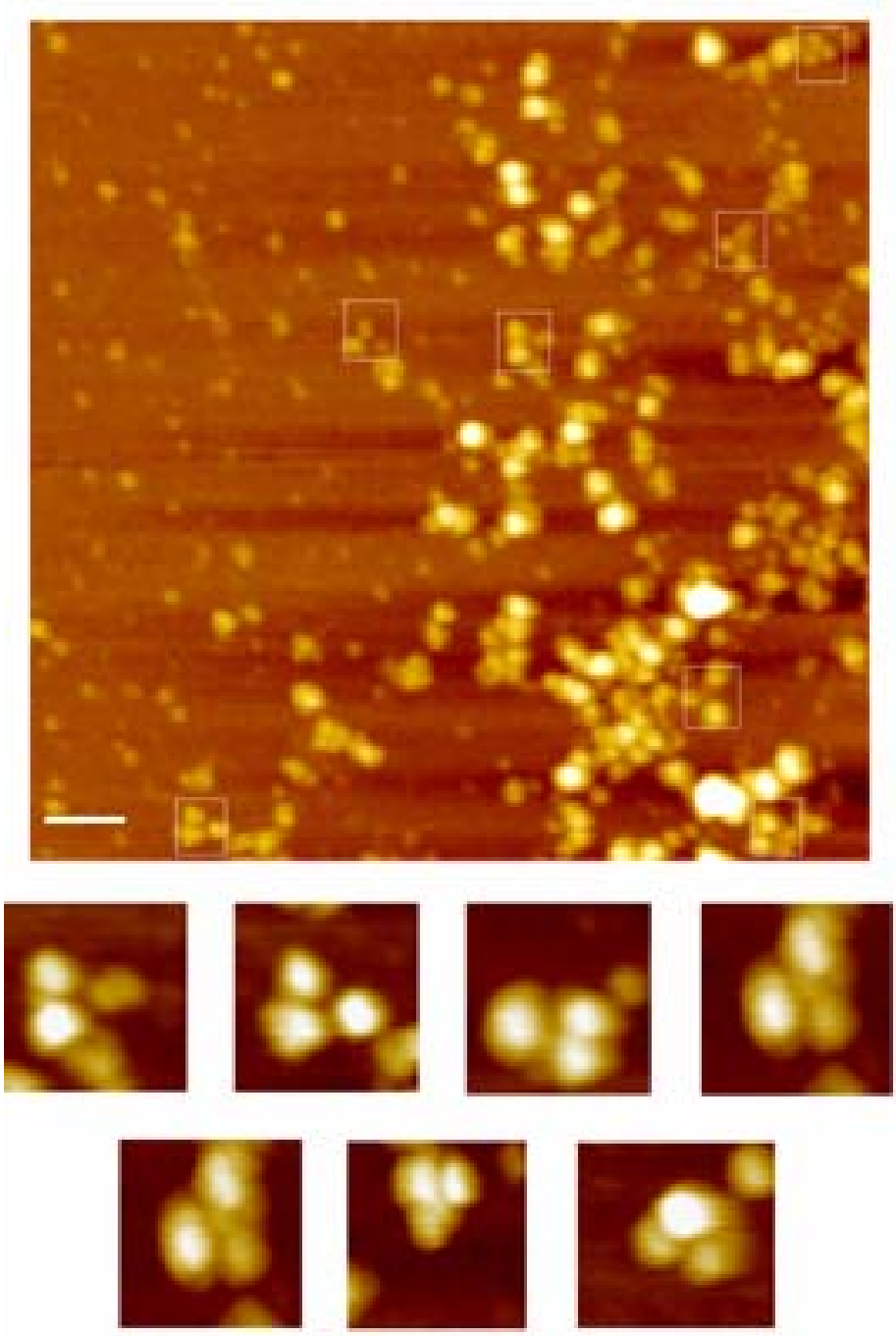

Figure 4.8: Topographical AFM image in air of *Bacillus stearothermophilus* DnaB-DnaG complex. A representative field view showing the complete population, with 3-fold symmetric rings highlighted by squares. Scale bar represent 100nm. Zoomed in highlights (50nm) show the detail of representative 3-fold structures.

4.3.4 Subpopulations

The size data can be interpreted as three molecules of DnaG bound around the outside perimeter of a 3-fold symmetric DnaB ring ($DnaB_6$-$DnaG_3$). However more detailed analysis of the ring complexes show that although the majority appear to represent the $DnaB_6$-$DnaG_3$ conformation, a few complexes represent $DnaB_6$-$DnaG_2$ and $DnaB_6$-$DnaG_1$ complexes with only one, or two molecules of DnaG bound to the DnaB respectively (figure 4.9).

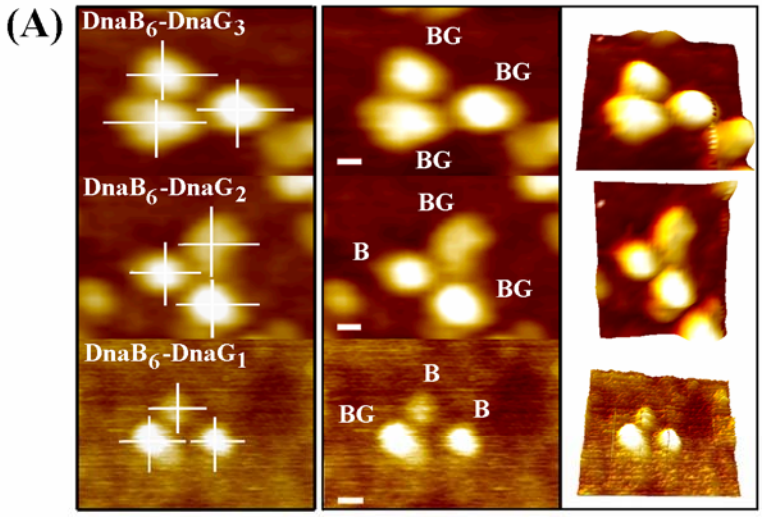

(B)

	X	Y
DnaB		
Mean (nm)	14.50	14.52
s.d.	2.48	2.75
n	48	48
DnaG		
Mean (nm)	10.55	15.77
s.d.	3.01	2.91
n	20	20
$DnaB_6$-$DnaG_3$		
Mean (nm)	26.11	25.14
s.d.	5.00	4.96
n	18	18

	X_{BG}	Y_{BG}	X_B	Y_B
$DnaB_6$-$DnaG_2$				
Mean (nm)	24.40	24.90	20.00	19.80
s.d.	4.67	3.11	0.00	0.45
n	10	10	5	5
$DnaB_6$-$DnaG_1$				
Mean (nm)	21.50	26.50	16.69	16.38
s.d.	6.56	7.19	2.58	2.50
n	4	4	8	8

Figure 4.9: A) Representative 3-fold symmetric rings showing $DnaB_6$-$DnaG_3$, $DnaB_6$-$DnaG_2$ and $DnaB_6$-$DnaG_1$, as indicated. Each of the subunits was measured individually in the X and Y direction. Scale bars represent 10nm. B indicates a DnaB subunit alone; BG indicates a DnaB-DnaG subunit. B) The data from analysis above and previously mentioned experiments. *n* stands for sample size whilst s.d stands for standard deviation. Sizes of the individual subunit are shown by XB and YB for DnaB subunits and XBG and YBG for DnaB-DnaG subunits.

Analysis of nine such complexes (from different AFM image experiments) identified five were potentially $DnaB_6$-$DnaG_2$ and four were potentially

$DnaB_6$-$DnaG_1$. The small number of these populations makes it only possible to speculate if stoichiometries other than $DnaB_6$-$DnaG_3$ exist *in vivo* and their potential biological relevance. Though such subpopulations hint at sequential method of adding of the DnaG to the DnaB and some degree of cooperatively towards the $DnaB_6$-$DnaG_3$ state as the $DnaB_6$-$DnaG_2$ and $DnaB_6$-$DnaG_1$ populations are under represented.

4.4. Complementary Work

4.4.1 Mutations in the N-Domain and interdomain linker region of DnaB

5 previously identified amino acids (page 53) are thought to be essential in the helicase-primase interaction where positioned on the *B.stereothermophilius* DnaB protein. The residues E15, Y88 and I119 are conserved between the *E.coli* and *Bacillus* DnaB proteins, they are all located together in the N-domain forming a potential DnaG interacting pocket. Ill9 is the last residue of a helix at the C-terminal of the N-domain. The residues I125 and L138 are located in the flexible linker region that joins the N-domain with the C-domain (figure 4.10).

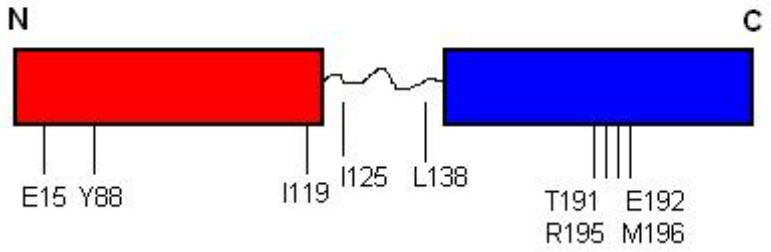

Figure 4.10: A schematic diagram of DnaB highlight the residues thought to be involved in its interaction with the primase

Mutations of these complexes where investigated by gel filtration of mutant DnaB-DnaG complexes to examine the effects in ATPase and helicase stimulation by DnaG *in vitro*.

E15A and Y88A point mutations both formed stable complexes under low ionic strength; these complexes were functional, since the ATPase and helicase activities of both mutants were stimulated by DnaG. At high ionic strength, 500mM NaCl the Y88A mutant could not form a stable complex with DnaG whilst the wild type DnaB and E15A mutant could.

The E15A-Y88A double mutant behaved like the Y88A mutant. Forming stable complexes and interacting with DnaG, stimulating the ATPase and

Helicase at low ionic strengths but not high ones. The data suggests that Y88 is involved in the interaction of DnaB with DnaG in a subtle manner, whereas E15 is not.

The ability of I119A and I125A point mutations to form stable complexes with DnaG was impaired at low and high ionic strengths. This was also evident by the inability of DnaG to stimulate the ATPase or helicase activities. The L138A point mutation was unaffected at low and high ionic concentrations and formed stable complexes and were stimulated by DnaG in there ATPase and helicase activities.

Overall the data indicates that I119 and I125 contribute directly to the formation of the helicase-primase complex, whereas E15 and Y88 may mediate allosteric effects of other replisomal proteins on the helicase-primase complex.

4.4.2 Mutations in the C-domain of DnaB

Previous studies concluded that the D212A-D213A and K216A-K217A double mutants in *E.coli* DnaB were defective in DnaG binding and priming (Yu *et al*, 1996). The equivalent residues in *B.stereothermophilus* DnaB (T191, E192, R195, M196) are located in the C-domain and are situated on the outer periphery of the ring forming a potential reaction interface with the primase. Double mutants of T191A-E192A and R195A-M196A were constructed and tested for their interaction with DnaG in a manner similar to the N-domain mutaions, described above.

Both mutants behaved just like the wild-type DnaB protein, they formed stable complexes with DnaG under high and low ionic conditions and in that there helicase and ATPase activities were stimulated by DnaG. It is concluded that these residues are not involved in the primase interaction. However, the amino acid sequence homology between *E.coli* and *B.steareothermophilus* is not good in this region and other amino acids nearby maybe involved instead.

In order to test this possibility and also to see if the N- and C- domains interact transiently the yeast two-hybrid assay was utilised.

4.4.3 The N- and C-domains of DnaB do not interact with DnaG

DnaB from *Bacillus steareothermophilus* has a two domain structure, the two domains have been cloned, overexpressed and purified and none of the domains either alone or in a mixture formed a tight complex with DnaG. However there is a possibility that DnaG interacts transiently with the N- and C-domains of DnaB. These interactions were investigated by Y2H, the interaction between DnaB and DnaG revealed a strong signal but neither the N- or C-domains of DnaB revealed significant signals to suggest an interaction with DnaG. Any potential primase interacting residues on either the N- or C-domain of DnaB do not contribute the main binding energy of this interaction. The direct involvement of the linker region was confirmed by limited proteolysis protection studies.

4.4.4 Primase-mediated protection of the linker region from limited proteolysis

The domain organisation of *B.stearothermophilus* DnaG is similar to that of *E.coli* DnaG. A 16kDa C-terminal domain (P16) is sufficient to bind stably to DnaB and stimulate its ATPase and helicase activities. If P16 binds to the flexible linker region of DnaB then it should protect it from proteolytic cleavage. Cleavage with trypsin showed that P16 could be cleaved into a smaller fragment $P16_N$. Protection of the linker region in the presence of P16 was evident in the first 10mins of the assay, but then P16 was cleaved into a smaller fragment and protection was lost. This data implies indirectly that P16 itself comprises two sub-domains with only its C-terminal subdomain interacting with DnaB. This subdomain is sensitive to multiple trypsin cleavages and its extensive digestion with time abolishes the interaction with DnaB.

Papain produced clearer results as it did not digest P16 and cleaved at a defined site within the linker region. In the presence of P16 this site was protected from papain cleavage as judged by the resistance of the fragment containing it to treatment and the disappearance of it and appearance of two fragments in its absence. Overall, the data presents direct evidence that P16 binds across the flexible linker region between the N- and C-terminal domains of DnaB. Furthermore, P16 itself comprises of two subdomains with its C-terminal subdomain being responsible for the interaction with DnaB.

4.5. Discussion

The helicase-primase interaction is a vital step in DNA replication. The helicase associates with the primase introducing it to the replication fork and activating its priming activity. The primase initiates DNA synthesis by priming the DNA for DNA polymerase III. The interaction between the main bacterial helicase DnaB and its primase DnaG is a very important one in bacterial replication. To date little is known about the structural details of this interaction.

AFM images of the helicase DnaB show a mixture of 3-fold and 6-fold symmetric rings as well as intermediates. Both types of structure are known to exist in the presence and absence of nucleotides (Yang *et al*, 2002) and have been previously visualised using AFM (Haranoiti *et al*, 2004). It could be that these two populations have distinct structural roles *in vivo* with the two populations existing in an equilibrium. The presence of intermediates supports the idea (that previous studies on the electron microscope have seen) that there is a transition from one form to the other (Yu *et al*, 1996).

Topographical AFM images and size data of DnaB-DnaG complexes suggest that the population distribution of DnaB switches from a mixture of 3-fold and 6-fold symmetric ring upon the binding of the DnaG to primarily a 3-fold symmetric ring population. Presuming this change is DnaG induced, and knowing that the helicase-primase interaction involves two or three primase molecules per helicase hexamer (Bird *et al*, 2000), it is thought that the complexes are arranged in a trimer of dimer structure with one molecules of DnaG bound across two molecules of DnaB (figure 4.11).

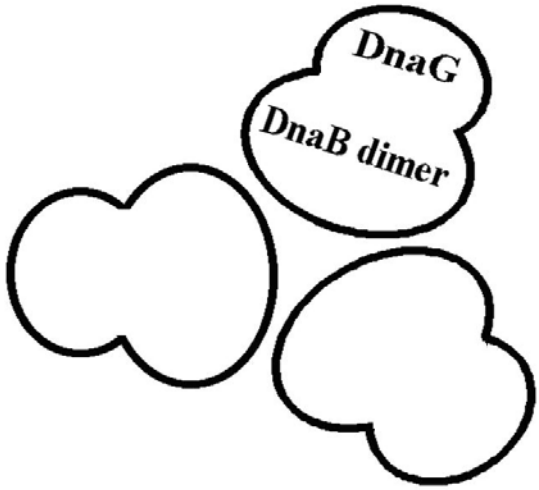

Figure 4.11: A schematic model showing the 3-fold symmetric architecture of the helicase-primase complex. The six monomers of the helicase adopt a 3-fold (trimer of dimers) geometry with three primase molecules bound around periphery of the ring.

The AFM images are not at a high enough resolution to reveal structural details of the individual protein molecules, however size data shows that the size of a BG complex subunit is equal to the size of a DnaB dimer plus a DnaG monomer, this supports the idea that DnaG is indeed bound across two molecules of DnaB. As well the fully saturated $DnaB_6$-$DnaG_3$ complexes a small number of $DnaB_6$-$DnaG_2$ and $DnaB_6$-$DnaG_1$ complexes where also detected, the biological relevance of these subpopulations is unknown but it supports a sequential mechanism of loading of the DnaG onto the DnaB.

Mutagenesis data suggests that the primase primarily interacts with the flexible linker region connecting the N- and C- terminal domains of the helicase. Residues such as Y88 that have a minor effect on binding and are present on the N-domain are likely to modulate subtle functional aspects of the interaction rather than provide the main binding energy of the binding.

It can be said that based on the data from these experiments that the DnaB-interacting p16 domain of DnaG (Tongu *et al,* 1996, Bird *et al,* 2000) interacts with the linker region between the N- and C- domains of either the same DnaB monomer or adjacent monomers in the same dimer. The orientation of the rest of the DnaG molecule is unknown, however the most likely postion is that its N-terminal domain containing the zinc-binding and

polymerisation domains is in the vicinity of the N-terminal domains of the DnaB ring, where it is ideally located to interact with the ssDNA as it emerges from the ring of the forward moving helicase. Whether the primase active site faces outwards from the central hole, as is the case in T7 gp4 helicase-primase or inwards towards the central hole, as suggested for the *E.coli* DnaG, is not clear.

Electron microscopy studies of the *E.coli* DnaB protein (Yang *et al*, 1998) support this idea by revealing there are dynamic interactions between the N- and C-domains around the ring, with the N-domain of alternating monomers interacting with the C-domain of neighbouring monomers (Figure 4.12a). However it is not clear if the primase interacts across the flexible linker region within the N- and C- domains of the same DnaB monomer or alternatively across the N- and C-domains of neighbouring monomers, both orientations can be accommodated in the model (Figure 4.12b).

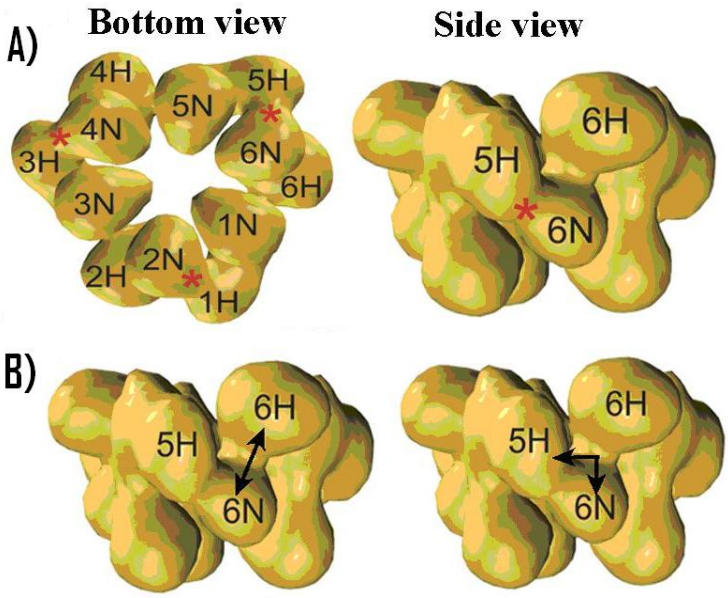

Figure 4.12: A) The proposed architecture of the 3-fold hexameric *E.coli* DnaB ring, viewed along the 3-fold symmetry axis (bottom view) and perpendicular to the axis (side view), The N- and C- (helicase) domains of adjacent monomers that constitute the three dimers are labelled and the interacting domains are highlighted by red asterisks. B) Side views of the 3-fold symmetric ring. Double arrows show the two possible ways that a molecule of DnaG could interact with one of the DnaB dimers. It could interact with one subunit (6N-linker-6H) or both subunits (6N-linker-5H) (from Thirlway *et al*, 2004)

4.6. Recent Advances

Recent work using NMR and crystal structures have identified the C-terminal, DnaB interacting domain (P16) of DnaG in both *E.coli* and *B.sterothermophilus* (Oakeley *et al*, 2005; Syson *et al*, 2005). These studies using NMR and crystal structures analysed the helicase interaction domain of the primase DnaG and identified two helical subdomains, C1 and C2 which, where both shown to have limited interaction. The C1 domain was shown to have a strong structural homology to the N-domain of DnaB from *E.coli* (there is a 44% sequence identity between *E.coli* and *B.stearothermophilus* DnaB proteins so it is likely that this structural homology will be retained in *B.stearothermophilus*). It has also been shown that the C2 domain is sufficient to mediate structurally the interaction with DnaB, but is not sufficient to stimulate the functional effects of the full length P16, therefore the C1 domain is important for the stimulation of DnaB ATPase activity.

The new structural data and similarities between the C1 subdomain of DnaG and the N-terminal domain of DnaB when combined with the model generated from AFM data (figure 4.12) suggest a plausible explanation for the molecular basis of the structural changes imposed on DnaB by the binding of the primase. The surface of the N-terminal domain of DnaB is acidic whilst P16 is primarily bipolar. This makes it likely that it acts as a spacer between the N-terminal and the helicase domains (C-terminal) of adjacent DnaB molecules in the 3-fold symmetry form of the hexamer (which, is known to predominantly occur when DnaG is bound, figure 4.8). It could be that a primase molecule C2 subdomain of P16 interacts with the linker region of a DnaB monomer whilst the C1 subdomain displaces the N-domain of the DnaB monomer (interacting with such residues as Y88) whilst maintaining the interaction with the C-domain which is necessary to preserve the 3-fold symmetry of the ring (Soultanas, 2005, Syson *et al*, 2005).

This data has lead to an improvement of the AFM model (figure 4.13) where the DnaG binding stabilises DnaB in its 3-fold symmetric conformation, leading to the shift in equilibrium in favour of 3-fold symmetric rings, (as seen by the lack of 6-fold symmetric rings in the DnaB-DnaG population, figure 4.8). However the precise molecular details that underpin this interaction will await the co-crystal structure of the helicase-primase complex itself

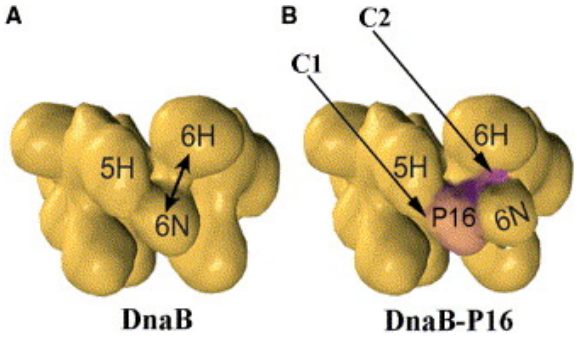

Figure 4.13: A model for DnaB-P16 interaction. A) The 3-fold symmetric ring of hexameric DnaB showing the N-domain of one monomer (6N) interacting with the C-domain (5H) of the adjacent monomer. B) In the P16-DnaB complex, the P16 protein (purple) interacts with the linker region that connects the N-terminal (6N) and C-terminal (5H) via its C2 domain. P16 C1 domain displaces 6N while at he same time maintaining the interaction with 5H that are essential to preserve the 3-fold symmetric ring in the helicase-primase complex

This new data also raises doubts upon the origin of helicase-primase genes, previous studies have identified a common origin for all the one component helicase-primase systems. It was thought that the system arose through fusion of ancestral helicase primase genes or by duplication of bifuntional helicase-primase gene followed by divergence with one gene retaining the primase and one the helicase activity. The homology between the C-terminal of DnaG and the N-terminal of DnaB suggests an alternative scenario (figure 4.14) where the gene duplication only applies to the linker region connecting the helicase and primase domains, followed by separation leaving one copy at the c-terminal of DnaG and one copy at the N-terminal of DnaB. Further sequence analysis of helicase and primase genes in other organisms may shed light on the origins of the helicase and primase genes.

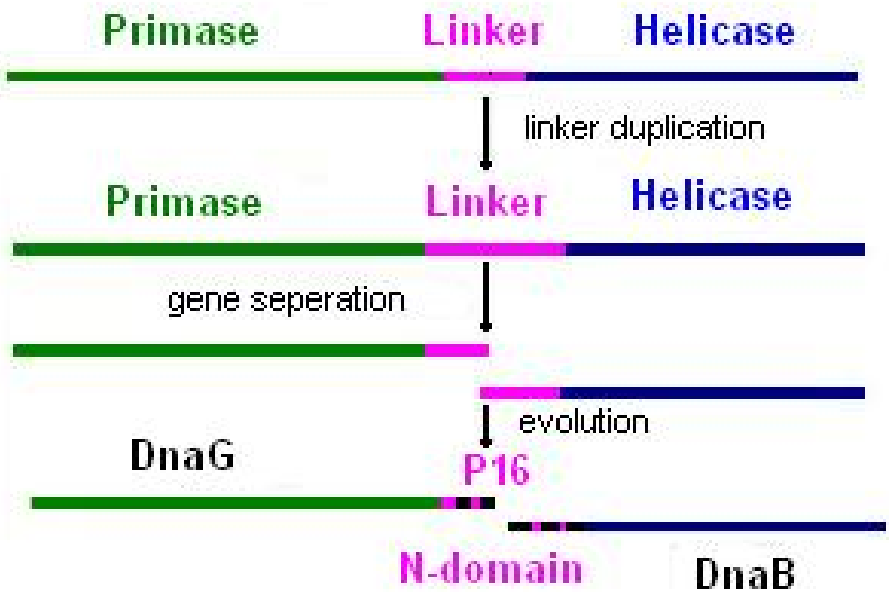

Figure 4.14: Evolution of separate helicase and primase genes. Schematic diagram showing the theoretical evolution of separate helicase and primase genes from a single ancestor gene. Adapted from Soultanas, 2005

5.What is the role of DnaD in the *Bacillus subtilis* Primosome?

5.1. Introduction

The DnaD gene of *Bacillus subtilis* (like many of the genes involved in the organism's DNA replication) was first identified in 1968 (as was the DnaB primosomal protein) through the isolation of a thermosensitive mutant. The mutant *dnaD23* affected the initiation of chromosome replication at a restrictive temperature, a temperature at which the bacteria displayed the mutant phenotype (Gross *et al* 1968) and lagging strand synthesis at the permissive temperature, a temperature at which mutants display the normal phenotype (Alonso *et al* 1988) both suggesting that DnaD is an important component of the *B.subtilis* primosome.

The *dnaD* gene was first mapped to a 104kb segment of the *B.subtilis* chromosome containing the *trp* operon that was cloned in a yeast artificial chromosome (Azevedo *et al*, 1993) and judged by its ability to transform *dnaD23* (Mael and Kasmata). The gene was sequenced (Bruand *et al*, 1995) using two factor transformation crosses through the insertion of the plasmid pSGMU2 with a chloramphenicol resistance (Cm^R) gene into the previously identified 104kb segment at various points. The mutants were then transformed with chromosomal DNA; transformants were measured by replica plating giving the genetic linkage value between the *dnaD* gene and the Cm^R markers.

dnaD was identified to a region which was used to construct a DNA library that was tested by it ability to transform the mutant *dnaD23*. The *dnaD* gene was found to be a 696bp long and encode a protein of 232 amino acids in length. The protein has a molecular mass of 27.4904 kDa and an isoelectric point of 7.174 (Bruand *et al*, 1995) No known homologues of DnaD have been found so far in *E.coli* despite the extensive studies of DNA replication in this organism. However DnaD is conserved among low G+C content gram-

positive bacteria including *Listeria*, *Staphylococcus*, *Enterococcus*, *Lactobacillu*s, *Streptococcus* and *Lacyococcus* spp. (Gross *et al*, 1968).

The essential role of DnaD was shown by point mutation studies in the *dnaD* gene of *Staphylococcus areus* (Kurokawa *et al* 2004). Through the identification of two temperature sensitive mutants, it was shown that DnaD protein is not only essential for the initiation of replication, as there was no replication at the non permissive temperature, but also to avoid blockage of the replication fork because replication that was started at permissive temperature ceased at replication forks at the non-permissive temperature. It was also suggested that the DnaD protein could be involved in DNA repair because both mutants had sensitivity to mitomycin C a drug that induces DNA damage.

It has been shown in *B.subtilis* that DnaD has an essential role in the two main pathways for loading the helicase and primase onto DNA (Bruand *et al,* 2001), one initiated at the *ori*C by DnaA and the other initiated at stalled replication forks and D-loops by PriA. DnaD as well as DnaB and DnaI have roles in these pathways which have been identified through mutation studies (figure 5.1). DnaD interacts with DnaA at the *oriC* (Ishigo-oka *et al,* 2001) suggesting that DnaD acts at an early stage of the primosomal cascade, presuming DnaD interacts in a similar way at PriA then it would act straight after the protein. There is also a third pathway for replication restart at stalled forks that has been seen in pUB110 mutants lacking *oriC* and PriA (Viret and Alonso, 1998) as these mutant cells are still viable though inefficient. DnaD is important in this third pathway because DnaD mutants of the cells are not viable.

Although DnaD has an essential role in the primosomal cascade at both the *oriC* and PriA the exact nature of its role is not understood. Most of the information about DnaD has been learned by its interaction with other proteins. It was shown that not only does DnaD protein interact with other DnaD molecules but that it also interacts with DnaA, the initiator of the primosomal cascade, suggesting an interaction between DnaD and DnaA is

important for replication initiation (Ishigo-oka *et al*, 2001). By creating a series of deletion mutants and carrying out the yeast two-hybrid assay it was shown that the amino terminal of DnaD is required for DnaD-DnaD binding and that an internal region of DnaD is required for interaction with DnaA (Figure 5.2).

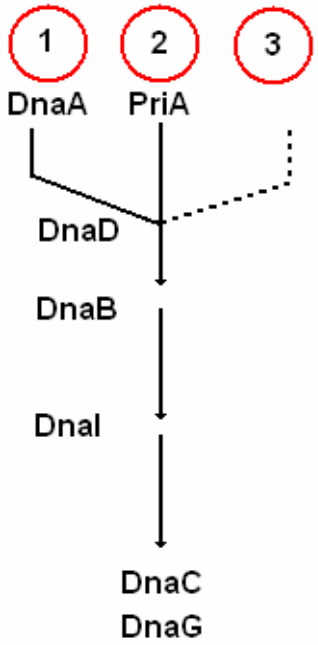

Figure 5.1: Schematic diagram showing the proposed different pathways for loading the DnaC helicase and DnaG Primase in *B.subtilis*. Numbers represents entry points for the different pathways. 1- DnaA dependent pathways acting at *oriC*, 2- PriA dependent pathways acting at stalled replication forks, 3- DnaD dependent pathways acting at any substrate containing ssDNA (Modified from Bruand *et al,* 2001).

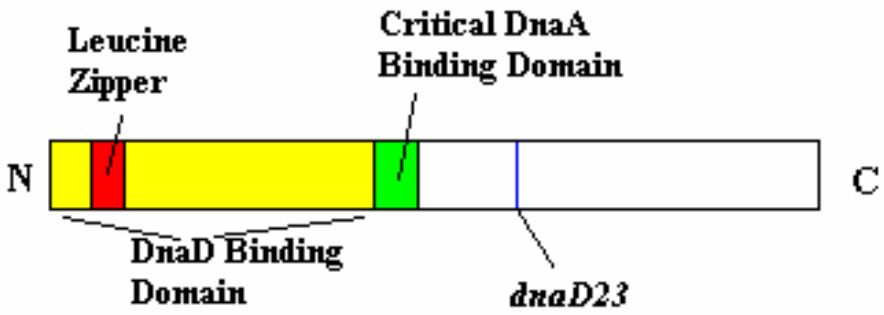

Figure 5.2: The structure of the DnaD protein showing the domains responsible for DnaA and DnaD binding, a leucine like zipper motif and the location of the previously identified *dnaD23* mutant.

The *dnaD*23 replication deficient mutant is positioned at amino acid 166. Although this is not in the domain critical for DnaD-DnaA interaction the mutation may affect the tertiary structure of DnaD, thereby affecting its interaction with DnaA. In the amino terminal of the DnaD gene there is a leucine zipper like motif (also in *S.aureus* DnaD gene, Kurokawa *et al*, 2004) these motifs are know to mediate homo and hetero dimerisation of proteins and may be involved in the dimerisation of DnaD molecules.

Both DnaD and DnaB are essential for replication initiation (Bruand *et al*, 2001) the interaction between the role of DnaD and the protein DnaB was investigated by looking at temperature sensitive repressors of both the DnaB and DnaD genes using chromatin immunoprecipitation assays (Rokop *et al*, 2004). Results show that during active replication initiation the membrane associated initiation factor DnaB interacts with DnaD to recruit it to the membrane. This interaction then acts to promote initiation of replication, through the loading of the helicase (DnaC). The signal to interact could be triggered by DnaA at the *oriC* or PriA at replication forks.

A genome wide search showed that gp49 a replication initiator protein in *Listeria monocytogenes* has 52% sequence homology with the C terminal of DnaD and 53% sequence homology with the C terminal of DnaB (Marcote *et al*, 1999). This suggests that gp49 is a fusion of the C terminals of DnaD and DnaB; often if two proteins are fused as a single polypeptide in one organism they interact in a second organism in which they are encoded separately. DnaD and DnaB have been previously shown not to interact in yeast two-hybrid experiments (Marsin *et al*, 2001, Noirot-Gros *et al*, 2002). A mutant of DnaD was show to give a positive result on the yeast two-hybrid experiment as well as increase the % of DnaD in the cell located at the cell membrane. The *dnabs1371p* mutant allowed increased/unregulated binding between DnaD and DnaB an event that normally occurs but is regulated and only occurs when the bacteria is actively initiating this physiological restraint, this may account for previous yeast two-hybrid negatives.

Bruand *et al* (2005), showed by looking at the roles of DnaD and the mutant *dnaD23* that d*naD23* cells where unable to grow, nor initiate and re-initiate chromosomal replication this was attributed to the much weaker binding affinity for ssDNA by DnaD23. This single stranded binding affinity of both DnaD and DnaB is increased by there binding with each other, an interaction which is known to take place in the primosomal cascade (Rokop *et al* 2004, Bruand *et al* 2005). DnaD binding affinity for ssDNA as well as its interaction with DnaB is seen to be essential for its biological role.

DnaD has also been shown to have an essential role in the primosomal cascade at the *oriC* as well as PriA and a third unknown pathway (Bruand *et al,* 2001, Marsin *et al*, 2001). DnaD removal from any of these pathways stops DNA replication. DnaD is thought to act at an early stage of the primosomal cascade through it direct interaction with DnaA (Ishigo-Oka *et al,* 2001), the initiator of replication at the *oriC*. DnaD is also known to interact with the membrane associated protein DnaB (Bruand *et al,* 2001, Rokop *et al*, 2004) its thought this interaction may be a key regulating step in the primosomal cascade as the DnaB-DnaD complex is involved in the disruption of the bond

between the helicase loader (DnaI) and the helicase (DnaC) and its loading onto DNA (Turner *et al*, 2005).

In this chapter (based on the published work, The Bacillus subtilis DnaD protein: a putative link between DNA remodelling and initiation of DNA replication; Ian J. Turner, David J. Scott, Stephanie Allen, Clive J. Roberts, Panos Soultanas, **FEBS Letters**, Volume 577, Issue 3, 19 November 2004, Pages 460-464) the global role of DnaD protein in bacterial replication will be investigated by studying the role of the protein through its interaction with DNA using AFM in conjunction with classical biochemical techniques.

5.2. Method

5.2.1 Atomic Force Microscopy

AFM images were carried out as under an air and liquid environment as described in section 2.1.1 and 2.1.2

All images were flattened and analysed as described in section 2.1

5.2.2 DnaD and pBR322 preparation

DnaD was purified as described in Turner *et al*, 2005. PBR322 was purified as described in section 2.2.

DnaD samples were diluted to between 0.5 and 0.005 lg/ml in 20mM Tris, pH 7.5, 2 mM EDTA, and 300 mM NaCl (Sigma-Aldrich, Poole, UK).

Plasmid samples were made up to a stock solution of 10 lg/ml in dH_2O before being diluted further to a desired concentration in 10% v/v PBS containing 0.5mM MgCl2. All solutions were filtered through 0.2 µMpore size filters (Sartorius) prior to use.

Protein DNA complexes were prepared by mixing protein samples diluted to 0.25–0.0025 lg/ml in 20 mM Tris, pH 7.5, 2 mM EDTA, 300 mM NaCl, with between 0.5 and 0.15 lg/ml of pBR322 diluted in 10% v/v PBS containing 0.5 mM MgCl2 to generate varying molar ratios of protein to DNA.

5.2.3 Complementary techniques

DnaD, and DnaD-DNA complexes were analysed using sedimentary velocity ultracentrifugation, gel shift assays and analytical gel filtration. Work was carried out by David J. Scott and Panos Soultanas, Centre for Biomolecular

Sciences, University of Nottingham, University Park, Nottingham, NG7 2RD. Brief details of the experimental conditions are described below.

5.2.3.1 Protein purifications

The *dnaD* gene was cloned by PCR from *B. subtilis* (strain 168 EMG50) genomic DNA into the *Nde*I-*BamH*I sites of pET28a (Novagen). Over-expression of DnaD was carried out in B834 (DE3) *E. coli* with 1 mM IPTG for 7-8 hours from exponentially growing cultures (OD_{600}=0.6). DnaD over-expressing *E. coli* grew noticeably slower than un-induced cells. Cells were harvested in 20 mM Tris pH 7.5, 2 mM EDTA, 1 mM DTT, 500 mM NaCl, 20 w/v sucrose, incubated for 30 min at 37^{o}C with benzonase (Novagen), sonicated and the cell extract was clarified by centrifugation at 17,500 rpm, 30 min. Total protein in the clarified supernatant was precipitated with ammonium sulphate (2.9 μg per 10 ml) and centrifuged at 17,500 rpm, 30 min. The protein pellet was re-suspended in GE (20 mM glycine pH 9.8, 2 mM EDTA, 1 mM DTT) buffer until the conductivity reached 40 mS and loaded onto a sourceQ column, pre-equilibrated in GE, at 10-12 mS. The column was washed with GE/100 mM NaCl and DnaD was eluted with a 100-400 mM NaCl gradient in GE. Relevant fractions were pooled and DnaD was precipitated with ammonium sulphate.

The protein pellet was re-suspended in BisTE (Bis-Tris pH 6.7, 2 mM EDTA, 1 mM DTT) buffer maintaining the conductivity at 40 mS and loaded onto a HiTrap 5 ml Heparin, pre-equilibrated in BisTE, at 15-20 mS. The column was washed with Bis-TE/100 mM NaCl and DnaD was eluted with 100-400 and stepping up to 700 mM NaCl. The relevant fractions were pooled and loaded onto a superdex S75 gel filtration column pre-equilibrated in TE/300 (20 mM Tris pH 7.5, 2 mM EDTA, 1 mM DTT, 300 mM NaCl) buffer. The molecular weight of DnaD is 27.5 kDa and its elution profile indicated an oligomer. Typically 8-9 mg of DnaD per litre of bacterial culture was obtained. Purity was assessed by SDS-PAGE and concentration was determined spectrophotometrically.

5.2.3.2 Sedimentation velocity ultracentrifugation experiments

Analytical ultracentrifugation sedimentation velocity experiments were carried out in a Beckman XL-I analytical ultracentrifuge using cells with two channel centerpieces, loaded into a four-hole AnTi 60 rotor. All experiments were carried out at 40,000 rpm. Cells were scanned every 5 minutes at 280 nm, and the temperature was set at 20^0C. DnaD concentrations were 4.9, 2.4 and 1.2 μM.

Sedimentation coefficient distributions were generated using the program SEDFIT (Schuck, 2000) using the c(s) method of analysis. Errors in the distribution were estimated at the 67 % and 95 % confidence levels using 1000 runs of a Monte Carlo simulation. Frictional coefficients for theoretical distributions of oligomers were estimated using the program SEDNTERP (Laue, 1992).

Experiments designed to observe the DNA dependent behaviour of aggregation were carried out with a 5' HEX labeled 33mer oligonucleotide (5'-HEX-TGCATGCCTGCAGGTCGACTCTAGAGGATCCCC-3') and data were obtained at a wavelength of 536 nm.

5.2.3.3 Gel shift assays

DNA binding reactions were carried out using a radioactively labeled 33mer oligonucleotide (5'-TGCATGCCTGCAGGTCGACTCTAGAGGATCCCC-3') at 2.5 nM in 50 mM Tris pH7.4, 100 mM NaCl, 1 mM EDTA, 1 mM DTT and increasing concentrations of DnaD (123-738 nM). Mixtures were incubated for 10 mins at room temperature and complexes were resolved by non-denaturing PAGE. Gels were dried and radioactive bands were visualized using a phosphorimager.

5.2.3.4 Analytical gel filtration

Gel filtration experiments were carried out as described before (Soultanas, 2002) using mixtures of *B. stearothermophilus* DnaB (4.52 μM), DnaD (1.96 μM) and DnaI (11.22 μM), as appropriate. Proteins were incubated in 50 mM Tris pH 7.5, 250 mM NaCl, 1 mM EDTA, 1 mM DTT for 10 mins on ice before fractionated through a superdex S200 10/30 column (Amersham Pharmacia Biotech). Fractions from the peaks were analysed by SDS-PAGE. Mixtures of DnaB/DnaD/DnaI, DnaB/DnaI, DnaB/DnaD, DnaI/DnaD as well as the individual proteins alone were analysed in a similar manner.

5.3. Results

5.3.1 Imaging of DnaD Protein

AFM images at increasing concentrations of DnaD show an increasingly complex structure of DnaD aggregation. At the lowest concentration of 0.49nM (figure 5.3) the DnaD population is predominantly monomers of DnaD. Size analysis of the dimensions of the protein monomers shows the average width of a protein molecule in both the x and y co-ordinate is 23.0 nm (with a standard deviation of 3.7nm). There are several structures that appear to be the aggregation of two DnaD monomers, similar width measurements of the individual proteins visible in the aggregated structure show an average size of 23.3 nm (with a standard deviation of 3.2nm) confirming they are DnaD dimers. Population distribution analysis (figure 5.4) shows that 67 % of the population are monomers (length of 10nm-30nm) and that 25 % are dimers (length of approximately 30nm-50nm) there are also a small number of larger aggregates, for example a 4 –mer structure (80-90nm).

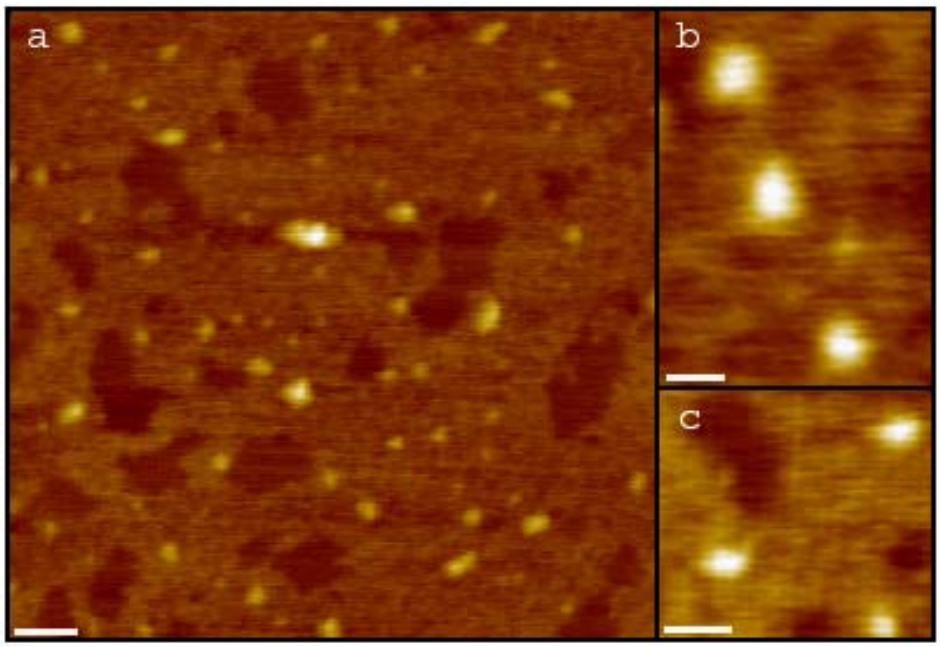

Figure 5.3: Topographical images of *Bacillus Subtilis* DnaD protein in air at a concentration of 0.49nM. A) Represents a typical field view showing a mixture of monomers and dimers. Scale bar represents 100nm. B) and C) Show zoomed in images of the proteins visible in the field view. Scale bars represent 50nm.

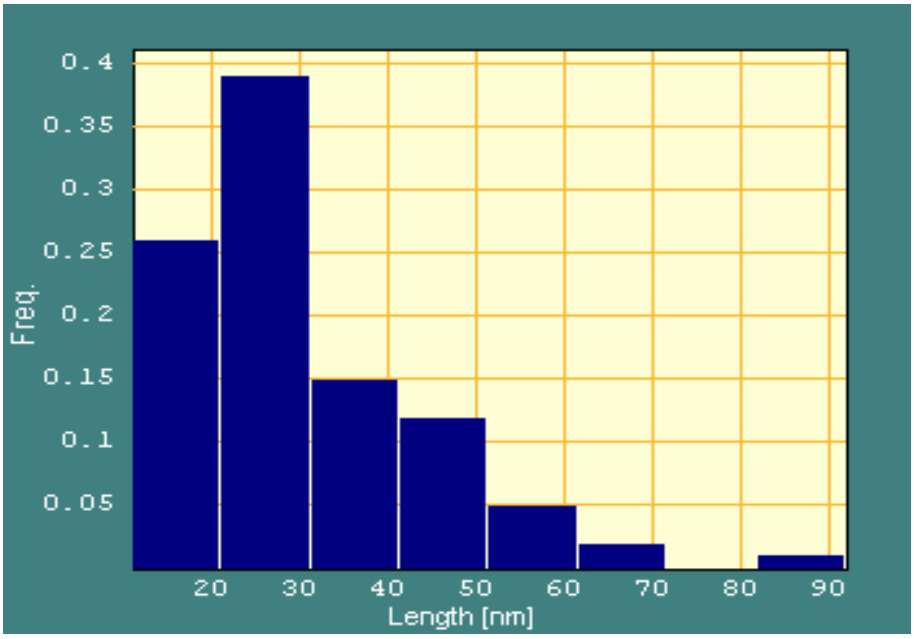

Figure 5.4: A histogram showing the population distribution of the lengths of DnaD aggregates at a concentration of 0.49nM.

At a concentration of 4.9nM coverage of DnaD on the mica surface is much higher than that at 0.49nM (45% as apposed to 5%) (figure 5.5). As well as an increase in the number of monomers and dimers there appears to be more extended structures such as trimers and pentamers. Zoomed sections of the image show both trimers and pentamers (figure 5.5b) in which the individual protein molecules can be clearly seen (figure 5.5c). Size analysis of the proteins that comprise the proposed trimers and pentamers have an average width of 23.6 nm (with a standard deviation of 3.4nm) in both the x and y direction. This is the size of a DnaD monomer as seen in the lower concentration images of DnaD (figure 5.33a). Population distribution (figure 5.6) shows that 33% of the population are monomers (10-30nm), dimers account for 34% (30-50nm) an the rest of the population is higher order aggregates (50nm +)

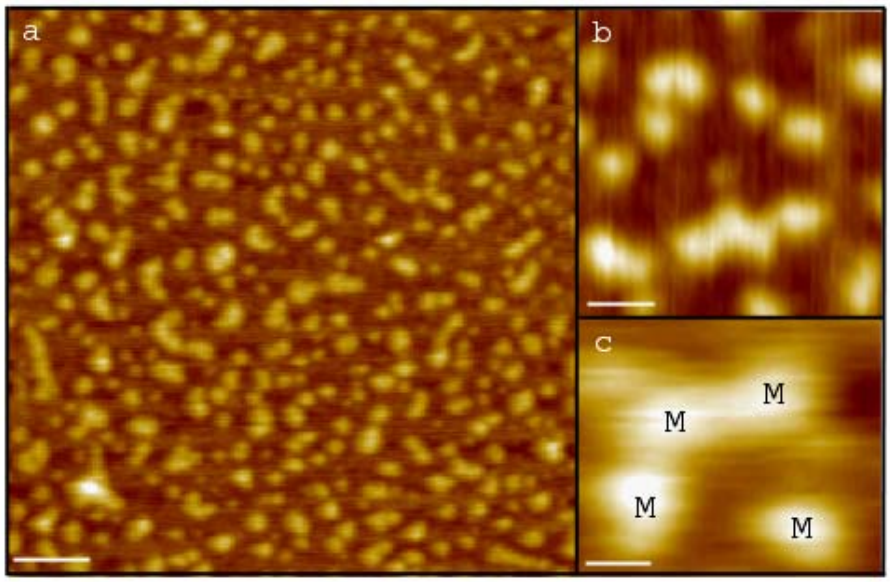

Figure 5.5: Topographical images of *Bacillus Subtilus* DnaD protein in air at a concentration of 4.9nM. A) Represents a typical field view showing a mixture of structures ranging from monomers to pentamers. Scale bar represents 100nm. B) Show a zoomed in section of the field view seen in A, where a pentamer a trimer and several monomers can be seen. Scale bar represents 50nm. C) Shows a trimer and a monomer, with individual proteins denoted by the letter M. Scale bar represents 50nm

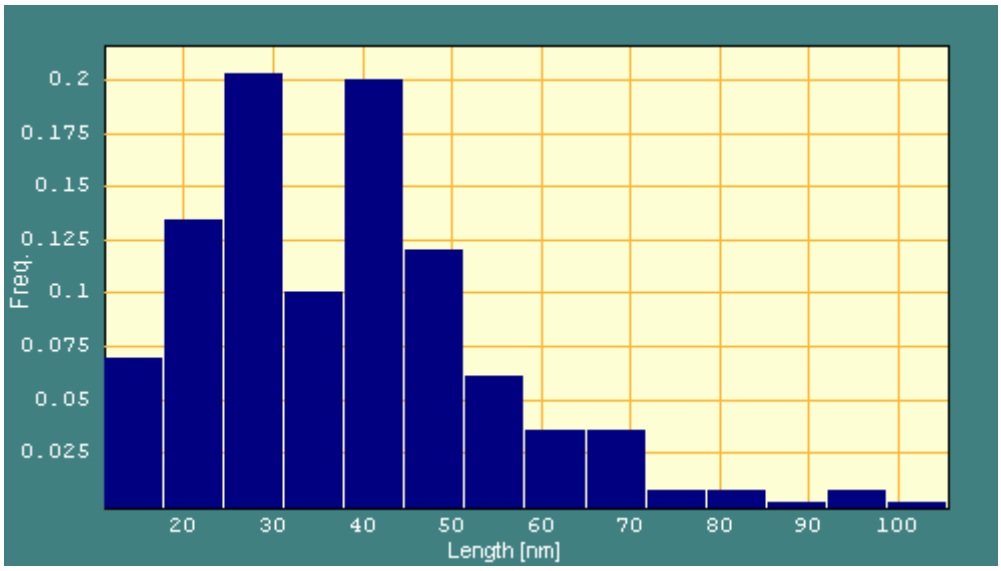

Figure 5.6: A histogram showing the population distribution of the lengths of DnaD aggregates at a concentration of 4.9nM

At a DnaD concentration of 49nM DnaD is densely packed on the surface of the mica (figure 5.7a). There are several large 'chains' of DnaD proteins as well as the trimers, dimers and monomers evident at lower DnaD concentrations. Zoom sections of the image (figures 5.7b-e) show chains of DnaD that are many monomers in length and appear to be almost circular in shape. The individual proteins of these chains are clearly visible and are up to 10 monomers in number (figures 5.7f-g). The width of individual monomers in these higher order chains is approximately 14.8nm (with a standard deviation of 3.3nm), which is smaller than the size of a monomer as calculated in lower concentration experiments. This could be due the DnaD molecules orientating in a specified way in the larger ring structures or possibly the DnaD molecules are more rigid in ring structures meaning there is less lateral deformation of the sample from the force of the tip.

The range of concentrations investigated shows that as concentration increases higher order oligomers are more evident, with the transition progressing from monomers and dimers to elongated 'chain' and 'circular' structures.

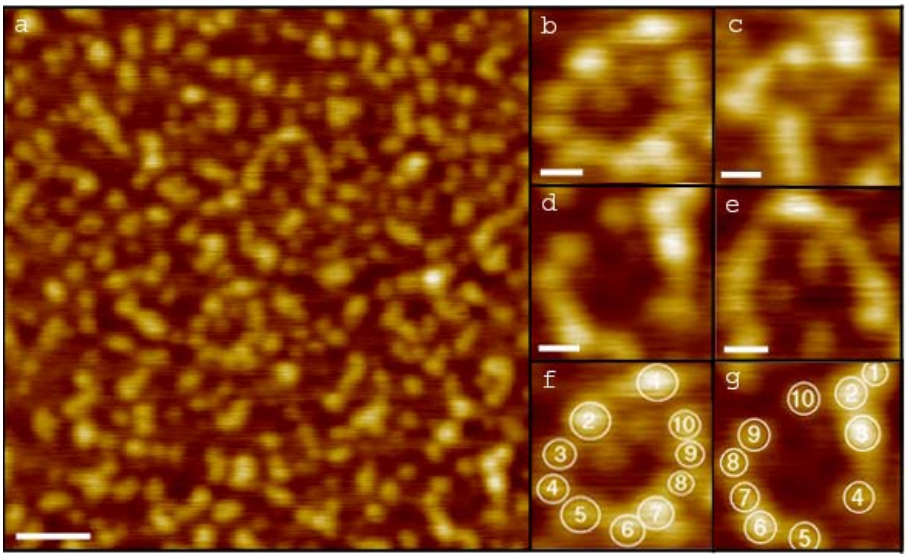

Figure 5.7: Topographical images of *Bacillus Subtilus* DnaD protein in air at a concentration of 49nM. A) Represents a typical field view showing a mixture of structures ranging from monomers to higher oligomer 'chains' and 'circles'. Scale bar represents 100nm. B), C), D), and E) Show zoomed in sections of the field view seen in A, where a higher order oligomers comprising a large number of proteins can be seen. F) and G) Shows the individual proteins that comprise the 'chain' seen in B) and D). Scale bars represent 50nm

5.3.2 Imaging of supercoiled pBR322

The plasmid population prepared by transformation and amplification in *E.coli* (section 2.2) which is used to bind DnaD, is approximately 80% in the supercoiled conformation, and 20% in the open circle conformation (Soultanas, personal communication, 2004). In topographic AFM images of the plasmid pBR322 both species can be seen (figure 5.8). The majority of the plasmid appears to be highly coiled and looped, a few open circle conformations are also present. The average contour length of a representative selection of supercoiled plasmids was measured and shown to be 1315nm with a standard deviation of 57nm.

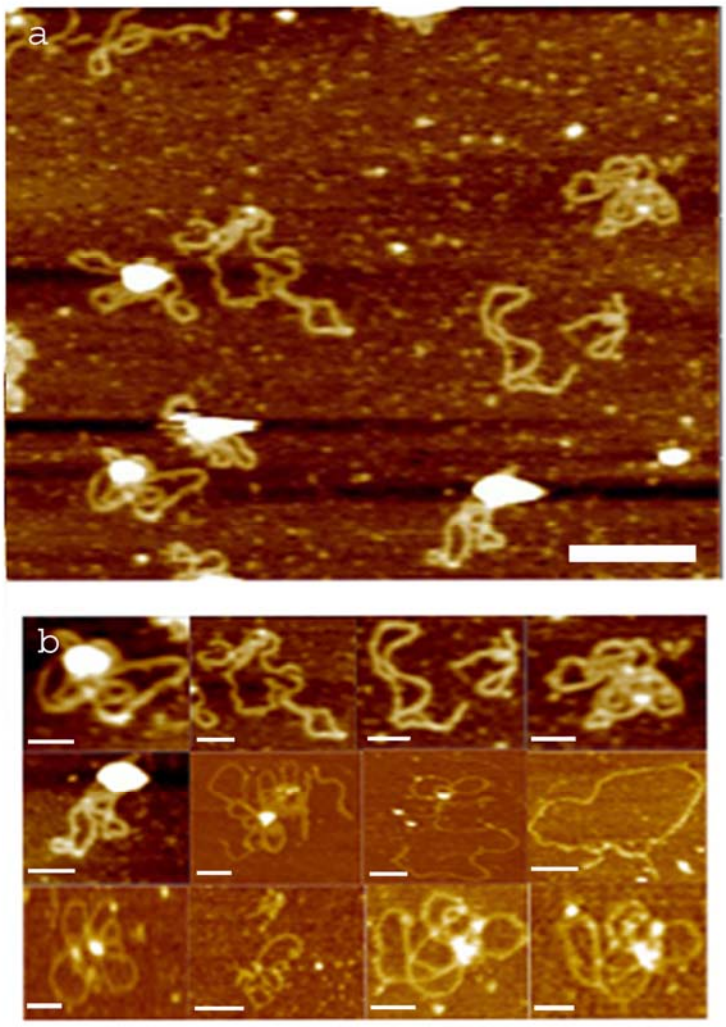

Figure 5.8: Topographical AFM image of bacterial plasmid pBR322 in air (a) a representative field view showing a selection of supercoiled structure. Scale bar represents 250nm. (b) Zoomed in AFM images of a

variety of supercoiled and open circle structures in air and liquid. Scale bar represents 50nm.

5.3.3 Imaging of pBR322 DNA and DnaD Protein complexes

The interaction between the protein DnaD and the exposed AT rich region of DNA has been shown to be a key step for normal replication in bacteria (Bruand *et al*, 2005). This interaction was investigated here by binding DnaD to DNA *in vitro* and imaging any formed complexes on the AFM (section 5.2.2).

Topographical AFM images in air (figure 5.9) show that the usual supercoiled plasmid conformation (figure 5.8) is not present and instead the plasmid exists solely in an open circular form. DnaD not associated with the plasmid is evident, as seen in the control images (figures 5.3, 5.5 and 5.7), the majority of this free DnaD appears to be in the monomer, dimer and trimer forms and not in higher order oligomeric forms as seen at similar concentrations of DnaD alone (figure 5.7), instead it appears as if the DnaD has become associated with the DNA forming DnaD-DNA complexes.

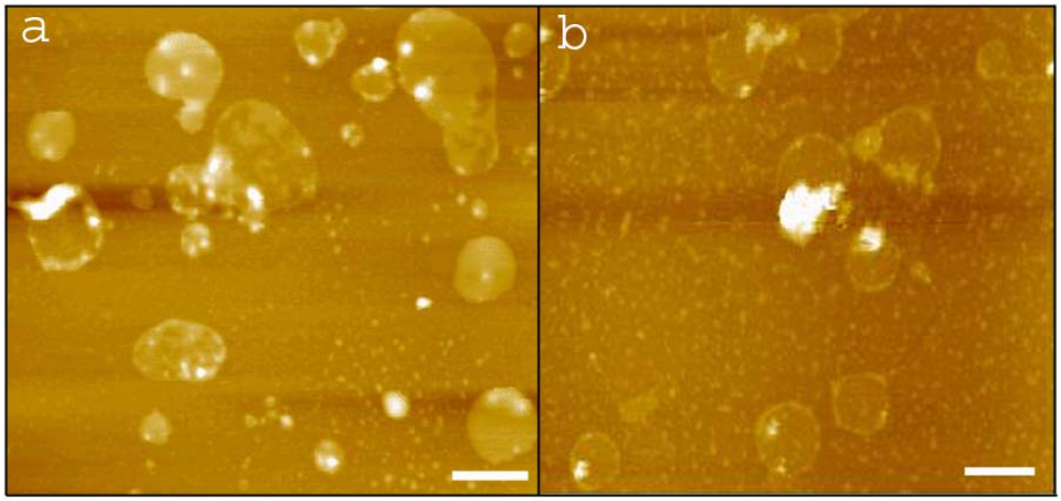

Figure 5.9: AFM topography images in air showing two representative AFM field views of DnaD-DNA complexes. Non-associated DnaD is also visible in a variety of oligomeric forms (dimers, trimers). Scale bar represents 1μm.

The DnaD-DNA complexes visualised have varying dimensions but they all have a similar geometry, as well as some similar structural features (figure 5.10). The DNA although circular appears to be elevated around its entire outer contour length as if the DnaD is preferentially bound there. The apparent height of naked DNA in AFM is 1nm (the real height of DNA is 2nm, this difference is commonly seen in AFM), whilst in the DnaD-DNA complexes it is 1.6nm. The distribution of DnaD bound to the DNA is non-uniform and varies from individual monomers to larger build-ups of many DnaD protein molecules, in some cases small side-chains of the DnaD protein can be seen branching off from the DnaD-DNA complexes (figure 5.10b).

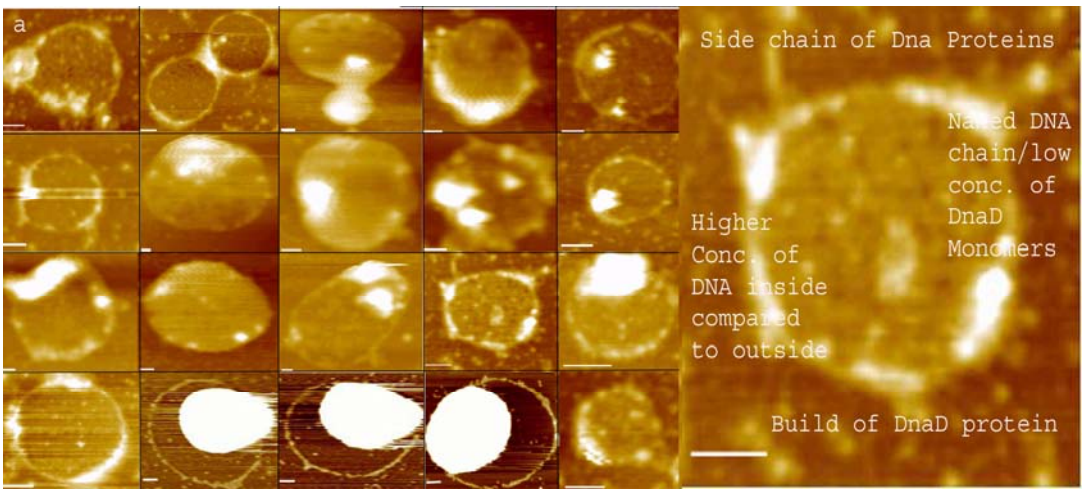

Figure 5.10: (a) Representative topographical AFM images in air of DnaD-DNA complexes, these structures vary in size but display similar geometry and structural features. (B) Zoomed in DnaD-DNA complex with selected structural features highlighted. Scale bars represent 100nm.

Several of the DnaD-DNA complexes display a large build up or 'loci' of DnaD protein at one point along their length. This loci does vary in size considerably but its presence on many complexes suggests there is a region of the plasmid DNA that has higher sequence specificity for the DnaD protein. This could be an AT rich region as DnaD is known to activate DNA replication at such a region. The DnaD protein appears to be localised within the centre of the DnaD-DNA complexes. Comparison between the areas

outside and inside the complexes show a higher abundance of the protein inside compared to the unassociated protein outside of the complexes, this can be seen by a step height comparison between the DnaD-DNA complexes and the unassociated DnaD (figure 5.11). There is a 1.2 nm height difference between the DnaD in the centre of the complex compared with unassociated DnaD outside the complexes, this could be due to the protein preferentially associating with the DNA rather than itself.

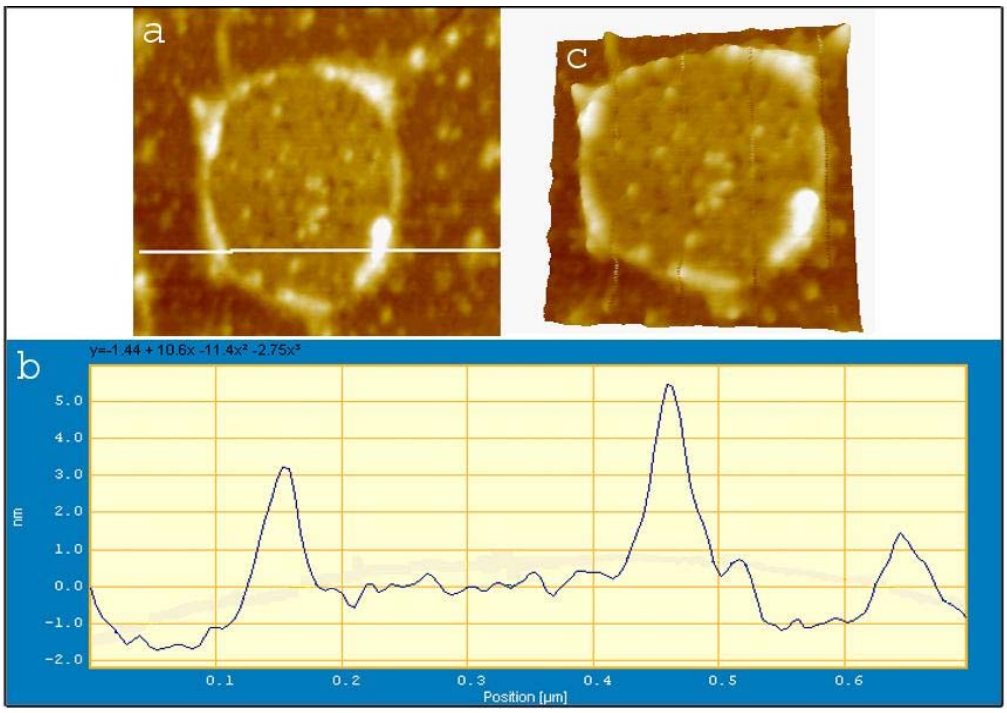

Figure 5.11: (a) Topographical AFM image in air of a DnaD-DNA complex with a line bisecting it illustrating the area step height analysis was carried out upon (b) Step height for line illustrated in (a) two peaks representing the raised DNA contour of the circle can be seen. The step height between the DnaD inside the circle and that of the background is 1.2nm (c) a 3D image of (a) which highlights the height difference between the centre of the circle and the background.

5.3.4 DnaD-DNA Complexes in Liquid

Circular DNA-protein structures have previously been visualised and attributed to the drying effects generated by the imaging of DNA in air (Williams *et al*, 1996, Williams *et al*, 1996a). To check the validity of the observed constructs and any effects drying may have had on the dimensions and organisation, the DNA protein mix was imaged at the same concentration in liquid (section 5.2.2).

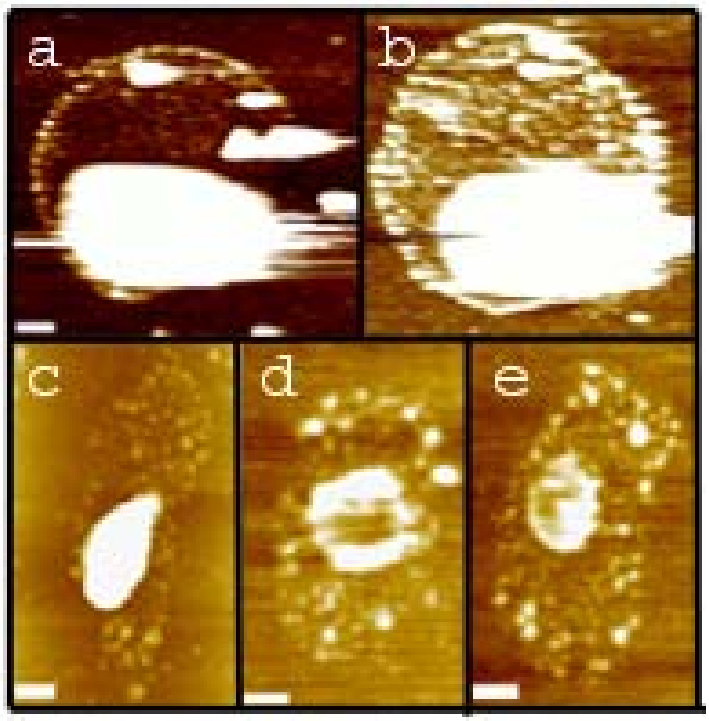

Figure 5.12: Topographic AFM images in liquid of DnaD-DNA complexes. (a) and (b) show large circles displaying many of the features seen in air such as protein coating the DNA, an abundance of protein inside the circle as apposed to outside and a large 'loci'. (c)-(e) smaller structures were also visualised which, have all the structural features previously mentioned but have adopted a different spatial conformation. Scale bars represent 100nm

Topographical AFM images showing circular DNA-protein complexes are also visible in a liquid environment (figure 5.12). The DnaD-DNA complexes exhibit many of the features seen in the air AFM images; many individual

DnaD protein molecules are visible along the length of the DNA and within the centre of the complex, these appear to exist as mixture of monomers, dimers and higher order oligomers. As seen in the air AFM images, in liquid there also appears to be a much lower concentration of protein molecules of any oligomeric length outside of those in the complex, there is a step height of 1.9nm between the DnaD in the centre of the complexes and the DnaD unassociated with a complex. This suggests that the protein is preferentially binding to the complex because of an attraction for either DNA or DNA bound protein over the unassociated protein. This binding of a large amount of protein to the inside of the complex may explain the circular geometry of what should be a supercoiled plasmid. The protein molecules may initially bind to the DNA causing some DNA structural change, subsequent protein is then either attracted to the newly exposed 'opened up complex' or the protein molecules already bound to the DNA (in preference to forming free DnaD oligomers). This interaction forms a scaffold which acts to 'push-out' out the DNA to a circular form as the DnaD build up inside it.

Comparing the contour lengths of both the unbound supercoiled plasmid (Table 5.1) and the DnaD bound plasmid there appears to be an average increase (across a range of concentrations) of approximately 680nm to the contour length of the DNA upon the addition of the protein. A considerable force (see section 5.5) would need to be applied to the supercoiled plasmid in order to covert it into an open circular form without nicking, which doesn't appear to have happened (Soultanas, personal communication, 2005). The plasmid is 4,361 bp long and from 18 images the average contour length is 1,314nm with a standard deviation of 56nm. Similar measurements of 134 DnaD-DNA complexes (imaged in air and liquid) show an increase in the plasmid contour length to 1,994nm with a standard deviation of 680nm. The sizes increase between the addition of DnaD divided equally among all the helical turns of the plasmid corresponds to 16.1 bp per helical turn. Since the DNA has not been nicked, we propose that the increase in the bases per turn has increased from 10.5bp per turn to 16.1 bp per turn to relieve the stress that would build up from the conversion of the plasmid from a supercoiled form to a open circle form.

	Average Contour Length	Standard Deviation	Number of Samples
Unbound Plasmid	1315nm	57nm	18
DnaD Bound (Molar Ratio 70)	1342nm		24
DnaD Bound (Molar Ratio 347)	2303nm		3
DnaD Bound (Molar Ratio 6944)	2819nm		5
DnaD Bound (Molar Ratio 6944)	2819nm		117
DnaD Bound Average	1995nm	689nm	134

Table 5.1: Size comparison between unbound plasmid and plasmid with DnaD bound

Experiments at a range of concentrations reveal an interesting trend, as the molar ratio of protein to base pair increases the size of the DnaD-DNA complexes increases (see figs 5.9 and 5.10). At a ratio of 70 protein molecules per plasmid which is fewer than 1 protein every 62 base pairs there is only a marginal increase in the contour length of the plasmid, though the plasmid still exhibits a circular structure and similar features to those described previously. As the molar ratio increases the size of the complexes also increases up to 2800nm where there are almost 7000 protein molecules per plasmid, which corresponds to 3 proteins for every two base pairs. Although there is a possible correlation between proteins per base pair and contour length (Figure 5.13), further experiments may reveal a levelling off of this effect as at concentrations where the number of proteins per base pair exceeds one, the system must be reaching physiological limits. Although more DnaD could bind in the centre of the complex to DnaD already bound to DNA, the DNA would be theoretically fully bound (there is a limit to how many proteins can be bound to one base pair) and cannot adapt any more by unwinding to reduce the stress induced by the mass protein binding.

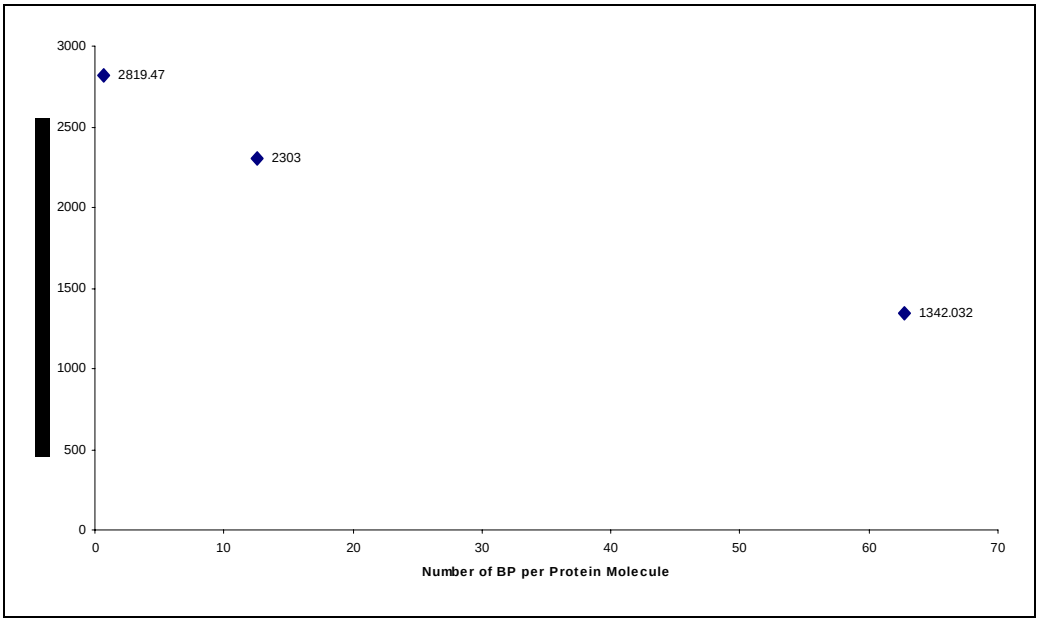

Figure 5.13: The relationship between the contour length of DnaD-DNA complexes and the number of base pairs per protein molecule.

5.4. Complementary Data

5.4.1 DnaD Oligomeric State

Sedimentation velocity experiments over a range of three concentrations revealed sedimentation coefficient distributions values consistent with three species being present in solution that interact in a concentration dependent manner (Fig. 5.14).

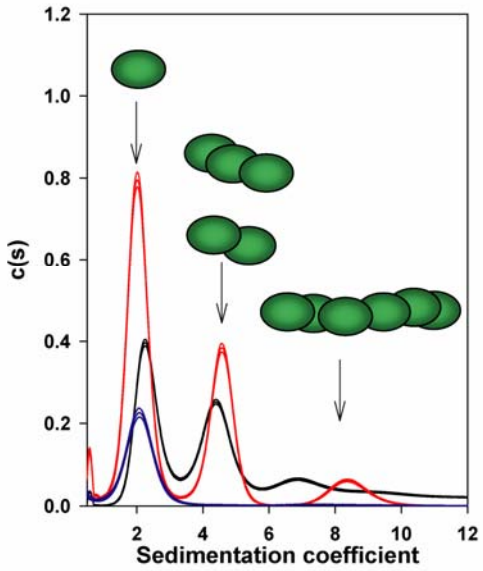

Figure 5.14: Analysis of DnaD oligomers by sedimentation velocity ultracentrifugation. Data was analyzed by the c(s) method of Schuck and errors were plotted at the 95% confidence limit. At low 1.2 μM (blue lines), there is a species corresponding to a monomer of DnaD. At 2.4 μM (black) and 4.9 μM (red), species corresponding to dimers or trimers and to higher order aggregates of at least pentamers and hexamers are apparent.

At the lowest concentration (1.2 μM), frictional coefficients expected for each oligomeric species (figure 5.15) reveal that only a monomer (sedimenting at around 2.0 s) has a physically reasonable value. Increasing the concentration leads to a second peak at around 4.5 s (corresponding to a compact dimer or an extended trimer), with higher order species in excess of 6 s (pentamer and hexamer, as judged by reasonable frictional coefficients) present at the highest concentration.

Species	2*s*	4*s*	6*s*	9*s*
Monomer	1.488			
Dimer	2.363	1.182		
Trimer	3.059	1.549	1.032	
Tetramer	3.750	1.875	1.250	
Pentamer	4.352	2.176	1.451	
Hexamer	4.914	2.457	1.638	1.092
Heptamer	5.446	2.723	1.815	1.210
Octamer	5.953	2.977	1.984	1.323
Nonamer	6.440	3.220	2.147	1.431
Decamer	6.908	3.454	2.3027	1.535

Figure 5.15: Table showing possible frictional coefficients versus species type for DnaD. Physically unreasonable values are in grey. Frictional coefficients are calculated higher values indicate a more elongated molecule.

Separation of the species into distinct sedimentation coefficient distributions also reveals a specific type of behaviour for the species interaction with each other. It is known both theoretically and experimentally that it is impossible to separate out a rapidly reversible monomer/dimer equilibrium using sedimentation analysis; a weighted average distribution is produced. If the second species is a dimer in these experiments, this would mean that the rate of dimerization is slow on the timescale of sedimentation. A second possibility is that the samples undergo irreversible aggregation, and separates into distinct species, as there is no appreciable off rate of aggregation. This, however, is unlikely as dilution of the sample for sedimentation yields only one small species: irreversible aggregation would yield the same proportion of species, irrespective of concentration, upon dilution. A third scenario is that the species are in a monomer/n-mer rapidly reversible equilibrium, where $n > 2$. Theory and experiment show that separation of species is possible if its assumed that there is a cooperative transition from monomer to trimer or tetramer. These would be present as highly extended conformations (as judged by physically reasonable frictional coefficients).

AFM images of DnaD at various concentrations show the formation of higher extended oligomeric species at high concentrations, giving weight to this third hypothesis. Elongated strand-like and also circular and semi-circular structures were visible at high concentrations (Fig. 5.7). This is a feature that has been observed in other nucleoid associated proteins such as the H-NS protein in *E coli* (Dame *et al*, 2000).

4.2 DnaD Mediated Nucleoprotein Complexes

Sedimentation velocity analysis of the binding of DnaD to DNA with a HEX-tagged synthetic oligonucleotide (so that the sedimentation of protein and the DNA can be followed independently at 280nm and 536nm respectively) was investigated. Upon addition of the oligonucleotide to DnaD, an extremely large nucleoprotein complex was formed (1-2 million Daltons) that was impossible to investigate further with analytical ultracentrifugation.

Instead the DNA binding activity was investigated by gel shift using the same untagged but radioactively labelled oligonucleotide (figure 5.16).

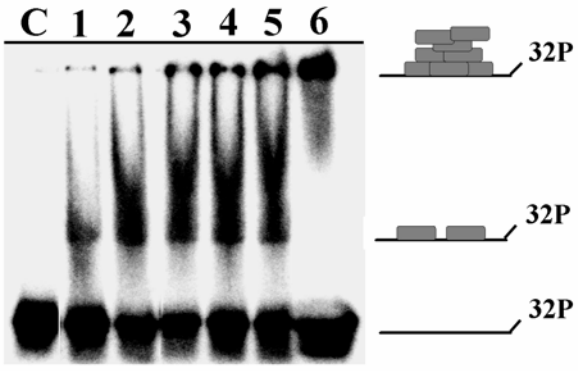

Figure 5.16: Gel shift analysis of DnaD binding to an oligonucleotide at increasing concentrations. Binding reactions were carried out at 2.nM oligonucleotide substrate and 123, 246, 369, 492, 615 and 738nM DnaD, lanes 1-6, respectively. Lane C shows the control radioactively labelled oligonucleotide

DnaD bound to the oligonucleotide produced a clear shifted band and as the DnaD concentration increased a band started to appear higher up the gel until the shifted band ended up in the well at the highest concentration. This observation shows that additional DnaD molecules were directed exclusively to the initial nucleoprotein complex rather to the free oligonucleotide, although not shown at very high concentrations all of the substrate could be forced into the well. This data seems to suggest that once DnaD forms an initial nucleoprotein complex it acts as a nucleus to recruit additional DnaD molecules forming a large complex. This matches the AFM data that suggests that the DnaD acts in someway to recruit other DnaD molecules to the DnaD-DNA complex acting to stabilise its structure.

5.5. Discussion

DnaD protein has been shown to form dimers and trimers as well as higher order oligomers in a concentration dependent manner. At low concentrations AFM topographical images and sedimentation velocity analysis show that DnaD is in a monomeric form but with an increase in concentration it assumes either a compact dimer or an extended trimer conformation. Further increasing the concentration shows DnaD forms higher order species such as pentamers and hexamers, as judged by sedimentation velocity frictional coefficients, although chains of up to nine proteins are seen in AFM images. It's known DnaD can bind to itself through the DnaD binding domain and form both dimers and trimers (Ishigo-oka *et al*, 2001). The size analysis of the protein molecules suggests that they are all spatially orientated in the same way. The higher order oligomers that form have some interesting circular and coiled geometries, the resolution of the AFM images is not high enough to reveal detailed structure of the proteins but the smaller average protein size (compared with the monomers/dimers) suggests that the proteins could be in varying orientations or conformations.

There are a number of possible scenarios for the nature of DnaD suggested by sedimentation velocity data (see figure 5.14) the most likely scenario considering the AFM data, is that DnaD monomers and the *n*mer are in a rapidly reversible equilibrium. This is physically possible if there is a cooperative transition from monomer to trimer or higher order oligomers, such higher order oligomers are present in the AFM images. A summary of this interaction (figure 5.17) shows the individual proteins, though their exact orientation is not known.

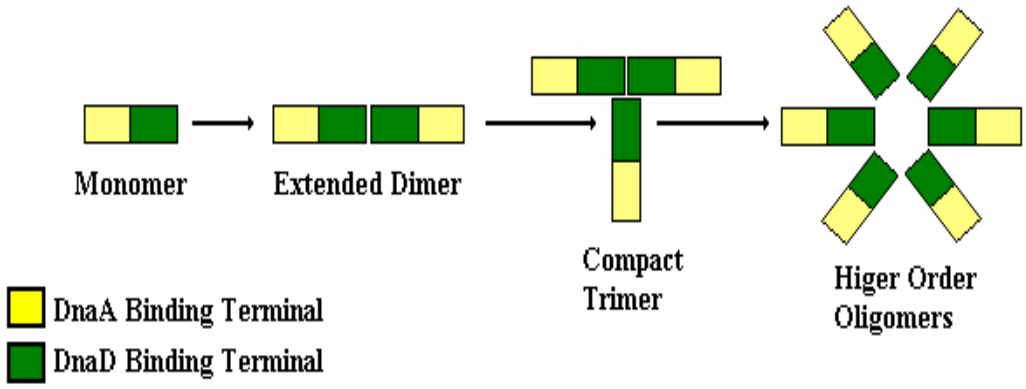

Figure 5.17: Diagram showing the behaviour of the DnaD proteins, concentration dependent increase as shown by sedimentation velocity frictional coefficients and AFM data. Each protein molecule is represented by a coloured rectangle. Orientation of the protein molecules is unknown.

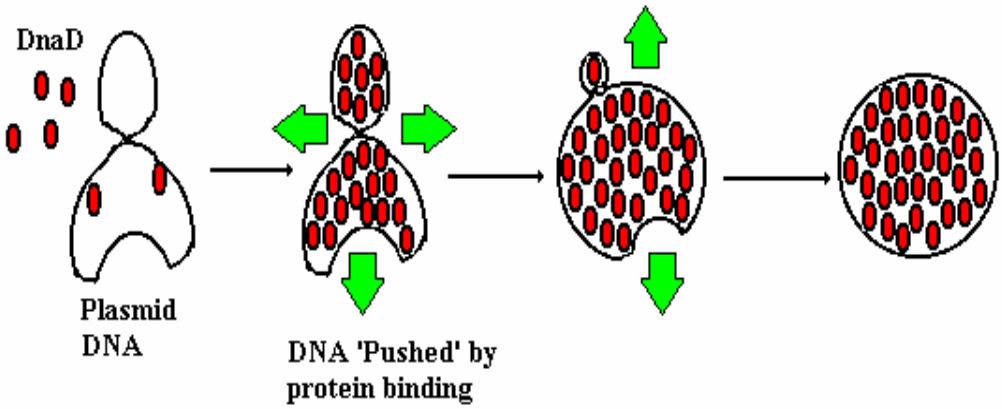

Figure 5.18: Diagram showing proposed model of DnaD binding to DNA. Initial DnaD molecules bind to the DNA which, recruits more molecules of DnaD to the already formed complex. As more DnaD binds it acts on the supercoiled structure of the DNA 'pushing' it out into an open circle form.

Interactions between DnaD and DNA cause the predominantly supercoiled plasmid population to assume an open circular geometry. DnaD has been shown to have DNA binding properties (Marsin *et al* 2004, Bruand *et al*, 2001) In this case there is an abundance of DnaD bound to the DNA as apposed to unassociated protein with the DNA. This phenomenon was seen in both AFM images (figures 5.9 and 5.12) and in gel shift analysis (figure 5.16) where, new DnaD seemed to be directed to the existing protein-DNA complex rather than formation of new complexes or self-binding. This affinity for DNA is an important property of DnaD (as seen in ssDNA experiments, Bruand *et al*, 2005) binding to DNA to stabilise the open loop is an initial step for DNA synthesis to proceed. Initial DnaD molecules bind to the plasmid; subsequent DNA molecules are then actively recruited to the complex. Since all newly recruited DnaD molecules can also bind to the DNA it becomes saturated, as the number of protein molecules increases the DnaD 'pushes out' the DNA into an open circle form (figure 5.18).

Although side chains of molecules are visualised on some of the DNA-DnaD circle complexes the majority of the DnaD molecules have bound to the DNA with their C terminus orientated towards the centre of the circle. Since the protein can bind to both DNA and other DnaD molecules it could be expected that DnaD would bind to DNA in both directions, instead it appears that the DnaD is only orientated towards the centre of the complex. It could be that the protein orientates itself in closest proximity to other DnaD molecules, which are associated with the complex than attached to DNA causing the protein to orientate inwards.

Several of the DNA-DnaD complexes structures observed have one area where the protein has aggregated in abundance. It is not possible to say if these features occur in the same place due to the circle structure of the complexes, however, the abundance suggests a common cause is responsible. It is know DnaD opens up a region of DNA at an AT rich region *in vivo* to initiate cell replication, it could be an AT rich region(s) of the pBR322

genome (that DnaD preferentially binds to). Sequence analysis of the pBR322 genome show two stretches of predominantly A and T bases (figure 5.19) which could be a region of preferential binding either individually or in combination.

Startpoint = Basepair no. 1 Length = 70 base pairs

ttctcatgtttgacagcttatcatcgataagctttaatgcggtagtttatcacagttaaattgctaacgc

Startpoint = Basepair no. 3229 Length = 42 base pairs

ttttaaattaaaaatgaagttttaaatcaatctaaagtatat

Figure 5.19: Two AT rich sequence in the pBR322 genome. Starting base and length are shown. A and T bases are highlighted in yellow.

The contour lengths of the DNA-DnaD complexes show an increased length compared with supercoiled plasmid DNA. An increased length in DNA could be explained by the DNA undergoing a nicking event and becoming unwound, however there is no evidence in this or other experiments that DnaD acts to nick DNA, and most DNA nicking enzymes would require a source of energy such as ATP that is not present in the reaction mix used in these experiments. Ruling out nicking activity as a cause there remains three reasonable possibilities to explain the increased contour length using the following relationship that describes topographical changes in DNA.

$$L = T + W$$

L (linking number)= number of turns,
T (twist) = Basepairs per turn,
W (writhe) = Supercoil

1) The number of basepairs per turn could be adjusted throughout the molecule; this would result in the DNA becoming underwound as a result of a decrease in the twist value.

2) The DNA could adopt a more supercoiled structure (writhe) to maintain the given twist with the given linking number.
3) The DNA could exist with the normal twist for most of the structure and have a region with zero twist

The DnaD protein acting to 'push out' DNA would (figure 5.18) stop the DNA becoming more supercoiled or existing with an area of zero twist (which is highly thermodynamically unstable). It is therefore most likely that the DNA has increased the number of basepairs per turn to cope with the stress of the increased contour length. Using an average value the DNA has increased its basepairs per turn from 10.6 to 16.1

Subpopulations at different ratios of DnaD to DNA show that the contour length increases as the amount of DnaD increases. This effect is explainable using the relationship described above. As DnaD is added it causes the DNA to extend, The DNA compensates by increasing the number of bp per turn (L). As more DnaD binds the DNA is stretched further requiring a greater alteration of L to cope with the stress and strain. The contour length of DNA would not be able to increase much beyond the lengths seen in these experiments as the DNA is saturated in terms of protein. At higher concentrations DNA-DnaD complexes can be seen where the DNA aggregates on top of the complex forming a massive dome like structure (figure 5.20).

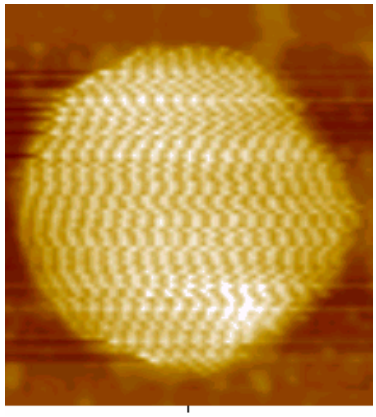

Figure 5.20: Topographical AFM image in air of a DnaD-DNA complex at a high concentration of DnaD, where the complex is completely covered by a mass of protein. Scan size is 600nm

The DNA-DnaD complexes seen show some similarity to work carried out on the *E.coli* HU and H-NS proteins. This system (figure 5.21) studied on the AFM shows that H-NS and HU work in equilibrium, with HU condensing the DNA during the resting phase of the cell cycle and H-NS 'opening up' the DNA when the DNA is needed for cellular processes such as cell replication.

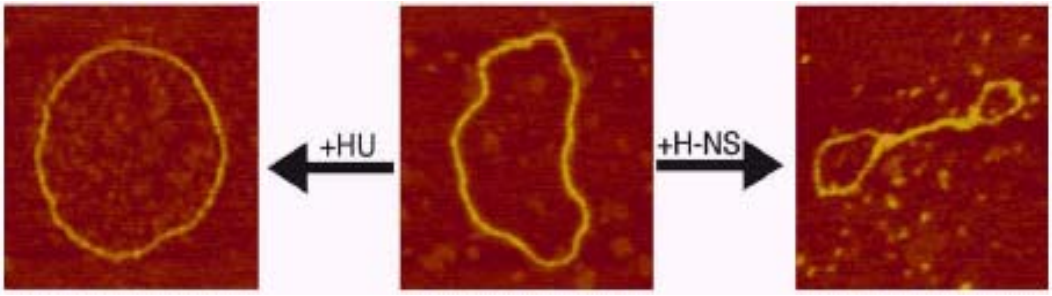

Figure 5.21: The effect of the *E.coli* proteins HU and H-NS on DNA as observed by Dame *et al* 2004 by AFM

The replication initiator RepE45 protein encoded by the mini-F plasmid shows a similar structural transition and in this case this relaxation is not the result of strand break or local melting of the DNA Interestingly HU reduced DNA structures have a similar build up 'loci' on the DNA surface. This could also be due to sequence homology but it maybe an important feature of how such proteins begin DNA replication.

This link between DnaD and HU suggest DnaD may effect the structure of a supercoiled plasmid in a similar mechanism, DnaD has already been shown to be important in DNA replication, restart and repair (Bruand *et al* 2001, 2005, Rokop *et al*, 2004). The recruitment of large amounts of DnaD may be important for the reorganisation of the bacterial nucleoid rendering it replication proficient. The DnaD may act as a scaffold for the attachment of other proteins in the primosome cascade whilst at the same time attaching the bacterial chromosome to the membrane via its interaction with the DnaB primosomal protein. If DnaD can impose global DNA architectural transitions, a property that is biologically important in primosome assembly then it may be a link between chromosomal reorganisation and DNA replication.

5.6. Model

The experimental evidence shows that DnaD forms large nucleoprotein assemblies affecting global DNA architecture. Previous studies have shown that DnaD disrupts a complex between the ring helicase (DnaI) and the replicative helicase (DnaC), and that DnaD interacts with the primosomal protein DnaB that is associated with the cell membrane. Its has been previously suggested that the initiation of DNA replication is regulated by recruitment of DnaD to the membrane, by maintaining DnaD in the cytoplasm prevents excessive over-initiation and its regulated recruitment to the membrane.

After activation of replication DnaD may bind to chromosomal DNA (figure 5.22) forming a scaffold to open up the nucleoid (either locally in the vicinity of *ori*C or globally) and render it replication proficient. DnaC is recruited from the DnaI-DnaC complex in the cytoplasm to the membrane attachment site by a direct interaction with DnaB. DnaD will then disrupt the DnaI-DnaC complex thus facilitating its loading onto the *ori*C. DnaD provides a possible link between nucleoid reorganisation and initiation of DNA replication. Its interaction with the membrane associated DnaB may be the prime regulatory event that couples chromosomal remodelling to DNA replication.

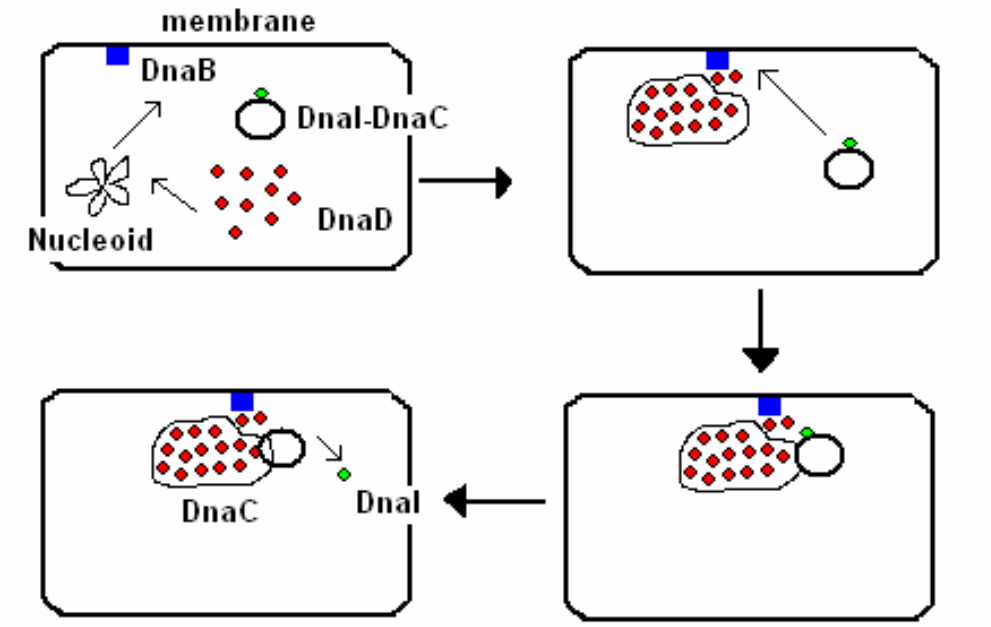

Figure 5.22: Speculative model for the coordination of nucleoid remodelling and initiation of DNA replication in *B.subtilis*. Indicated stoichiometeries of complexes and the membrane attachment site are not precise and have not been established. The sizes of various components are not drawn to scale. Although DnaD is depicted to remodel the whole of the nucleoid, also localized remodelling in the vicinity of the *ori*C may be the case.

6. Is DnaD a global regulator of DNA architecture?

6.1. Introduction

6.1.1General

DnaD has been implicated to have a role in the organisation of global DNA architecture as judged by its ability to open up the structure of supercoiled DNA (chapter 5). Bacterial histone-like proteins are an example of universal bacterial proteins that have a vital role in the organisation of the bacterial nucleoid. The bacterial histone-like proteins, so named because of a functional analogy with eukaryotic histone proteins (there is no structural similarity), have a similar role in the organisation of the bacterial nucleoid to the eukaryotic histone proteins. They share many similar properties such as a comparable DNA binding ability, low molecular mass, copy number and electrostatic charge. The four most characterised histone-like proteins are Fis (factor for inversion stimulation), H-NS (histone-like nucleoid structuring), HU (heat unstable) and IHF (integration host factor) (Dorman *et al* 2003).

Two of the histone-like proteins; HU and H-NS have been studied in detail and reveal structural and physical insights into their role of global regulating proteins. In this chapter the role of DnaD as a global regulator protein will be investigated by comparison with H-NS and HU and further studying the complexes formed by its interaction with DNA (figure 5.10).

6.1.2 H-NS

H-NS is a 15,600 Da protein that is present at about 20,000 copies per cell. The protein exhibits a global neutral pI but harbours many patches of charged amino acids. The protein has a C-terminal DNA binding domain and a N-teminal oligomerisation domain, separated by a flexible linker region (Figure 6.1) (Schroder *et al,* 2002, Dorman *et al,* 2004). The N-terminal is mainly α-

helical and because of the presence of a coiled coil. H-NS exists as a dimer, (Bloch *et al*, 2003) where the dimer can self associate to form larger oligomers (Smyth *et al* 2000) and often aligns to form oligomeric structures that are effectively zippered stretches of DNA through a H-NS cross-linking of adjacent DNA segments (Dorman *et al*, 2004).

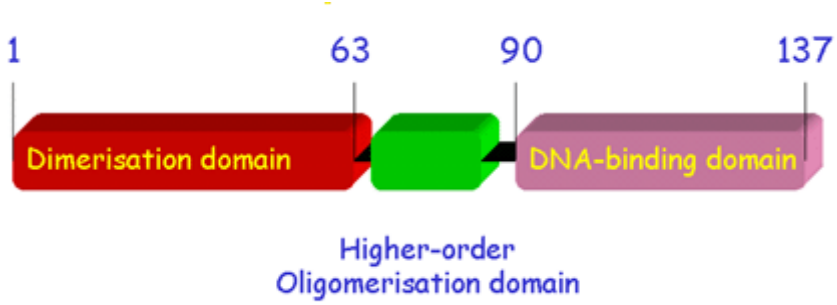

Figure 6.1: A schematic diagram showing the two binding domains and the flexible linker region of the H-NS protein.

Up to 5% of the genes in *E.coli* have been shown to respond to the presence or absence of H-NS. The exact mechanism of H-NS repression of transcription has been characterised in a few cases. The protein is attracted to a region of DNA in close proximity to the promoter it is repressing, it then causes DNA to loop around the promoter; the loop is then closed by the two patches of H-NS decorated DNA (Dame *et al* 2001 & 2002, Schroder *et al*, 2002). This mechanism of H-NS repression is called H-NS bridging (figure 6.2) and is exploited when H-NS exerts its regulatory role in transcription.

H-NS does not normally exhibit sequence specific binding, but it has been shown to bind preferentially along A/T rich tracts which extend into flanking DNA sequences. This might explain the observed rigidification caused by the formation of a H-NS patch (Rimsky 2004). This ability is the molecular basis for the recognition of intrinsically curved DNA for example, AT sequences have been shown to have a large impact in overall DNA flexibility (Hangerman *et al,* 1984, 1995), which is an essential feature of many genes

that are repressed by H-NS. Bridging provides an explanation for the mechanism by which RNA polymerase is trapped in the open initiation complex at the *rrnB* P1 ribosomal RNA promoter (Dame *et al*, 2005).

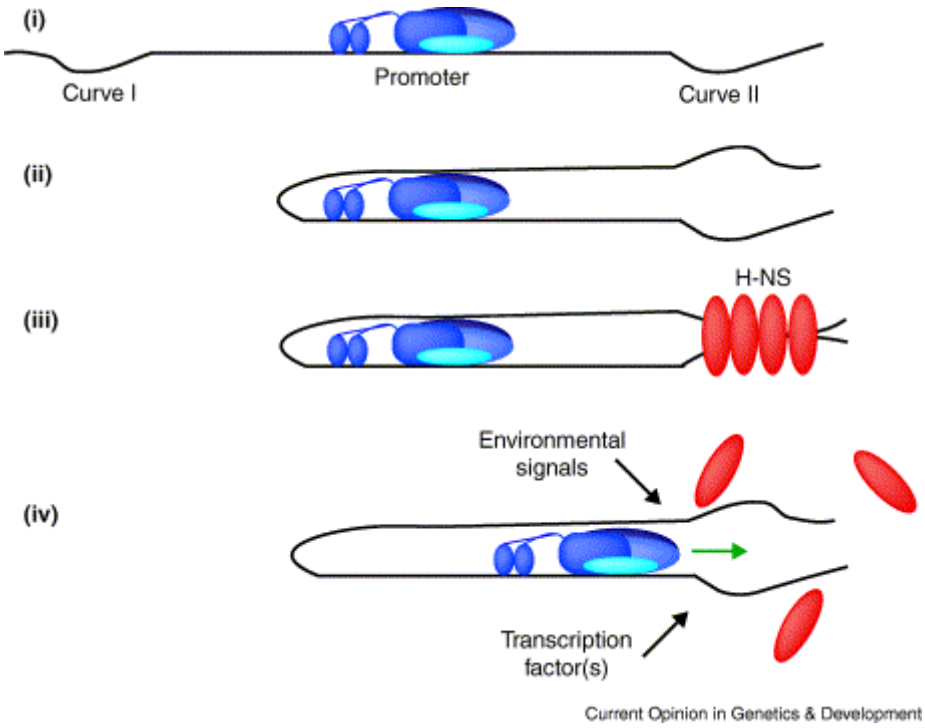

Figure 6.2: A scheme showing the repression of transcription by H-NS. (i) RNA polymerase binds to a promoter flanked by regions of intrinsically curved DNA. (ii) DNA wraps round the polymerase bring curves close together. (iii) H-NS binds to the curved regions, forming a patch/bridge that traps the polymerase and represses transcription. (iv) complex is disrupted by environmental signals or positive transcription factors. (adapted from Dorman *et al*, 2003)

H-NS has many homologues (e.g. StpA with a 58% sequence homology and MvaT) which, despite a low sequence identity, have been shown to have strong structural homology which suggests they employ similar mechanisms. They both have recently been shown to exhibit DNA bridging forming dimers between two exposed independent DNA binding domains (Dame *et al,* 2005).

6.1.3 HU

HU is a 18,000 Da protein, present at 50,000 copies per cell during the logarithmic phase. It has been discovered and resolved to a high degree of structural resolution in *Bacillus stearothermophilus*. HU protein was refined at 2.0 Å (using x-ray crystallography) and shown to be a dimeric molecule that consists of a compact body of several intertwined α-helices from which two protruding β-ribbon arms wrap around the minor groove of DNA upon binding (figure 6.3). A positively charged surface extends down the side of HU which has been directly implicated in DNA binding and important for DNA binding over a variable distance (Tanaka *et al*, 1984 & 1986, White *et al*, 1999)

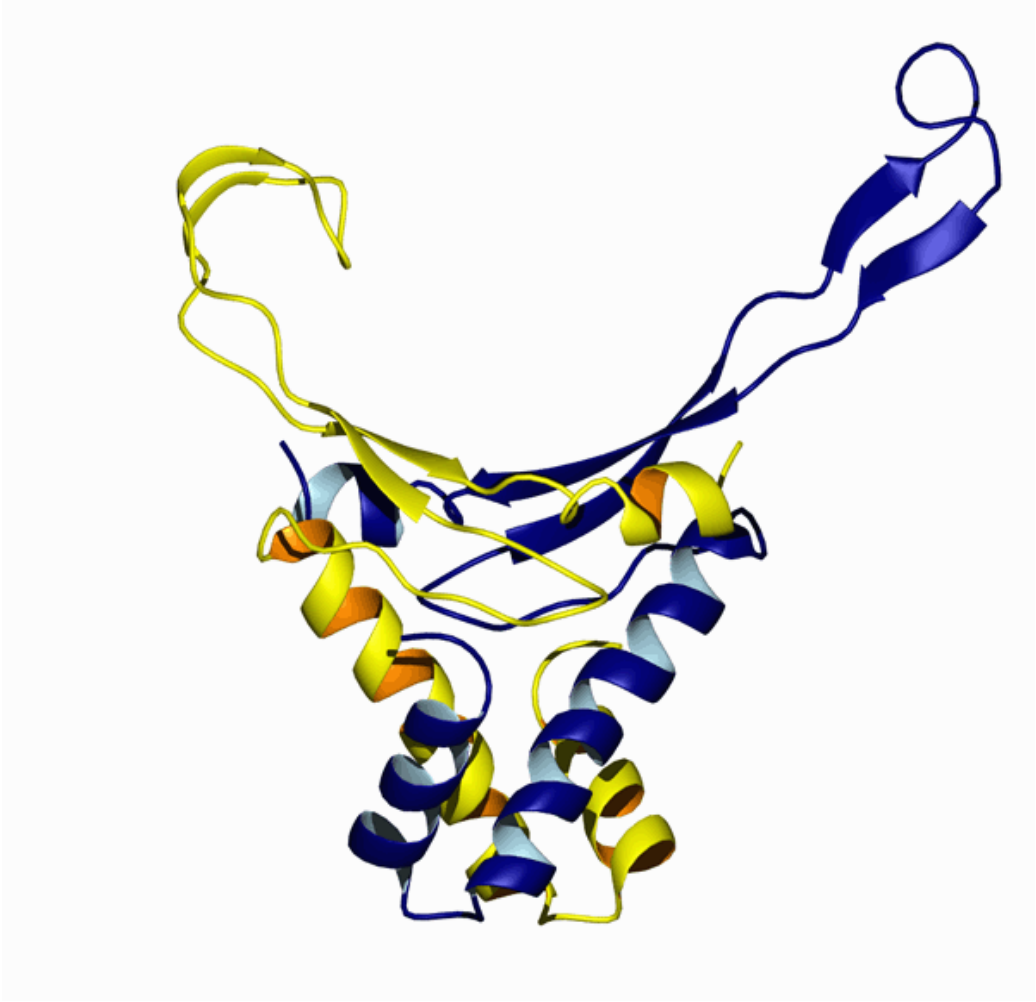

Figure 6.3: Molecular model showing the structure of HU protein in *Bacillus stearothermophilus*, highlighting the α -helix core and the protruding β-ribbon arms (adapted from White *et al*, 1999).

HU shows little sequence specificity, though it does bind preferentially to supercoiled DNA (Shindo *et al* 1992) and can constrain negative supercoils *in vivo*, this can be seen by looking at the DNA-HU co-crystal in which, in addition to bending, HU induces underwinding and writhe (Swinger *et al*, 2003).

HU protein is attracted to DNA containing structural aberrations such as single strand lesions and plays an architectural role, binding as a dimer and bending DNA. Genetic evidence links HU to promoter function but often without further molecular detail, one such example is the GalR-dependent repression of the E.coli gal promoter, where HU and DNA supercoiling combine to form a repression loop at the promoter (Kar *et al* 2001).

HU has been shown by AFM and magnetic tweezers to induce localized DNA bending and to generate condensation effects (van Noort *et al*, 2004). At lower concentrations (less than 100 nM) HU dimers induce flexible bends in the DNA that are responsible for DNA compaction of up to 50%. At higher HU concentrations (more than 100nM), a rigid nucleoprotein filament was formed in which HU appears to arrange helically around the DNA without inducing significant condensation.

Sagi *et al* 2004, using FRET analysis showed that HU does not act by introducing bends in a random orientation; their findings support features of a previous model (Tanaka *et al*, 1984) in which HU-DNA complexes form a nucleosome-like structure, with DNA lying in the periphery around a scaffold formed by HU dimers. However above a threshold HU DNA compaction gives way to rigidification resulting in a complex with higher bending stiffness than bare DNA.

The bending angle induced by HU into undistorted DNA cannot be easily estimated because of the lack of sequence specificity. In biochemical assays, the protein may not necessarily associate to the same site. AFM studies show a range of bend angles from 0-180º. This provides support to the evidence that HU acts as a flexible hinge and can accommodate a range of different bending

angles. HU is also a structural homologue of IHF, a protein that can induce bends into DNA of up to 160º when bound to its recognition site. (Rice *et al* 1996).

Genetic data and an increasing number of examples of HU bound to distorted DNA substrate (some with very high affinity) continue to suggest that HU is involved in DNA repair. The exact nature of its role and its importance is yet to be determined (Swinger *et al*, 2004).

6.1.4 H-NS and HU

H-NS is present at a constant level with respect to the DNA content of the cell whilst the level of HU fluctuates; HU helps to displace H-NS from DNA when HU is available. Consistent with this model is the observation that the HU/H-NS ratio is 2.5 in log phase and only 1 in stationary phase (Amit *et al*). This offers an explanation as to why in the stationary phase the nucleoid is more condensed.

HU and H-NS have different roles which have been shown to work antagonistically and their roles are in opposition in the nucleoid. H-NS has been shown to compact DNA whereas HU has not, it lacks the ability of H-NS to compact the nucleoid when over expressed, though it can constrain supercoils in DNA. In fact it has been shown using the atomic force microscope that HU acts to open up circular DNA molecules such as the pUC19 plasmid (Dame *et al*, 2002) (figure 6.4) whilst H-NS causes these plasmids to adopt a highly compact dumbbell shape.

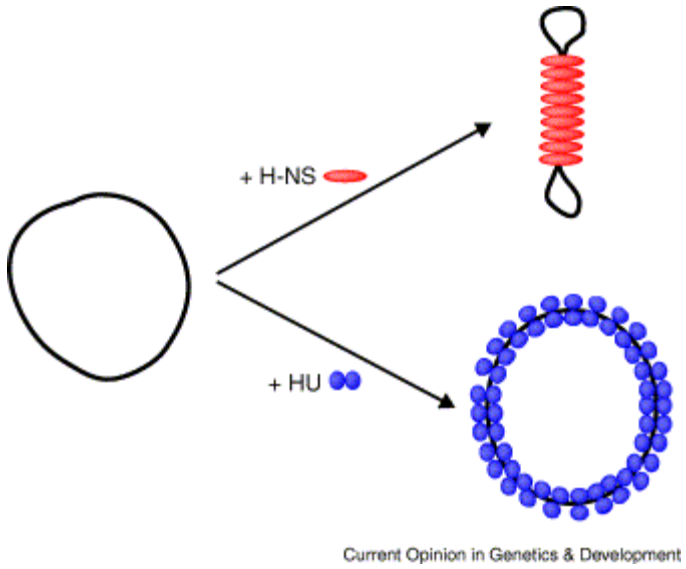

Figure 6.4: The counter influence of the proteins H-NS and HU in DNA compaction. H-NS causes the DNA to become highly compact whereas HU produces an open nucleoprotein complex (adapted from Dorman *et al*, 2003)

HU has an ability to relieve the repression activity of H-NS as shown by H-NS increased ability to repress the transcription of several genes in mutants lacking HU. It is also known that many of the H-NS promoters are organised so other DNA binding proteins can antagonise the H-NS mediated repression (Schroder *et al*, 2002) such as Fis or IHF. It is thought that HU plays a similar role but at a more general level. HU non-specifically antagonises H-NS so that regions compacted by H-NS will be of a limited size and stability, which could be important for transcriptional activity (Dame *et al* 2002).

In this chapter (based in part on - The *Bacillus subtilis* DnaD and DnaB Proteins Exhibit Different DNA Remodelling Activities; Wenke Zhang, Maria J.V.M. Carneiro, Ian J. Turner, Stephanie Allen, Clive J. Roberts and Panos Soultanas, **Journal of Molecular Biology**, Volume 351, Issue 1, 5 August 2005, Pages 66-75) the role of DnaD as global regulator of DNA will be further investigated by AFM and related to the functions of known global DNA proteins such as HU and H-NS.

6.2. Method

6.2.1 Atomic Force Microscopy

AFM images were carried out in an air and liquid environment as described in section 2.1.1 and 2.1.2.

All images were flattened and analysed as described in section 2.1

6.2.2 DnaD preparation

DnaD was purified as described in Turner *et al*, 2005

DnaD samples were diluted to between 0.5 and 0.005 µg/ml in 20mM Tris, pH 7.5, 2 mM EDTA, and 300 mM NaCl.

6.2.3 DNA Preparation

PBR322 was purified as described in section 2.4.

Plasmid samples were made up to a stock solution of 10 µg/ml in dH_2O before being diluted further to a desired concentration in 10% v/v PBS containing 0.2mM $MgCl_2$.

Digested plasmid samples were incubated at 37ºC for 4 hours with pstI restriction enzyme (Sigma-Aldrich) then raised to 75ºC to kill the enzyme. The DNA was purified with Potassium Acetate and 100% cold ethanol before being stored in EB buffer.

Lambda DNA (Sigma-Aldrich) was made into a stock solution of 1 μg/ml in 10% w/v PBS before being further diluted in PBS containing 0.2 mM $MgCl_2$ - at volumes required in individual experiments.

6.2.4 Complex Preparation

Protein DNA complexes were prepared by mixing protein samples diluted to 0.25–0.0025 μg/ml in 20 mM Tris, pH 7.5, 2 mM EDTA, 300 mM NaCl, with between 0.5 and 0.15 μg/ml of pBR322 or Lambda DNA diluted in 10% v/v PBS containing 0.2 mM $MgCl_2$ to generate varying molar ratios of protein to DNA.

Trypsin was diluted to 5mg/ml in 10% w/v PBS and added to protein DNA complexes prepared as above at concentrations as described.

All solutions were filtered through 0.2 μm pore size filters (Sartorius) prior to use.

6.3. Results

6.3.1 Linear Plasmid

Plasmid pBR322 was synthesised and digested with the *E.coli* restriction enzyme *pstI,* the digest was checked for completion by gel electrophoresis and the digested plasmid analysed by the AFM.

The digested plasmid was complexed with DnaD at two different concentrations. At a lower concentration of approximately 1 DnaD molecule per plasmid (see figure 6.5) the cut plasmid DNA still retained its linear conformation.

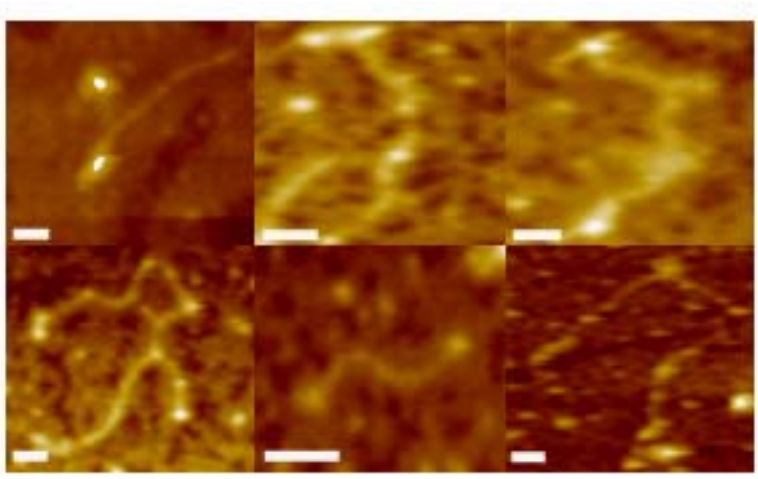

Figure 6.5: Six representative topographical AFM images in air of plasmid-DnaD complexes at a lower concentration. DnaD has bound to the ends and 'bends' in the DNA. Scale bars represent 100nm.

Although the cut plasmid still has a primarily linear conformation, DnaD molecules can be seen bound along its length. On most of the linear plasmids one or two molecules of DnaD can be visualised along its length, the DnaD is bound at varying positions, however many of the linear plasmid-DnaD complexes have DnaD bound at the AT rich 'sticky ends' where the DNA was cut by the restriction enzyme. On several of the linear plasmids there is also a point where DnaD has bound, that is in close proximity to a bend in the length

of the linear plasmid, this bend could be induced by the binding of the DnaD at that location.

This observation is of particular interest when considering at a higher concentration DnaD causes uncut plasmid DNA to undergo a major structural change and adopt an open circle conformation (chapter 5). The regions where DnaD has initially bound have not been mapped in this experiment; however there could be some links between these areas of initial binding and the areas where loci form at higher concentrations.

At a higher concentration of DnaD (100 molecules per plasmid) there is a dramatic difference in the appearance of the linear plasmid (figure 6.6) the DNA has adopted a open circular conformation as seen with uncut supercoiled plasmid DNA (chapter 4) the DnaD appears to have bound along the entire length of the DNA as judged by its much thicker appearance than naked DNA of 11.2nm as opposed to 8.2nm (figure 5.11)

DnaD is visible in the centre of the DnaD-DNA circles, as seen with the uncut plasmid, however there does appear to be less DnaD bound than the uncut plasmid. This is probably due to the lower concentration of DnaD (in this experiment compared with previous experiments, 5.10) though cutting the DNA may result in less DnaD being able to bind to the DNA. There is also a low amount of free DnaD present (figure 6.6a) that is not associated with DNA, this was also seen previously with the uncut plasmid.

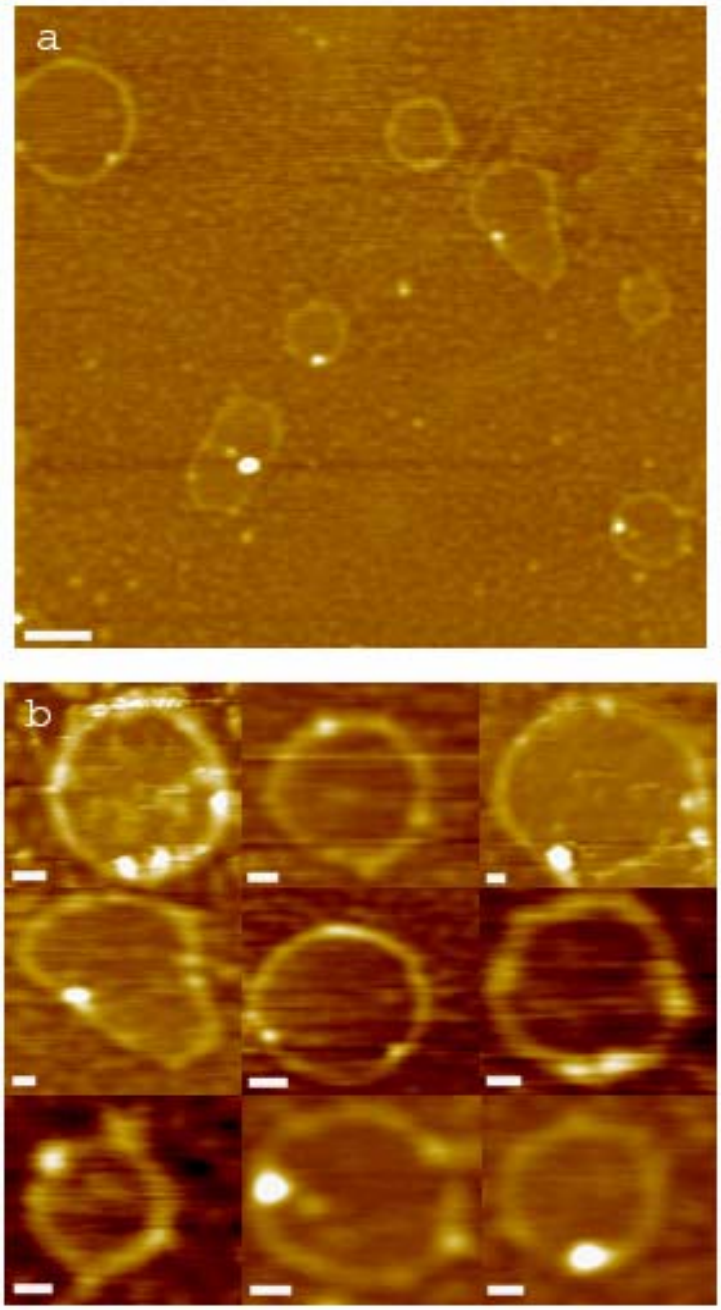

Figure 6.6: a) Representative topographic AFM image in air of linier plasmid DNA-DnaD complexes at a higher concentration. Scale bar represent 500nm. b) representative zoomed in images of linear plasmid DNA-DnaD complexes. Scale bars represent 100nm

The observation that DNA coils into a circle is quite remarkable given its linear nature, in some circles (figure 6.7) the gap between the two ends can be clearly identified. It does appear in this case that DnaD has preferentially bound to the open ends (as judged by the higher amount of DnaD present) possibly explaining why the gap (between the ends) cannot be seen in all samples. There is a point along the contour of the circle that is slightly higher than others. This could be at similar location to the loci seen with the supercoiled plasmid, the smaller size being due to the lower concentration of DnaD.

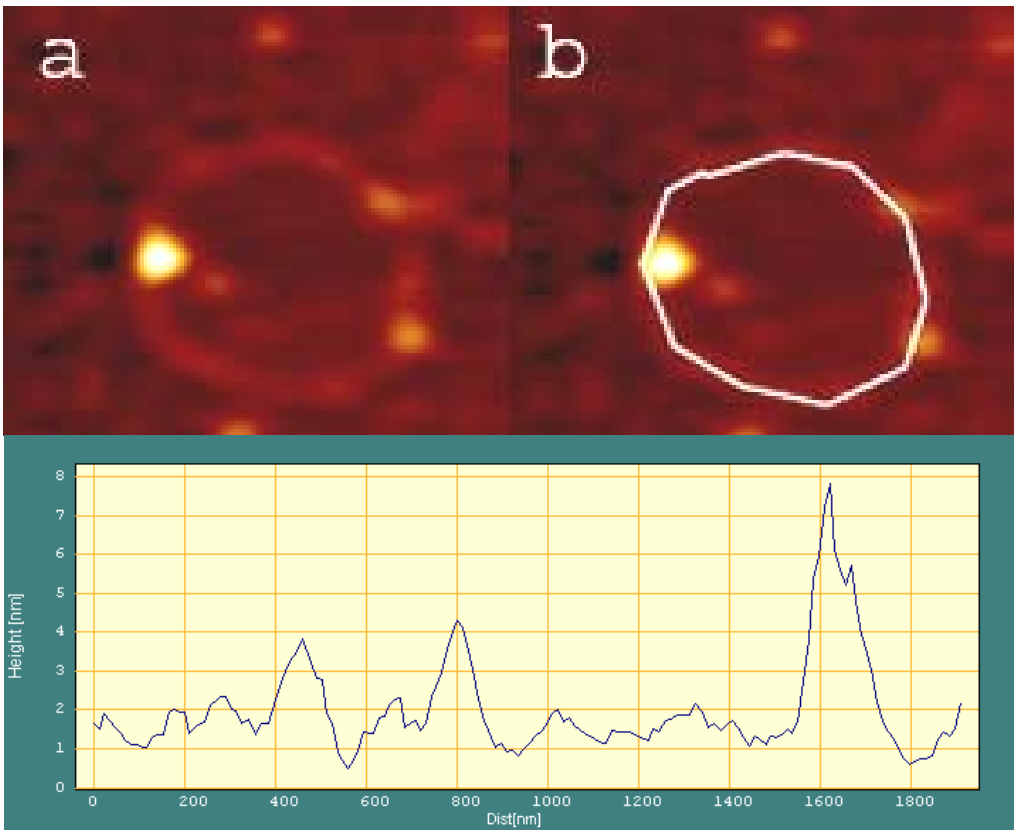

Figure 6.7: a) linear DNA-DnaD complex from figure 6 b) same complex as in a) with cross sectional line illustrating areas of measurement c) line profile of height from b) showing loci on surface as well as 'gap' between cut ends of plasmid.

The average contour length of the linear plasmid-DnaD complexes has a value of 2743 nm. Direct comparison cannot be made between the two types of complex due to the difference between supercoiled and linear plasmid. However the linear DNA-DnaD complexes have a comparable contour length to that induced by varying DnaD concentrations with supercoiled plasmid

(figure 6.8). This suggests that the DnaD effect alters the conformation of PBR322 in a very similar way, independent of whether the DNA is linear or supercoiled.

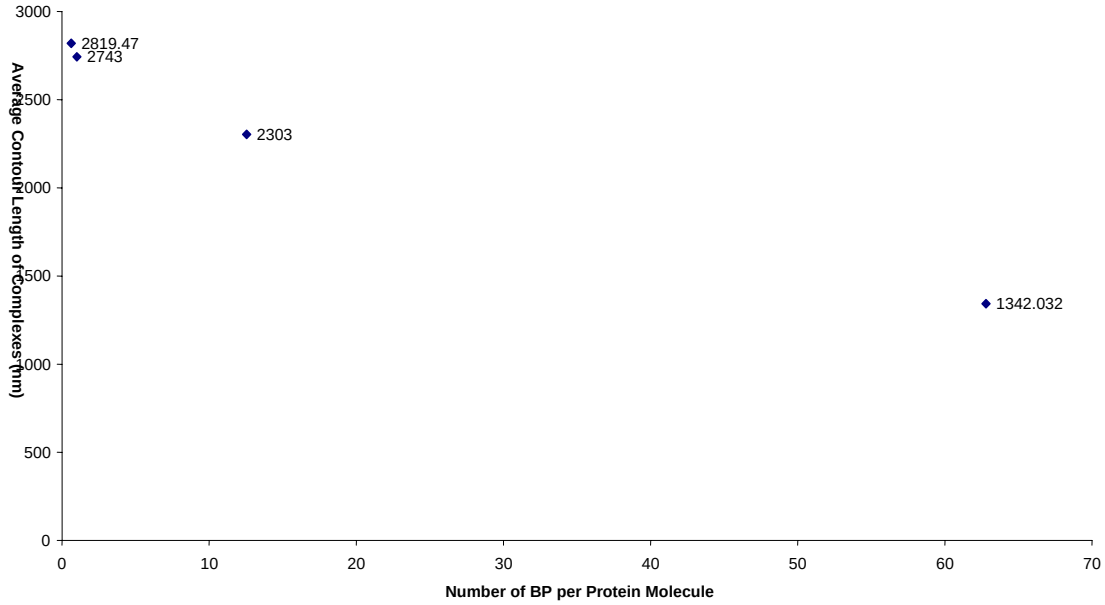

Figure 6.8: A graph showing the relationship between BP of DNA per molecule of DnaD and DNA contour length

6.3.2 Protease Experiments

If DnaD is, as speculated a global regulator of DNA replication, then it must operate as part of an equilibrium. Not only must it be able to bind DNA quickly and alter its structure but its removal should cause the reverse effect. There is a basic understanding of what causes DnaD to bind to DNA; the same cannot be said for the reverse step. It could be that *in vivo* DnaD regulates itself or is regulated by another component of the primosomal cascade (which may or may not have yet been discovered).

The reversibility of DnaD binding, in the DnaD-DNA complexes was examined by subjecting the complexes to the activity of trypsin, a 24 kDa protease enzyme over a period of time to examine if a supercoiled conformation reformed after the DnaD has been removed.

Prior to the addition of the enzyme the DnaD-DNA complexes where imaged as a control (figure 6.9)

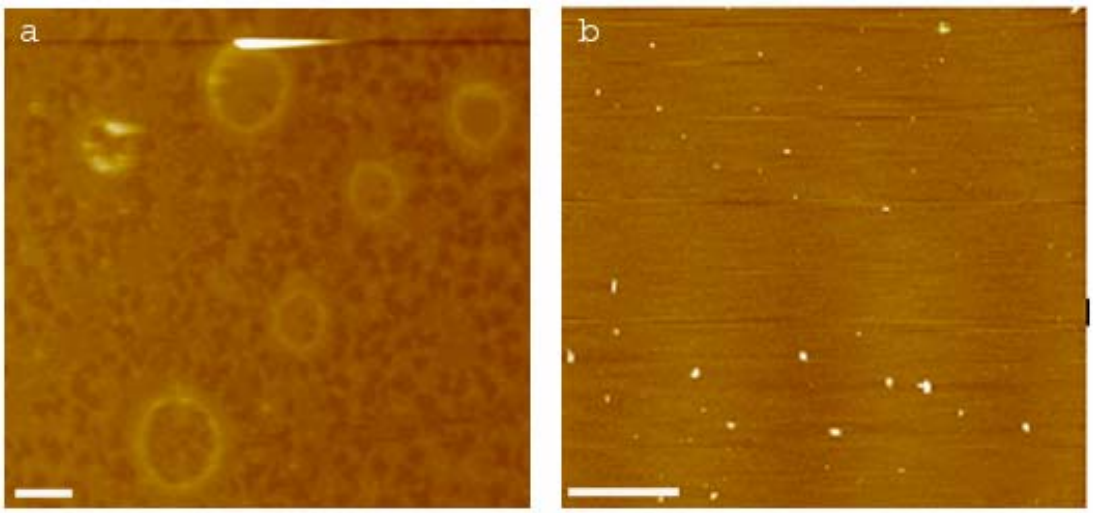

Figure 6.9: a) Control topographical AFM images in air of supercoiled plasmid DNA-DnaD complexes at time zero, prior to the addition of the protease. Scale bar represents 500nm. b) Control image of the protease trypsin. Scale bar represents 100nm.

The DnaD-DNA complexes were evident with an average contour length of 1563 nm, this value falls with in the previously generated graph showing the ratio of DnaD to protein (figure 6.10). It appears that the size of open circles induced by DnaD is dependent on the ratio of DnaD to base pairs. A control image of trypsin (figure 6.9b) shows trypsin to be a small protein of approximately 6nm in the x and y dimensions (previous EM studies show trypsin to be 3.8nm in length, Diaz *et al*, 1996).

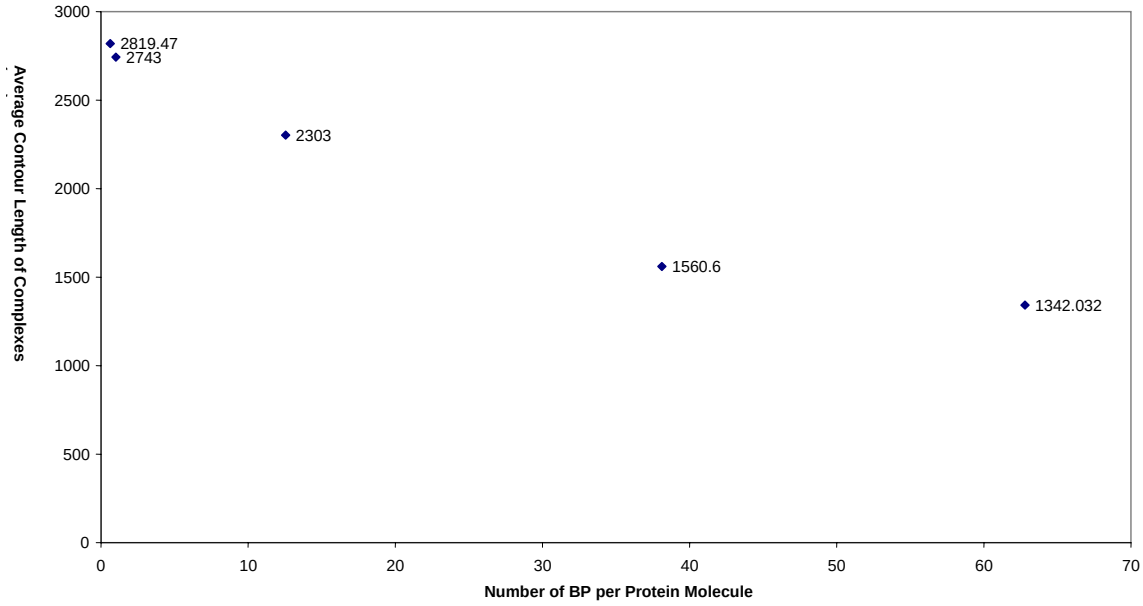

Figure 6.10: A graph showing the relationship between BP of DNA per molecule of DnaD and DNA contour length.

After addition of the enzyme to the complexes the solution was left at 37°C for 24 hours and then imaged again (figure 6.11) The complexes are still predominantly circular in geometry (note some complexes have had more protein digested than others) although some complexes appear to have lost some of there rigidity and much of the DnaD that was present in the centre of the complexes has been broken down. This would explain why some of the complexes appear looser in their circle shape, since DnaD is no longer acting to push out the DNA into a rigid circle.

In a few complexes without any DnaD remaining in the centre of the complex stabilising the circle structure it appears as if DnaD molecules have linked two

strands of dsDNA. Approximately 78% (from 34 complexes) of the complexes are still in the circle geometry previously described; others have undergone more digestion and are discussed below.

After 48 hrs in the presence of the enzyme the circle structure of the complexes are not evident, the most abundant species ~82% are linear like fragments that in many cases are curved slightly (figure 6.12). It appears, as seen after 24 hours, that the enzyme has now degraded all the DnaD normally bound to the centre of the complexes, leaving the DnaD bound along the length of the DNA itself as the only DnaD in the complex. The linear like structure could be due the bridging effect occasionally seen after 24 hours. Also seen in this sample are a number of chains (figure 6.12c) that have begun to coil, this could be where the enzyme has degraded DnaD at certain points along the DNA itself allowing DNA to coil back to its native state.

After 72 hours the enzyme has degraded most DnaD along the length of the DNA allowing it to coil and reform supercoiled structure in some cases (figure 6.13). Some DnaD may still be present as judged by the thickness of the DNA and the presence of loci (which could be DnaD or trypsin) on some of the supercoils, it could be that DnaD is in someway sterically protected by being bound to the DNA making it more difficult for the enzyme to degrade. Of the DNA that has not fully supercoiled, all of it has at least partial coiled (figure 6.13c). One interesting example appears to have one molecule of DnaD on its entire length preventing it from supercoiling, although this height difference could just be from overlapping strands of DNA (figure 6.13c, right image).

Although the action of trypsin appears to vary from complex to complex (shown by the varying populations at different temperatures), in general it appears to have degraded the DnaD not directly associated with the DNA, in the centre of the complexes first, causing the complexes to adopted a more loose circle form. As more DnaD is removed the DnaD starts to locally cross-link the DNA. Finally the DnaD bound to the DNA is removed, exposed regions begin to coil until enough DnaD is removed for the DNA to form a supercoiled structure.

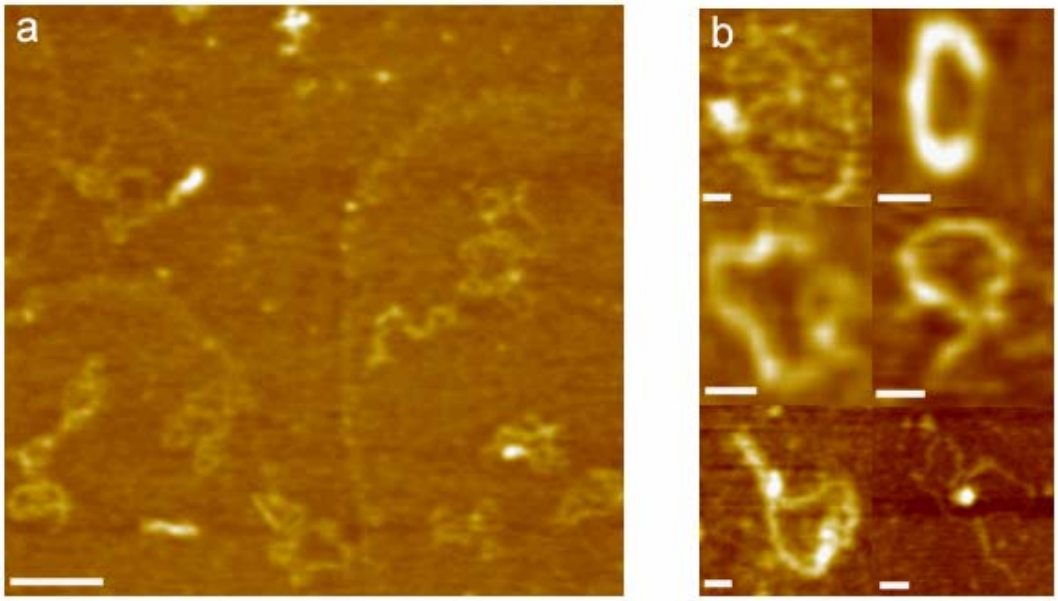

Figure 6.11: a) A representative topological field view in air of plasmid DNA-DnaD complexes after 24 hours in the presence of the protease enzyme trypsin. Scale bar represents 500nm b) zoomed in sections of individual complexes showing some loose circle formations and evidence of DNA bridging. Scale bars represent 100nm.

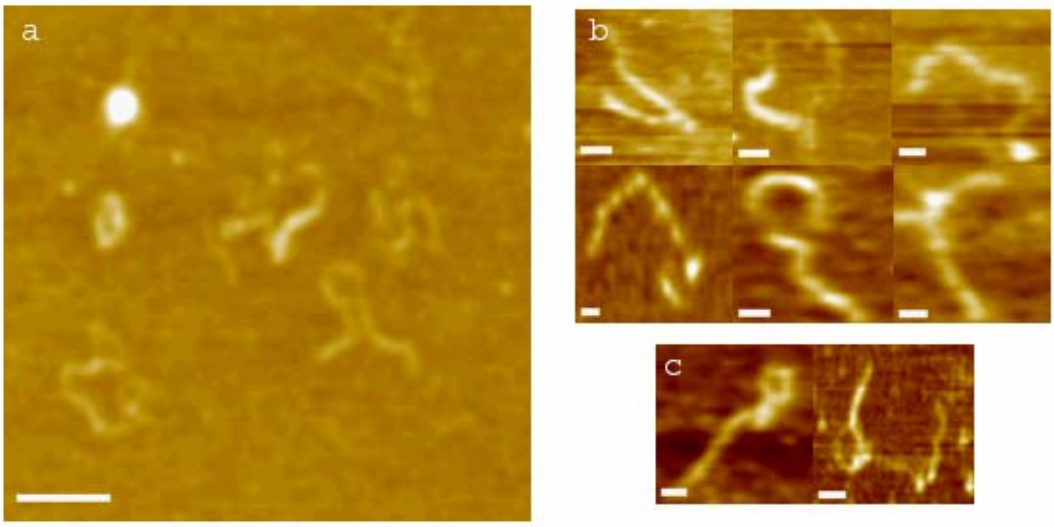

Figure 6.12: a) A representative topological field view in airof plasmid DNA-DnaD complexes after 48 hours in the presence of the protease enzyme trypsin. Scale bar represents 500nm b) zoomed in sections of individual complexes showing linear like DNA fragments and c) partially coiled DNA. Scale bars represent 100nm.

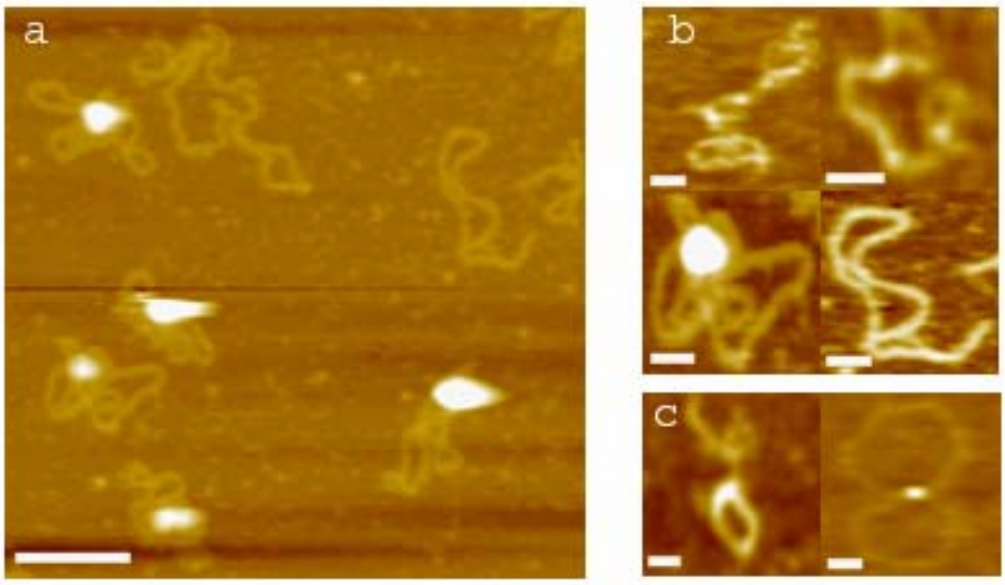

Figure 6.13: a) A representative topological field view in airof plasmid DNA-DnaD complexes after 72 hours in the presence of the protease enzyme trypsin. Scale bar represents 500nm b) zoomed in sections of individual complexes showing supercoiled DNA and c) partially coiled DNA. Scale bars represent 100nm.

6.3.3 Lambda DNA

The effects of DnaD have so far only been studied on one type of DNA the plasmid pBR322. The effect of DnaD was studied with linear lambda DNA of varying fragments sizes to identify if its effects on DNA are universal and to see if the circle structures seen with the plasmid-DnaD complexes, were related to the plasmid structure.

Control images of lambda DNA, sizes ranging from 3530bp to 21226bp (figure 6.14a) show the varying fragments present in the population whilst a higher magnification image (figure 6.14b) shows the detail of one DNA fragment. DnaD mixed with lambda DNA at a concentration of 4 molecules of DnaD per fragment causes no apparent major structural change to the lambda DNA however many of the linear fragments do appear to have a build up of a few molecules of DnaD bound to them. The location of this build up may be at a specific sequence, it is impossible to say in these experiments because of the differing sequences of the various fragments.

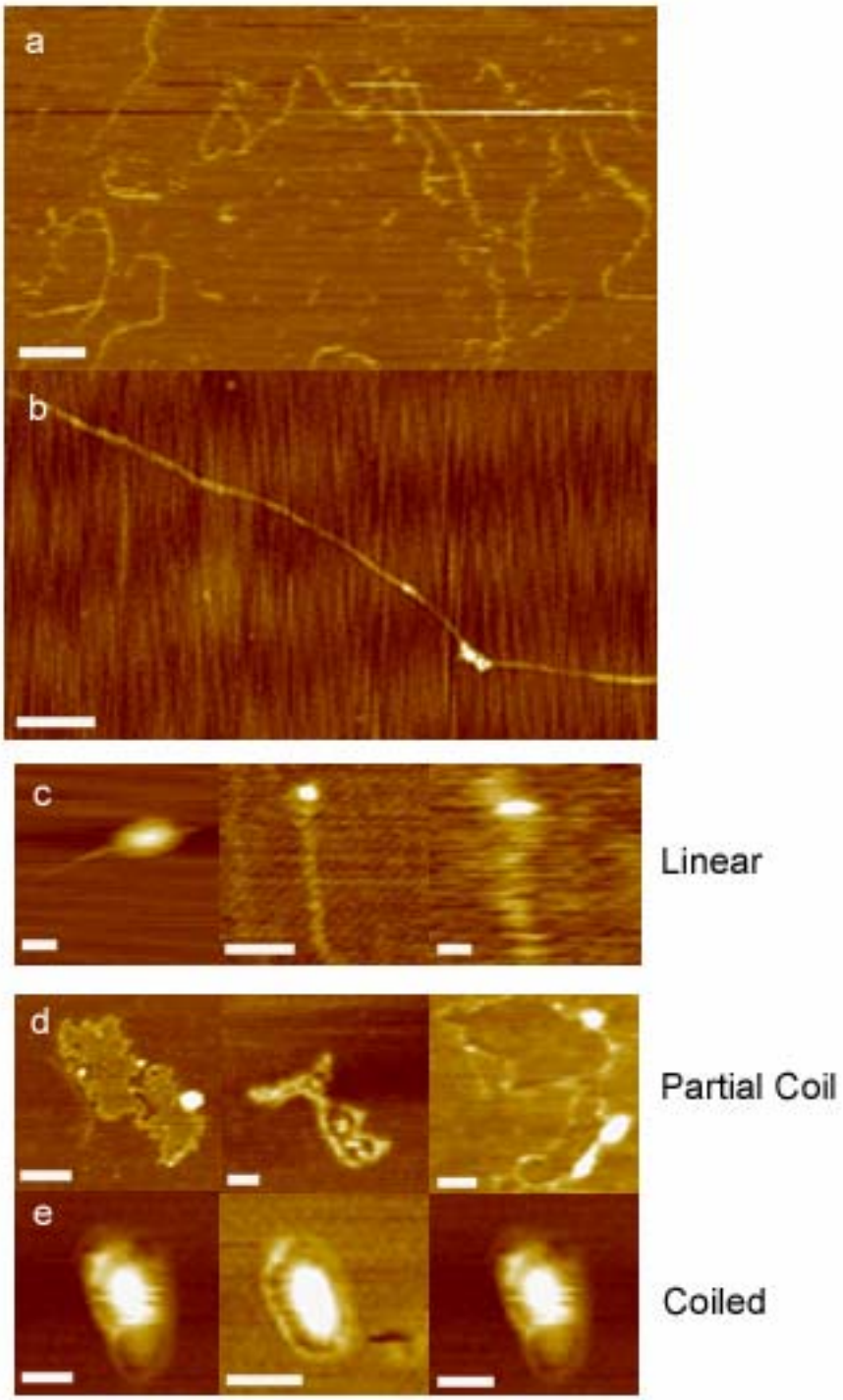

Figure 6.14: a) Representative topographical field view in air of lambda DNA showing a selection of fragments. Scale bar represents 500nm b) the detail of one fragment of lambda DNA. Scale bar represents 100nm. c) representative images of lambda DNA plus DnaD at the lower concentration, showing linear fragments with DnaD bound. Scale bar represents 100nm. d) representative images at the higher concentration showing partially coiled and f) fully coiled structures. Scale bar represents 100nm.

At a higher concentration of DnaD, 400 molecules of DnaD per DNA, there is a marked change in the structure of the lambda DNA with a mixture of structures which are partially coiled (figure 6.14d) and coiled (figure 6.14e). The partially coiled structures have a roughly circular shape with evidence of DnaD in the centre of the complexes, and at various points around the DNA contour length. The fully coiled structures are quite small 120nm (compared to previously seen coiled structures) but there is a build up of DnaD at the centre. It is possible that some of the smaller fragments of lambda DNA have completely coiled whilst the larger fragments have only partially coiled (average contour length of the partially coiled structures 1168nm). It appears that the DnaD induced DNA effect may be universal and affect all types of DNA.

6.4. Discussion

It has been shown previously that DnaD alters the structure of supercoiled plasmid DNA causing it to adopt an open circular conformation. This function has been linked to a global role in the architecture of DNA, which is essential for DNA and chromosome replication. In order to further investigate this hypothesis the interaction of DnaD with linear DNA (mimicking the *in vivo* situation), the interaction of DnaD with other sequences of DNA (to check the effects previously seen are not exclusive to pBR322) and the reversibility of the DnaD induced effect (when DnaD is removed from DnaD-DNA complexes) were investigated in this chapter.

6.4.1 Linear Plasmid

pBR322 cut with the restriction enzyme pstI and then bound to DnaD formed similar circle complexes to those seen with the supercoiled plasmid. Initially at low concentrations of DnaD there was some binding to the plasmid but not enough to cause coiling, the DnaD seems to have preferentially bound to the opened ends of the DNA. This could be due the fact pstI cuts at a sequence that leaves exposed A and T residues at the sticky ends, and as previously discussed DnaD binds to AT rich regions of the DNA *in vivo*. There also appears to be a point along the length of the plasmid where DnaD has bound. As seen for the supercoiled plasmid there are two AT rich regions in pBR322 sequence where DnaD may preferentially bind (figure 5.10). By digesting the plasmid with different restriction enzymes and noting the position of these loci, it may be possible to identify the region(s) to which DnaD preferentially binds. Interestingly where DnaD is bound there does seem to be a bend in the DNA. This could just be due to the orientation of the DNA on the mica surface but has parallels with other global regulator proteins that are known to preferential bind to bent DNA (Dame *et al* 2001) and to induce bends in DNA (Rice *et al*, 1996).

It is possible that initial DnaD binding which could be sequence specific (figure 6.15), causes small bends in the DNA, and as more DnaD binds these bends are exaggerated until DnaD is attracted to DnaD at the opposite end of the strand, causing the DnaD to form a circular structure with the DNA. As additional DnaD is added it binds to the now circular DNA and the inside of the circle, 'pushing out' the structure, as seen for the supercoiled plasmid.

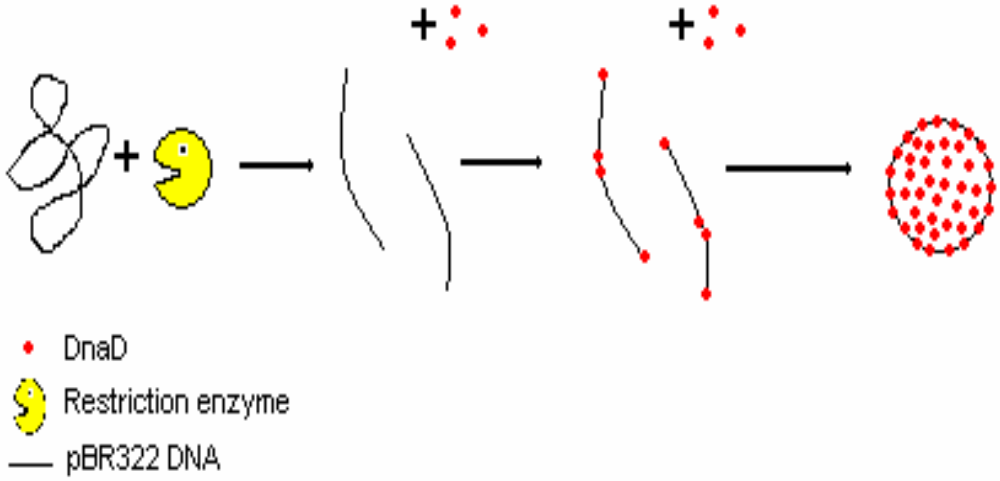

Figure 6.15: A proposed scheme for the mechanism of DnaD on restriction enzyme digested plasmid DNA

The DnaD-DNA complexes visualised are similar to those seen for the uncut supercoiled plasmid, and those visualised on pUC19 with HU (Dame *et al,* 2000) except that in some of the plasmids a gap can be seen between the two cut ends where the ends are not visible this is possibly due to DnaD binding in the vicinity.

The average size of these complexes is interesting, especially when combined with the additional data generated from the protease experiment (figure 6.11) because it is consistent with the data from the supercoiled populations. Although further concentrations with both supercoiled and digested populations need to be investigated before further comparisons could be made between the two populations, the data suggests that there is a relationship between the contour of the DNA in the complex and the amount of DnaD present. If this could be proved and related to the amount of cellular DnaD

during DNA replication some approximation of the size of the 'opening up' effect could be established.

6.4.2 Protease experiments

Digesting bound DnaD from DnaD-DNA complexes caused the DNA to reform its original supercoiled structure. The process over a period of 72 hours showed a gradual transition (figure 6.16). At first the trypsin degrades some of the DnaD in the centre of the complexes causing the circles to become slightly deformed and more flexible, as DnaD degradation continues the DnaD in the centre of the circle is removed causing the DnaD bound along the DNA's length to bridge across the gap, a similar effect has been studied in detail with H-NS (Dame *et al*, 2005). As the DnaD bound directly to the DNA is removed, the DNA can start to coil until almost all of the DnaD is removed allowing a complete recovery of the supercoiled structure.

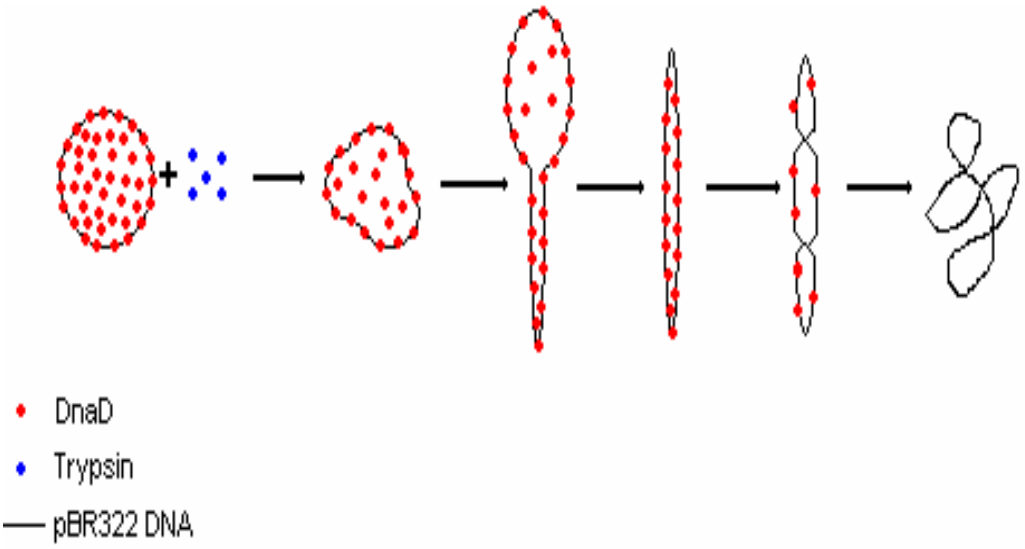

Figure 6.16: A Theoretical scheme for the digestion of DnaD from plasmid DNA-DnaD complexes and the reformation of supercoils.

It is not known why the DnaD bound to the DNA is better protected against the action of the enzyme, in fact it may be just as susceptible, for example as one of the DnaD bound to the DNA is removed one of those in the centre takes its place. In the future attacking the initial DNA-DnaD complexes with a

DNase would show if the DNA is protected by the protein or not. It can be seen in some of the complexes that one molecule of DnaD can stop the DNA resuming a supercoiled geometry. There is variation between the individual complexes after 72 hours with some complexes having formed supercoiled structures; this could be due to differences in the amount of DnaD bound or localisation of trypsin in the experiments. However, the trend described above accounts for approximately 75% of the complexes over the time course of the experiment and shows the recoiling process in general; *in vivo* the situation would take place over a much shorter time period because *E.coli* for example, can replicate its entire genome in 40 mins (Helmstetter *et al*, 1987).

The action of DnaD on the plasmid pBR322 occurs on both supercoiled and linear fragments and the action has shown to be reversible on supercoiled complexes. In order for this effect to be considered global it needs to be shown that it is not exclusive to the pBR322 DNA sequence. Investigating the interaction of DnaD with lambda DNA shows a similar trend to that seen with the linear plasmid.

6.4.3 Lambda DNA

At lower concentrations of DnaD the protein binds to specific locations along the length of the lambda fragments. Unlike the linear plasmid fragments there is no specific binding at the ends (as they are different sequences), there are no structural changes evident and some linear fragments appear to have no DnaD bound at all. At a higher concentration structural change is evident. There is a mixture of partial condensed structures and tightly coiled circles. Both structures display similar properties to the complexes seen with pBR322 such as DnaD build up in the centre of the complexes and DnaD bound along the contour length. There was almost 100% conversion of lambda DNA from a linear molecule to a partially coiled molecule. It could be that DnaD acts with a similar mechanism on lambda and linear plasmid (figure 6.17), and that the different structures could be accounted for by either; not all the DNA being converted to a complete circle (which it was at the same concentrations for linear plasmid) or by the varying fragments being altered to differing degrees.

i.e the smallest fragments being fully circular in shape whilst the largest fragments (larger than linear plasmid) only partially coiled, on account of there not being enough DnaD present.

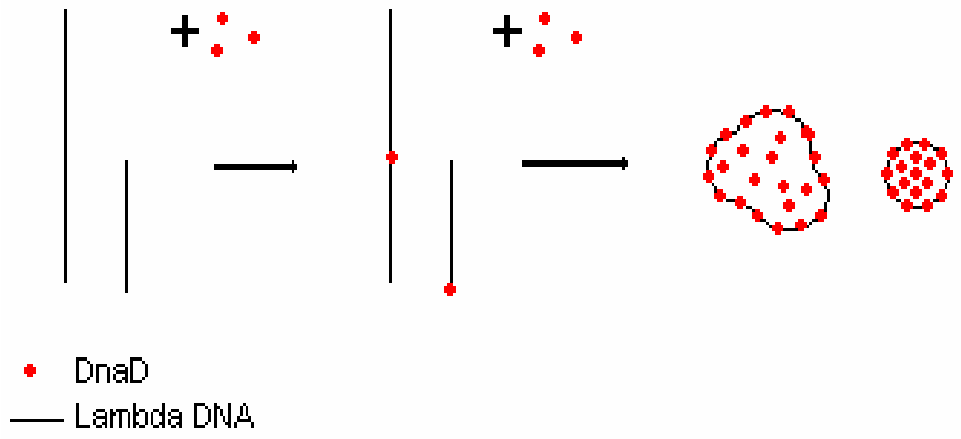

Figure 6.17: A theoretical scheme for the coiling of Lambda DNA by the action of DnaD

6.4.4 Summary

DnaD appears to universally alter DNA (figure 6.18) causing DNA of any length or conformation to form a opened form. This would allow *in vivo*, components of the primosomal cascade to bind and start DNA replication. The effects visualised may not be as dramatic *in vivo* because there is may be less DnaD present than in these experiments (currently no information exists on the cellular amount of DnaD) and in addition other components of the primosomal cascade may act to counter the effects of DnaD. The removal of DnaD as shown by protease experiments on the supercoiled complexes causes the initial DNA structure to reform, and presuming the same would happen for linear induced complexes, DnaD does appear to act as a dynamic regulator.

It is not certain if DnaD regulates itself in terms of binding and unbinding *in vivo* or if a component of the cascade does this. Two potential candidates are the helicase binder DnaI, and the membrane protein DnaB. As DnaI brings the helicase to the exposed to region of DNA opened up DnaD, it is known to

interact with DnaD to disrupt the bond between itself and the helicase. This interaction could also cause the unbinding of DnaD now that the helicase is bound. DnaB is a membrane associated protein that recently has been shown to act to compact DNA and work antagonistically with the action of DnaD (Zhang *et al*, 2005).

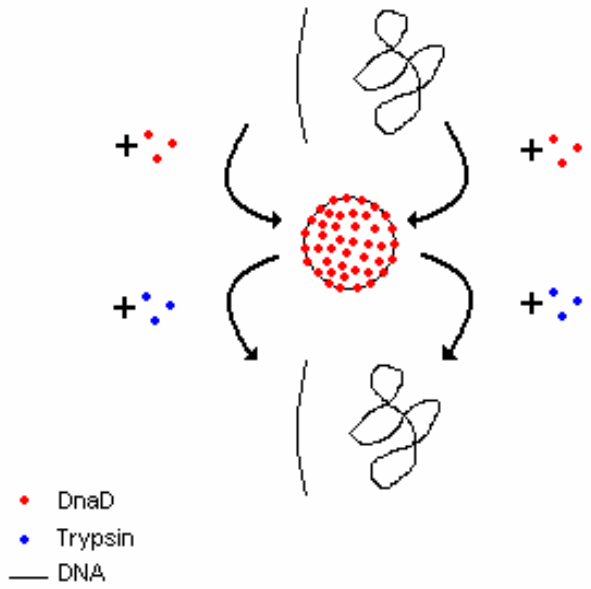

Figure 6.18: A schematic summary showing the proposed universal architectural effects of DnaD on DNA

6.4.5 DnaD as a global regulator

HU protein has been discovered and characterised in *Bacillus* whilst H-NS protein is yet to be isolated. Based on the evidence presented here DnaD could be a homologue of HU or H-NS. Despite little sequence homology it has been shown that the H-NS, StpA and MvaT proteins all have similar roles (Dame *et al* 2005). There are a number of direct structural comparisons between DnaD and H-NS and HU; Both DnaD and HU constrain negative supercoils, HU protein is critical in assisting the DnaA protein in the unwinding of DnaA at the *oriC* (Bahloul *et al*, 2001) DnaD has been shown to have a similar role at the *oriC* and PriA and H-NS and DnaD are both dimeric proteins that form higher order oligomers.

DnaD functional comparisons with the histone-like proteins HU and H-NS suggest DnaD may have an analogous role to one or both of them. There are similarities with both besides from its essential role in DNA replication. At high ratios of DnaD-DNA evidence shows that DnaD acts like HU to open up DnaD complexes (Dame *et al*, 2002). At lower concentrations as seen in the linear and lambda DNA experiments, there is no structural change, though DnaD seems to be linked to bends in the DNA, as seen for H-NS (Dorman *et al*, 2004, Rimsky, 2004). In the protease experiments it appears as though DnaD bridging could be taking place (Dame *et al*, 2005).

It could be that DnaD works as one part of a pair of proteins in a similar relationship to HU and H-NS. There is currently no data on the amounts of DnaD present in a cell at various points in it cycle, but if it acted in a role similar to HU it would be expected for there to be a large increase in its number during the logarithmic phase, when DnaD is recruited to the *oriC* and PriA sequences. Taking into account the recent advances in the understanding of the DnaB protein (Zhang *et* al, 2005) we suggest that DnaD and DnaB work together (figure 6.19), one compacting and one opening up the DNA in an antagonistic relationship. As DnaD binds to exposed DNA it allows the binding of components of the primosomal cascade, once the helicase is bound; DnaD is removed or its effects countered by DnaB, as it does it causes the

DNA to compact trapping the helicase and primase on the DNA in a similar mechanism seen for RNA polymerase in *E.coli* (Dame *et al*, 2005).

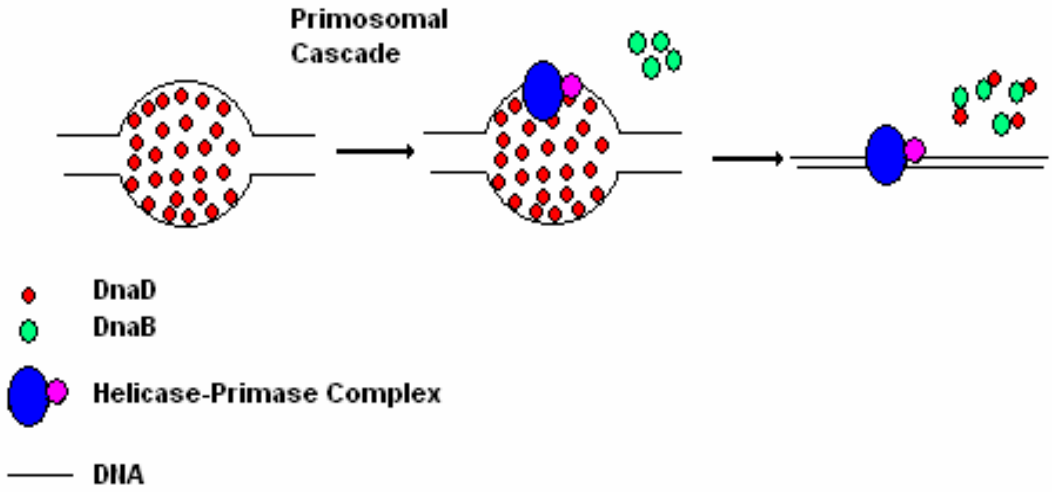

Figure 6.19: A speculative model for the interaction of DnaD and DnaB in the *Bacillus* Primosome. DnaD binds to a AT rich sequence of DNA opening up the DNA, allowing the primosomal cascade to take place and the helicase-primase to bind. DnaB has been shown to associate with DnaD, its effect on the DNA or the DnaD causes the DnaD effect to be reversed. This closes the opened up DNA trapping the helicase-primase on the surface.

7.Cryogenic Atomic Force Microscopy: A New Tool for Structural Biology

7.1. Introduction

7.1.1 General

The AFM since its initial development in 1986 has clearly become an established technique in a broad range of scientific disciplines. High-resolution imaging has been achieved on a variety of macromolecules such as immunoglobulins and membrane bound cholera b toxin oligmers showing surface features as small as 1-2nm (Mou *et al*, 1995), native purple membrane imaged to sub nanometer resolution (Muller *et al* , 1995) and the chaperonin protein GroEL with a resolution achieved up to 1nm (Mou *et al*, 1996). These systems all have extensive inter subunit contacts and a very regular shape that aids imaging as the biomolecules are less effected by deformation from the AFM probe.

Some of the reasons for the limited success to date with a wider range of biomolecules can be attributed to technical aspects of AFM (such as sharpness of the AFM tip), however two largely intrinsic factors (sample softness and thermal motion) are also partially responsible;

1) Sample softness – At room temperature the compression force of a tip in air or solution can damage and deform the sample resulting in an increase in the contact between the tip and hence poorer resolution (see figure 7.1). Although the force of the tip is only 0.1-1nN the pressure can be in the MPa range due to the small contact area. One theoretical study suggests that a probe force as low as 10^{-11}N is required to reduce deformation to an acceptable level (Persson, 1987). This distortion effect can be reduced by close 2D packing of the molecules being examined, due to a decrease in the contact area between molecules or balancing the attractive forces between the tip and specimen with the repulsive electrostatic force (at close distances) as seen on purple

membrane (Muller *et al*, 2000), but it is difficult to achieve for macromolecules that contain many flexible domains/subunits. Salts in the buffer containing the biomolecule of interest can act to counteract the electrostactic forces governing tip-sample interaction and reduce deformation (Scheuring *et al,* 2001, *Shao et al*, 1996).

2) Thermal motion - At room temperature macromolecules exhibit several types of thermal motion, transitional motion, rotation of the molecule and the random change of molecular shape. This can cause smearing/averaging out of the AFM image, which makes high resolution imaging extremely problematic, especially given the relatively slow acquisition speed of AFM. In addition when imaging in liquid thermal convection in the liquid, due to uneven temperature distribution may effect resolution (Takaki, 2004, Thomson *et al*, 1996, Nakamoto *et al*, 2001).

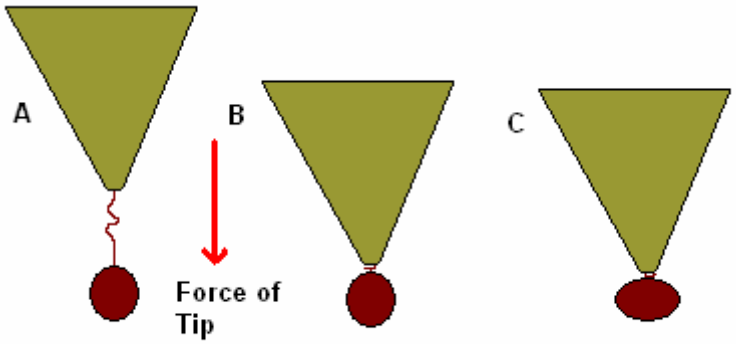

Figure 7.1: A schematic diagram showing how the force of an AFM tip can deform biomolecules and effect high resolution imaging. A) An ideal situation where the tip images the side chain of the biomolecule. B) No imaging of the side chain but biomolecule undeformed.C) No image of side chain and biomolecule deformed by force of tip.

Operation of the AFM at subzero temperatures could help minimize the effects of these two main intrinsic factors that are hindering high resolution imaging because, at cryogenic temperatures thermal motion would be greatly suppressed and the Young's modulus of the sample (elasticity) would be significantly higher. For example, protein and DNA Young's modulus at

cryogenic conditions are between 10^3 and 10^4 times of that at room temperature (Yang *et al*, 2003).

There has been a proof of principal development of a cryogenic AFM by Shao *et al*, (1996) their system was operated under ambient pressure in a cryogenic gas. The system had moderate success demonstrating the first molecular resolved images at low temperatures (figure 7.2). However, there where problems, at ambient pressures the level of contamination of the samples was high and freezing caused major ice formation. Removing water by dehydrating the samples caused structural damage. The AFM described in this chapter was designed to explore methods of overcoming some of these problems by operating in a vacuum on samples frozen in vitreous ice.

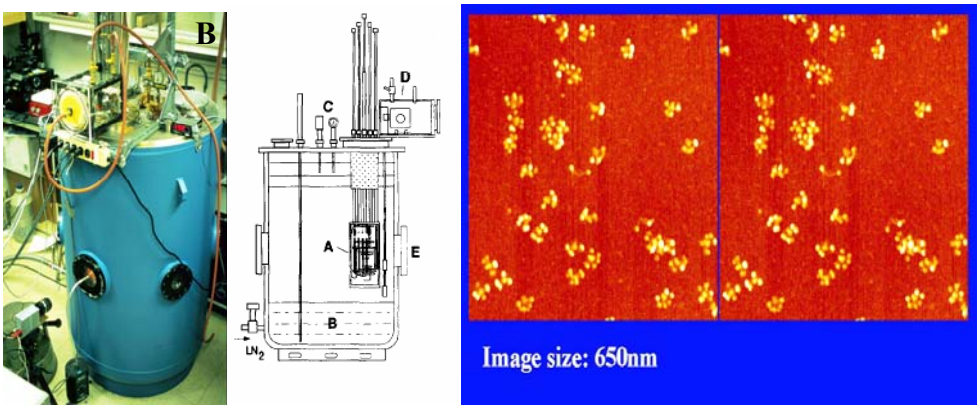

Figure 7.2: A) The cryogenic AFM developed by Prof. Shao at the University of Virgina, VA, USA. B) A schematic of the main components of the AFM C) A topographic cryogenic AFM image of the c1q1 component of human complement on the system, showing its high resolution structural compatability.

This system builds upon established cryomicroscopy techniques used in cryogenic SEM and TEM, such systems help identify the key considerations in converting a technique to enable cryogenic imaging. Key aspects of cryogenic sample preparation and imaging that were considered include the following.

7.1.2 Freezing Process

The most vital step of preparing samples for analysis by cryomicroscopy is the freezing step, as seen by the limitations of the previously developed cryogenic-AFM. The cooling rate must be sufficiently fast (ideally carried out in less than 10^{-9} seconds) so that the specimen is preserved with few or sufficiently small ice crystals (section 7.1.5) that can disrupt and rupture biomolecules. It is extremely difficult to totally prevent ice crystal formation in all but very small specimens (due to the slightly different freezing rates across larger samples). Chemical fixation or cryoprotectants can be used to prevent ice formation but these can cause an array of artefacts and in the case of cells lead to shrinkage.

7.1.2.1 Cryogens

A range of cryogens are currently used in cryomicroscopy to rapidly cool specimens (Table 7.1). As well as the temperature and cooling rate of the cryogen other factors such as the cost, flammability and availability along with the method of cooling, the types of specimen being prepared and the microscopic technique being used need to be considered.

Cryogen	Boiling Temperature (°C)	Mean cooling rate (10^{3} °C s^{-1})
Ethane	-118	-260 to -258
Ferons	-118	-267 to -265
Liquid Nitrogen	-196	-273 to -268
Slush Nitrogen	-210	-272 to -271
Propane	-190	-263 to -261

Table 7.1: A table showing some of the properties of cryogens used in cryomicroscopy

Ethane and propane are potentially the best cryogens as they have the highest cooling rate, however both cryogens are very inflammable and have flash points (the minimum temperature at which the liquid produces a sufficient concentration of vapour above it, that forms an ignitable mixture with air) well below zero (-130°C and -104°C respectively) and in order to be used safely they must be used in an atmosphere of liquid nitrogen, which makes them complex and expensive to use. These cryogens are hence normally used for the freezing of large samples such as cells.

Liquid nitrogen, however is non-flammable and relatively cheap upon comparison with other cryogens. Liquid nitrogen is commonly used as a cryogen in cryomicroscopy despite its low sample-cooling rate. Nitrogen slush, which is a mixture of solid and liquid nitrogen, can be used in conjunction with liquid nitrogen to increase this cooling rate. It is created by placing liquid nitrogen in a vacuum desiccators and reducing the pressure. One problem with liquid nitrogen and other potentially good cryogens such as liquid helium which has a very low melting point and a high heat conductivity is that film boiling occurs readily, causing the gas to coat any warmer object with a layer of insulating gas which lowers the cooling rate of the cryogen significantly (Echlin, 1992, Steinbrecht *et al*, 1987).

7.1.2.2 Freezing Methods

Several techniques exist for freezing the sample as quickly as possible, by bringing it into contact with a cryogenic surface.

1) High-speed plunging immersion – A simple technique that is frequently used in cryomicroscopy, it involves plunging a specimen into a suitable liquid cryogen as quickly possible. This technique is most commonly used for very small or thin specimens, with immersion into a cryogen such as liquid nitrogen causing freezing with few ice crystals, for larger specimens a more effective

cryogen such as liquid propane must be used or the freezing will be ineffective, and ice crystal formation will damage and distort the sample.

2) Slam freezing - a rapid technique in which a plunger brings the sample at speed into contact with a block, maintained at a cryogenic temperature, causing the sample to freeze. Provided the whole of the block is at a constant temperature this technique can reduce ice crystal formation due to the simultaneous touching of the surface by all parts of the sample.

3) Spray freezing – This approach is commonly used for freezing cells in cryomicroscopy. The cells are placed in a droplet of fluid that is sprayed with liquid nitrogen cooled propane; the cells will quickly freeze because of the large surface-to-volume ratio. After freezing the propane is extracted under vacuum and butyl benzene is added to form a paste. This technique achieves high freezing rates and reduces ice crystal formation in the cells, but due to the extraction is time consuming.

4) Jet freezing – In this technique a specimen is held between two metal sheets through which nitrogen-cooled liquid propane is propelled at high pressure causing the specimen to be frozen on both sides simultaneously.

5) High-pressure freezing - In this method a sample (often used for larger specimens) is placed between two metal planchets, placed in a high-pressure chamber, into which liquid nitrogen is forced under pressure to freeze the specimen. This high pressure causes a reduction in the cooling rate and therefore ice crystal formation (Echlin, 1992, Steinbrecht *et al*, 1987, Erk *et al*, 1997).

7.1.3 The Cryogenic Microscope

The cryogenic microscope will vary largely depending on the microscopic principle being used; however there are a number of consistent features that are found in all types of cryomicroscopy.

1) The cold stage – A cold stage is needed to keep the samples at a constant low temperature after freezing whilst analysis takes place. If the sample were to warm ice crystals could form or the sample could become softer, leading to deformation of the sample. The cold stages of cryogenic-SEM and TEM are often small modules fixed on the specimen platforms that are either liquid nitrogen or liquid helium cooled. The liquid nitrogen cooled modules (also the approach used in the cryo-AFM) described here can operate in one of three ways.

a) Liquid nitrogen is fed from a dewar outside the microscope to a small sealed reservoir close to the low-temperature module sitting on the microscope stage. The reservoir is then connected to the cold module by a flexible conductive coupling (often oxygen free, high purity copper, in the form of braid threads) to allow it to be moved on the stage. Such modules can theoretically achieve temperatures as low as -163°C though rarely get much colder than -123°C.

b) Liquid nitrogen can simply be circulated directly around the specimen area. Doing this generates temperatures as low as -193°C but problems can arise in feeding the nitrogen into the system whilst still allowing for sufficient specimen flexibility.

c) The cold stage is supplied with dry nitrogen gas that has been chilled by passage through a metal coil immersed in a dewar of liquid nitrogen. A low temperature of -178 to -173°C can be achieved without the delivery problem associated with liquid nitrogen.

2) The specimen stage – Most cryomicroscopy techniques operate under vacuum, and need to be able to quickly transfer the specimen to the cold stage after freezing, to prevent the sample heating. In cryogenic SEM there are two types of specimen stage, a drawer type in which a stage runs on rails into the microscope chamber. To load a specimen the chamber is brought up to atmospheric pressure and the specimen is loaded *al fresco*. A second type has the stage permanently fixed inside the microscope chamber and access is via an airlock, these stages are sturdy and allow a large freedom of movement (this approach is used in the cryo-AFM).

3) Anticontaminator – Contamination is a serious concern in cryomicroscopy, although vacuum systems are efficient there are potential sources of contamination, any contamination will be drawn to the coldest surface available, for example the sample. In cryomicroscopy anticontamination plates are normally located around the specimen stage, in cryo-SEM and TEM they are large copper plates colder than the working temperature of the module (attracting contaminants), this is achieved by supplying the anticontaminator with liquid nitrogen before the cold stage.

7.1.4 Post-Freezing

Cryomicroscopy allows a number of post-freezing strategies to be employed that allow increased structural details to be obtained that could not be easily visualized in air.

1) Fracturing - Specimens can be either fractured by tensile stress or shear forces (such as a knife cleaving the surface) to examine their internal structure (as in cells). The fracture pathway is largely unpredictable, however if present it often follows the inner, hydrophobic zone of the lipid bilayers. To be visualized in cryogenic SEM the fracturing process can be carried out in units that stand alone or are attached to the microscope, most units have fracturing, etching and/or surface coating capabilities.

2) Cryogenic-sectioning - This technique allows more predictable cuts to the sample. Slices are generated using either a cryoultramicrotome (glass or diamond knife) or a cryostat microtome and sliced into ultrathin (50 - 100nm), thin (100 - 1000nm) or thick (1-2 μm) slices. This technique is most often used with analysis of tissue samples.

3) It is also possible to remove frozen water from specimens by freeze-drying (where the ice is removed by low-temperature vacuum sublimination) or freeze-substitution (where the ice is dissolved in an organic solvent) this can be carried out on samples with a high water content, such as cells. Both these procedures are prone to cause major artefacts and structural damage to the specimen and must be carried out very carefully and on a specimen-to-specimen basis. The removal of the ice is often combined with replacement using a liquid resin (Erk *et al*, 1997, Walther *et al*, 1995, Steinbrecht *et al,* 1987).

7.1.5 The Structure of Ice

Cryogenic microscopy involves freezing samples at subzero temperatures. A common cause of artefacts is crystalline ice, hence an understanding of ice formation and structure is useful in developing strategies to prevent it forming in cryogenic samples.

There are 7 million cubic miles of ice on earth (2.14% of the total water). The structure of ice varies largely, depending on the temperature and pressure at which it is formed; there are at least nine different crystalline forms. Of these types, two crystalline (hexagonal, cubic) and amorphous ice can be expected to found at the temperatures and pressures utilised in cryomicroscopy (Table 7.2).

Ice State	Lower Temp. (°C)	Upper Temp. (°C)	Transition at upper temp.
Hexagonal	-273	0	Melts
Cubic	-273	-90	> Hexagonal
Amorphous	-273	-120	> Cubic

Table 7.2: A table showing the conditions at which, the forms of ice present in cryomicroscopy occur under

1) Hexagonal Ice – This is the most energetically favourable structural arrangement of ice and the most common type of ice seen in cryomicroscopy (as well as everyday life e.g. ice cubes and snowflakes). Its structure is a hexagonal lattice, each unit cell of the lattice consists of four oxygen atoms hydrogen bonded to four other oxygen atoms (~ 0.276 nm away) placed at the vertices of a regular tetrahedron (figure 7.3). The smallest polygons are the non-planar hexagonal rings of water molecules that can be in either the 'boat' or 'chair' form. The shafts running through the crystal (the centre of the hexagonal rings) account for the fact that hexagonal ice is less dense than the water from which it is formed.

The arrangement above is very stable at low temperatures, but as the temperature increases towards the melting point of the ice (0°C) there can be fluctuations in the molecular orientation (there are 10^{23} possible orientations for the hydrogen atoms in a crystal) which could affect imaging of samples and in retrospect the way samples are manipulated.

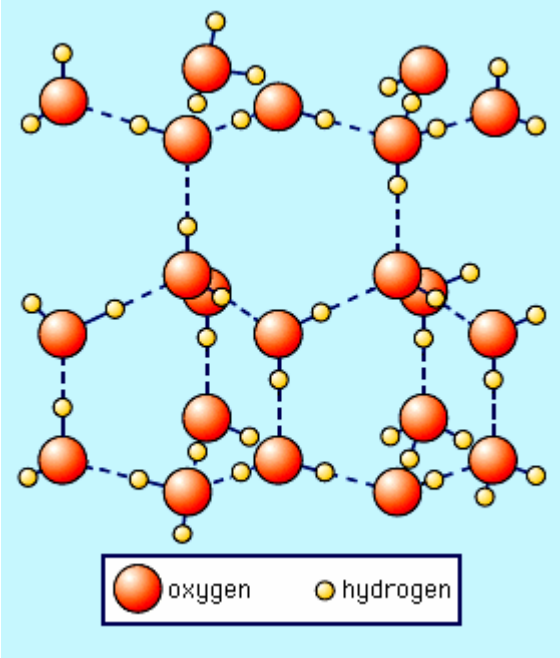

Figure 7.3: The structure of hexagonal ice (red spheres oxygen, yellow spheres hydrogen) (adapted from Echlin *et al*, 1977)

2) Cubic Ice – This form of ice is not thought to form naturally. Cubic ice is a meta-stable form of ice that exists between -80°C and -150°C. It can be formed in cryomicroscopy when either water vapour is allowed to condense on a clean substrate maintained at below -130°C or, more commonly when amorphous ice is warmed above -150°C. Cooling hexagonal ice below -80°C does not form cubic ice

Structurally, cubic ice is similar to hexagonal ice with the exception that the unit cell dimensions are different and each cell contains eight rather than four hydrogen atoms (figure 7.4). When cubic ice is heated above -80°C hexagonal ice is formed, only very small dimensional changes occur as this happens, but the transition could distort a sample in cryomicroscopy.

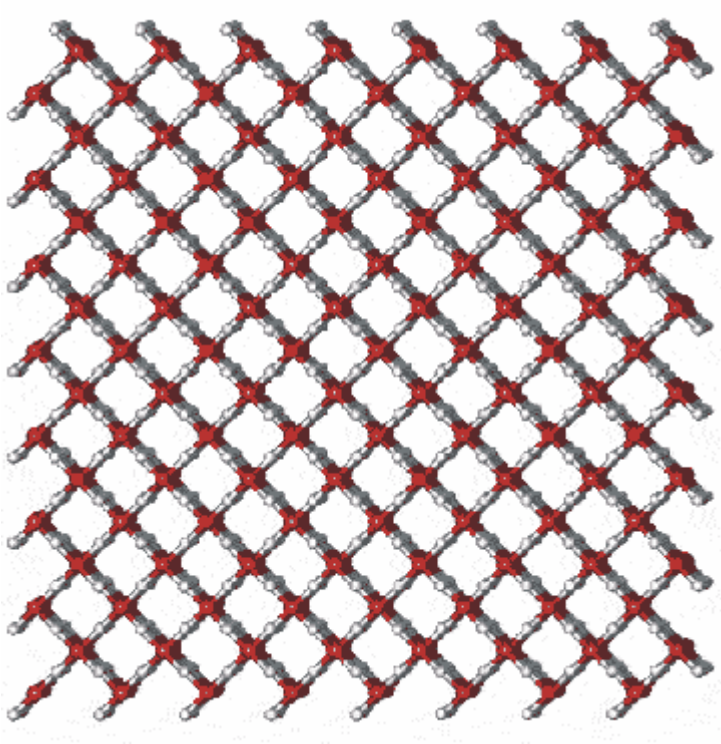

Figure 7.4: The Structure of cubic ice (red spheres oxygen atoms, white spheres hydrogen atoms) (adapted from Echlin *et al*, 1977)

Amorphous ice – This is a non-crystalline formed by the very rapid freezing of water or by condensing water vapour on a surface at less than -160°C. It occurs where water molecules landing on a surface lose there energy and remaining at the point of contact because there is not enough energy to migrate over the surface to positions of minimal potential energy which favors crystallization. Amorphous ice is the ideal type of from a cryomicrocopists point of view as it has the minimal effect on the structure of the sample (Echlin, 1992).

In cryomicroscopy, freezing the samples at temperatures and pressures and over timescales where amorphous ice is most likely to form is the ideal situation. This and making sure the sample is kept at a constant temperature help prevent the sample being to distorted by ice formation.

7.2. The Cryogenic AFM

7.2.1 General

An AFM designed for use at cryogenic temperatures and a high vacuum (figures 7.5 and 7.6) was custom designed and built by Dr. Shugang Liu and Prof. Clive Roberts, Laboratory of Biophysics and Surface Analysis, School of Pharmacy, University of Nottingham to a skeletal stage. This will be described along with further developments and applications by the author.

7.2.2 Operation Overview

The cryogenic-AFM system consists of three main components;
1) The AFM (modified for use at low temperatures)
2) The cryogenic chamber (for sample storage and imaging)
3) A slam freezer (for sample preparation).

The operation of the system is primarily by computer, separate modules control image acquisition and alignment of the laser on the cantilever (figure 7.6). In addition a cryogenic control, which is regulated by a temperature control monitor linked to three sensor/heaters in the AFM chamber unit, is responsible for maintaining the vacuum temperatures in the cryogenic chamber.

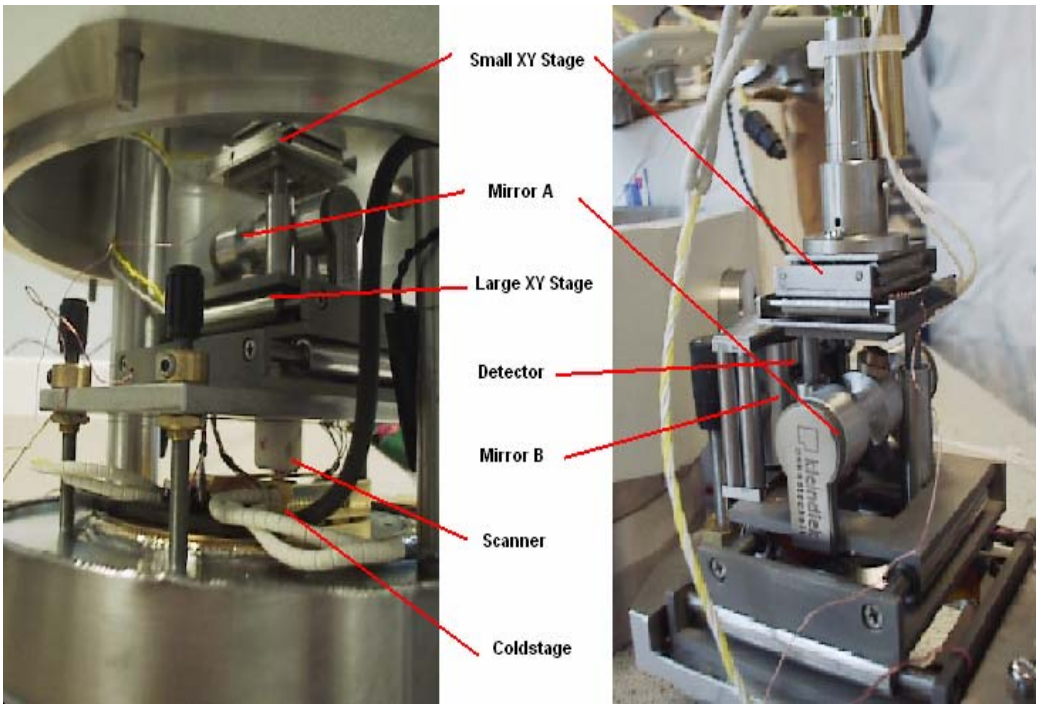

Figure 7.5: Photographs of the cryogenic-AFM, inside the chamber (left) and out of the chamber (right) with key features as described in the text highlighted.

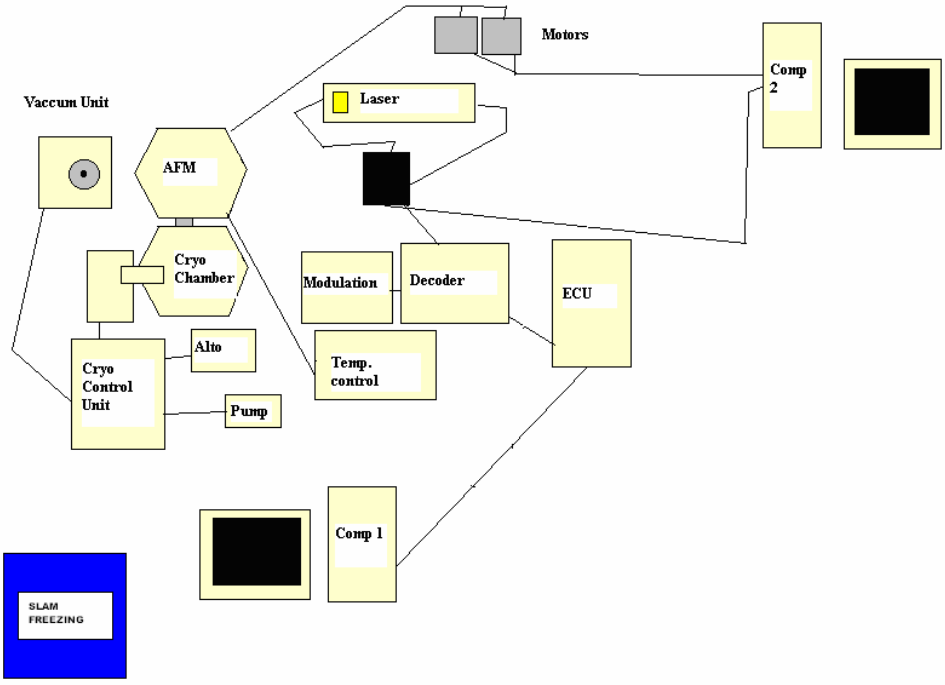

Figure 7.6: An overview of the cryogenic-AFM set-up. Connections are shown as black lines. The diagram is not to scale

7.2.3 The AFM

Movement in the AFM is controlled by five stages. The stages are controlled by custom built micromanipulator motors (Kliendiek Nanotecnik, Reutlinger, Germany) through an interface with a computer.

1) A small xy stage for moving the laser to focus on the cantilever
2) A large xy stage for moving the whole AFM (to move the tip over the sample)
3) A Z stage for lowering the tip (to contact the sample)
4) Two rotating stages which control movement of the mirrors.

The laser is focused via the small xy stage through a split mirror (A) on to the sample surface (figures 7.5 and 7.7) The laser is then reflected back to the mirror and on to a second mirror (B) that reflects the laser onto the detector. The mirror is at an angle of 2° from the normal line.

The AFM temperature is maintained via a reservoir of liquid nitrogen below the sample, which is supplied through an external dewer. This liquid nitrogen helps maintain the cold stage at a specified temperature. The cold stage is two tiered (figure 7.8) so that the lower part, is in closer proximity to the liquid Nitrogen reservoir and as a result it is slightly colder than the upper part (specimen stage). This causes it to act as a cold trap/anticontamination device.

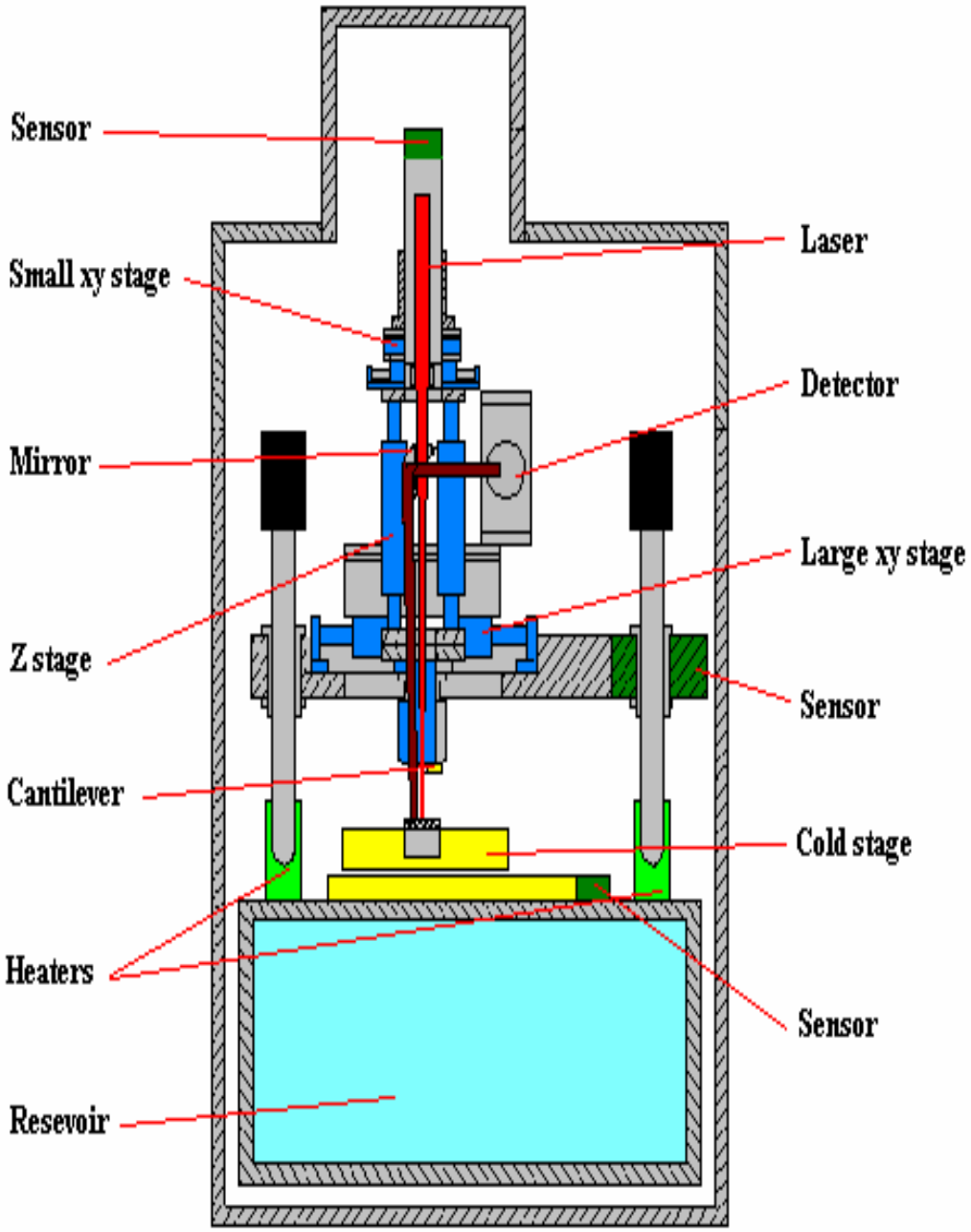

Figure 7.7: Schematic diagram of the cryogenic-AFM in the AFM chamber. Key described in the text are coloured and labelled

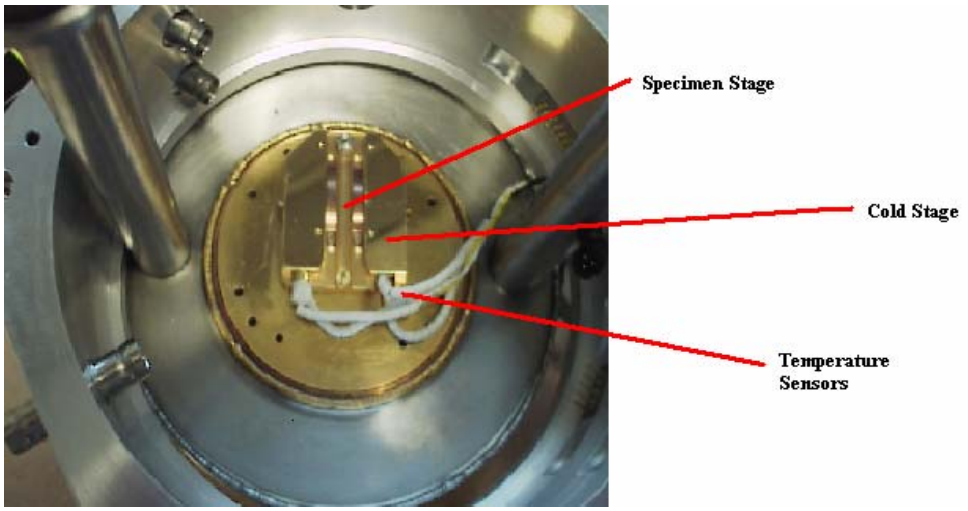

Figure 7.8: A photo of the cold stage of the cryogenic-AFM with key features highlighted

The cold stage as well as the cryogenic chamber is regulated by three heater/sensors in the chamber. These heater/sensors are connected to the cold stage (in two places) and the AFM frame, an additional sensor is located near the laser (to avoid it over heating in vacuum). These sensors are regulated by three internal heat modules (figure 7.9) located on the AFM frame legs as well as an external temperature control box.

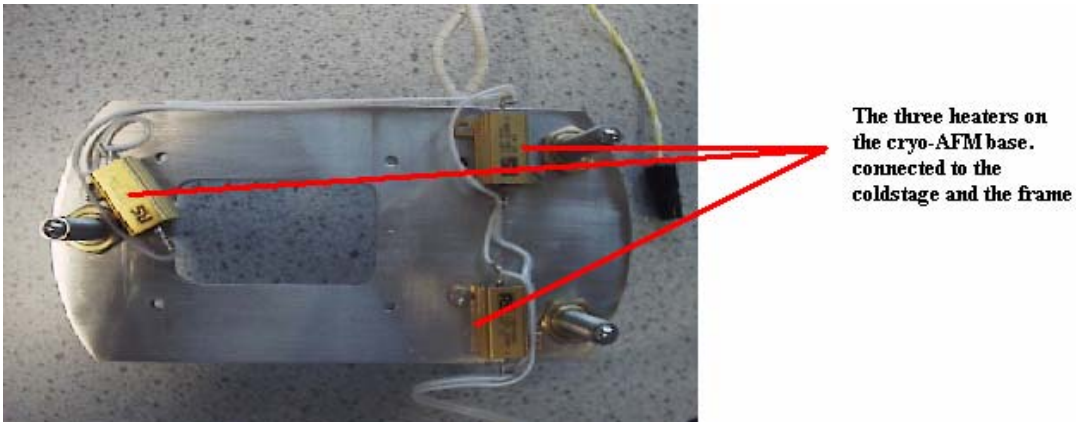

Figure 7.9: A photo showing the heater modules attached to the legs of the cryogenic-AFM

7.2.4 Sample Freezing

Samples are prepared in a CF100 (LifeCell Corporation, New Jersey, USA) (figure 7.10) which operates by the slam freezing principle with liquid nitrogen as the cryogen (7.1.2.2). The CF100 is supplied with ultra pure nitrogen to prevent the cryogenic block acting as a cold trap for any contaminants which maybe present; this is achieved by reversing the vacuum with the ultra pure nitrogen. The ultrapure nitrogen also has the additional function of preventing pre-cooling of the sample before it reaches the cryogenic block by forming a protective layer over the block, stopping the cold layer of gas that would form above the cryogenic block freezing the sample in the fractions of a second before it hits the block (figure 7.10).

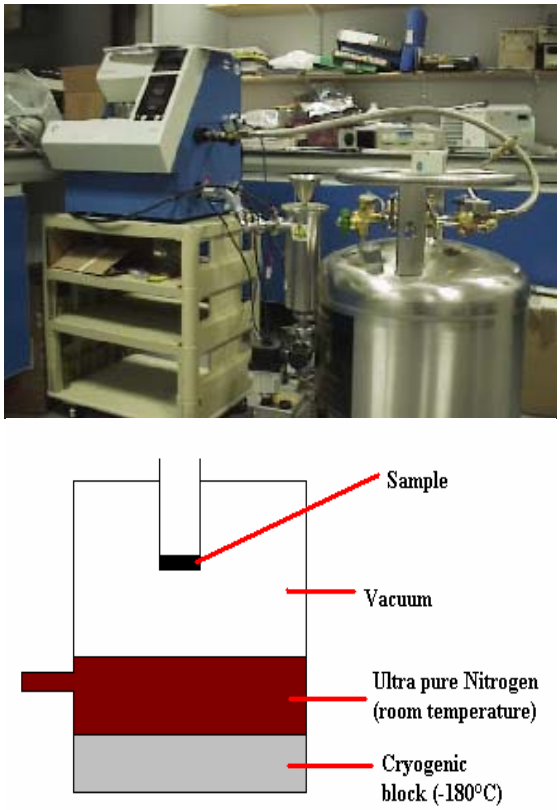

Figure 7.10: The CF100 system; a photo (left) and a schematic diagram of the basic operating principles (right) as described in the text.

7.2.5 The cryogenic chamber

The cryogenic chambers are ALTO 2500 (Gatan, Oxford, UK) specially modified for use with the Cryogenic-AFM (figure 7.11).

Figure 7.11: A photo of the cryogenic chamber and AFM chamber

There are two ALTO chambers, a cryogenic chamber and a AFM chamber. The cryogenic chamber is where; after it has been frozen, a sample is placed to maintain its temperature. In this chamber the temperature can be lowered and raised and also other post freezing strategies such as fracturing (7.1.4) can be carried out in this chamber

The chamber also contains an anticontaminator (figure 7.12) similar to the one in the AFM chamber, this anitcontaminator is supplied with liquid nitrogen before the cold stage, preventing contaminants being attracted to the specimen.

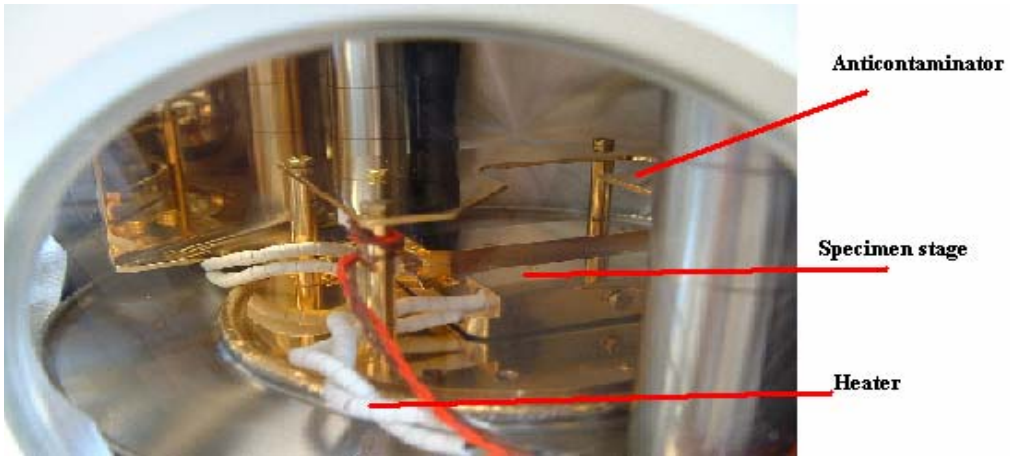

Figure 7.12: A photo of the inside the cryogenic chamber with features described in the text highlighted

7.2.6 Operation

Operation of the Cryogenic-AFM comprises of four steps

1) Aligning the laser

2) Preparing the vacuum and cryogenic chamber

3) Sample freezing

4) Imaging

7.2.6.1 Aligning the laser

The laser is aligned via an custom built interface (figure 7.13)

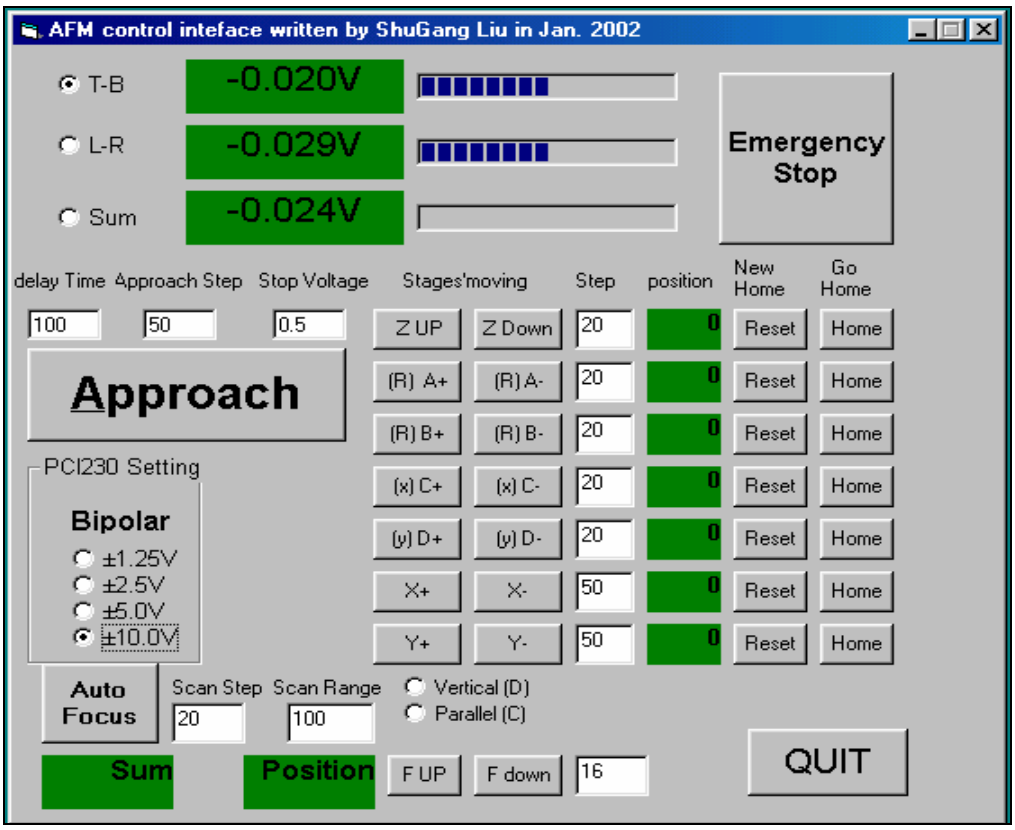

Figure 7.13: The custom designed interface for operation of the cryogenic-AFM. Various features are described in the text.

The interface has 5 controls that control each of the stages the mirror and the detector (figure 7.14).

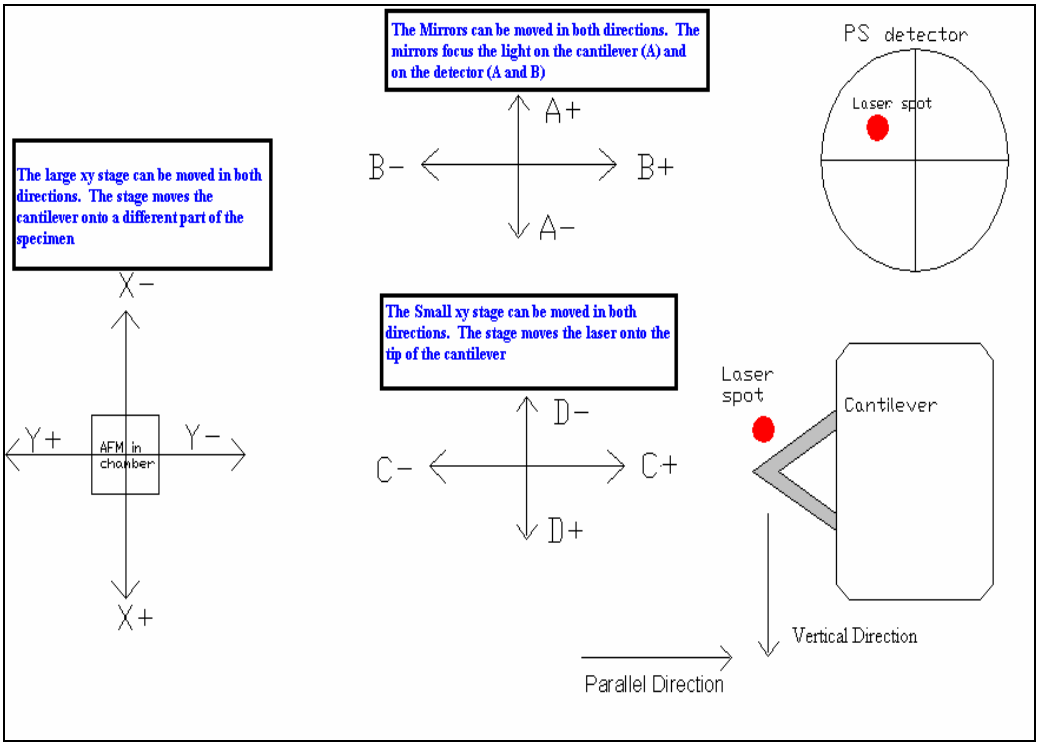

Figure 7.14: A diagram showing the relationship between the buttons on the control interface and movement in the cryogenic-AFM.

Each control can be moved in both directions (shown by the + and - buttons). The step feature of the control panel shows the increments that the control has been moved. These increments have no units and are simply a proportion of the movement for the particular stage. The stage feature shows the current position of the control; the home button returns the control to its starting position and the reset button zero's the step feature once the control is in the correct place.

Unlike commercial instruments such as the DI multimode, the cryogenic-AFM does not contain a CCD camera for alignment of the laser. This is because of the difficulties operating a camera at low temperatures and vacuum and space considerations in the cryogenic chamber. Before the AFM is placed in the cryogenic chamber the tip is placed on the tip holder and the laser is aligned. The aligning mechanism is unlike that found in normal AFM.

The small xy stage (C and D) is moved until a sum is found indicating the laser is on the cantilever holder. Then using the D- direction control the stage is moved until the sum disappears, signifying the location of the top edge of the cantilever, then it is moved back until the sum reappears. This process is then repeated using the C- directional controller to locate the top left hand corner of the cantilever holder

By scanning vertically with the auto focus function on the interface the laser scans downwards and a resultant trace indicates any height anomalies (such as the cantilever) with a peak, for example the two peaks (figure 7.15) resemble the two arms of the cantilever.

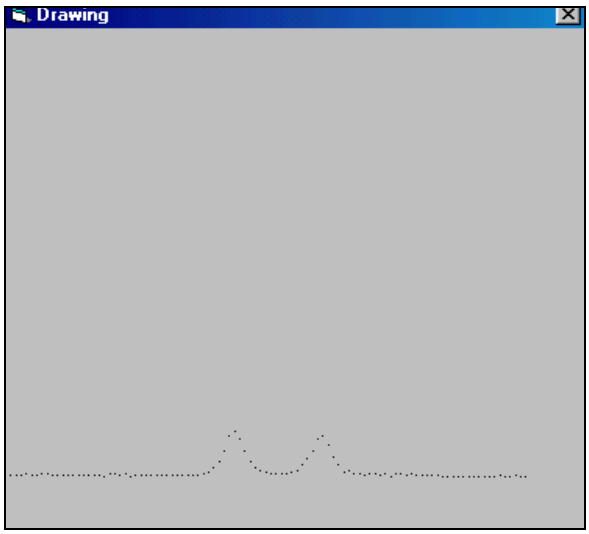

Figure 7.15: A vertical scan of the cantilever using the Cryogenic-AFM interface

After vertically scanning the laser must be manually realigned to the top left of the cantilever holder. The same procedure for aligning the laser must be repeated with adjustments made until the tip of the cantilever is shown by one peak on the sketch (figure 7.16).

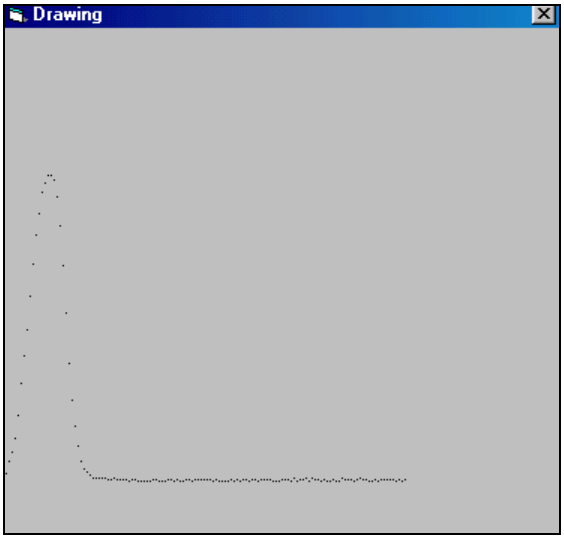

Figure 7.16: A second vertical scan of the cantilever (showing the tip of the cantilever) using the cryogenic –AFM interface

Once the tip of the cantilever has been located, minor adjustments using the C and D controls can move the laser to the very tip of the cantilever; as judged by the maximum obtainable sum value. Once the sum is at its maximum value a parallel auto focus scan should show one peak followed by a zero reading (the gap between the two cantilever arms) then a large peak (the cantilever holder) (figure 7.17)

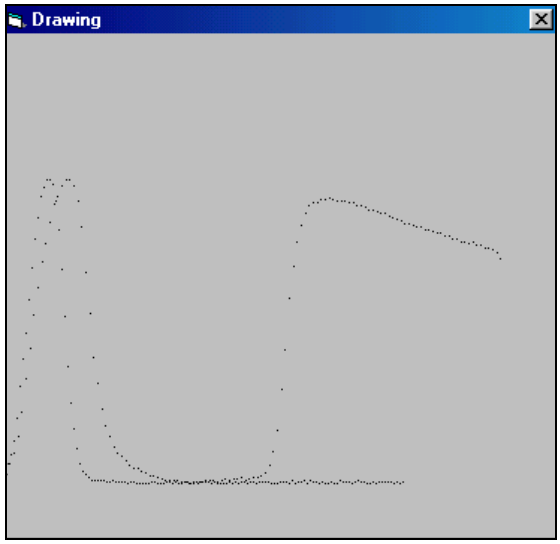

Figure 7.17: A vertical and parallel scan using the cryogenic-AFM interface that shows the laser is on the tip of the cantilever

This indicates that the laser is in the centre of the cantilever. Minor alterations to the detector and mirror using the A± and B± controls may increase the signal received by the detector (monitored by the sum value on the interface).

7.2.6.2 Preparing the cryogenic chamber

Once the laser is correctly aligned on the cantilever the system can be vented and a vacuum created. Once a vacuum of less than $1x10^{-5}$ Pa has been achieved the chamber can be cooled down by the addition of liquid Nitrogen to the external dewer. When it is at the desired temperature it is ready for a frozen sample.

7.2.6.3 Freezing the sample

The samples are frozen using a CF100 (LifeCell Corporation) (see section 7.2.4) then transferred immediately to a polystyrene cup containing nitrogen slush (made using the vacuum unit) (figure 7.18).

Figure 7.18: A photo of the sample in its holder in a polystyrene cup of nitrogen slush prior to its insertion into the cryogenic chamber

As quickly as possible the sample is transferred from the CF100 sample holder onto the Gatan gold sample holder using ceramic tweezers. Then the sample holder and sample are placed inside a vacuum transfer device in which, a vacuum is created allowing the sample to be placed in the cryogenic chamber. Once in the chamber the temperature can be altered until the sample is in the desired state before it is pushed through into the AFM chamber where scanning can commence.

7.3. Methodology

7.3.1 Atomic Force Microscopy

DI Multimode

AFM images were carried out as under an air environment as described in 2.1.1

Cryogenic-AFM

AFM images were carried out in air (as for the Multimode, 2.1.1) and at cryogenic temperatures as described in this chapter.

7.3.2 Polystyrene spheres

Air Imaging

Samples of 404nm ± 4nm and 19nm Nanosphere size standard, polystyrene polymers (Duke Scientific Corp, California, USA) were prepared by placing 40µl on freshly cleaved mice and drying under Nitrogen gas.

Cryogenic imaging

Samples of 404nm ± 4nm and 19nm ± 1.5nm Nanosphere size standard, polystyrene polymers (Duke Scientific Corp.) where prepared by placing 40µl on a Gatan sample holder and placing in cryogenic chamber (7.2.6).

7.4. Results

If the intrinsic factors such as sample softness and thermal motion that inhibit high resolution imaging of a large number of biomolecules could be reduced by cryogenic-AFM then there could be an increase in the resolution of many of the biomolecules currently imaged by ambient AFM techniques possibly to a resolution sufficient to reveal sub-molecular structure. The cryogenic-AFM in order to achieve these aims, when operated in air on a non-frozen sample, should be comparable to currently available AFM systems.

The Digital Instruments Multimode IIIa (DI Multimode) is a benchmark of AFM imaging technology. A comparison between the cryogenic-AFM and DI Multimode (the control system) will illustrate the potential of the cryogenic AFM system.

Polystyrene spheres with a size of 404nm ± 4nm where imaged in initial experiments comparing the two instruments. Such a sample represents a good test system since features of defined size and geometry can easily be created and imaged.

7.4.1 Air imaging

7.4.1.1 Cryogenic-AFM

404nm spheres imaged on the cryogenic-AFM in air reveal a population of features (figure 7.19) in which, although the spheres are evident they are not uniform in shape or size. The tightly packed nature of the spheres and the geometry of the AFM tip may have lead to probe convolution effects but some distortion due to non-linear scanning is also evident. This combined with the soft nature of the spheres and the force of the tip has led to distorted images. The shadowing that can be seen on the right side of the polystyrene spheres is caused by the scan direction (left to right) due to the slow response time of tracking topographical changes by the AFM scanner. The tightly packed

nature of the spheres and evidence of tip convolution are better highlighted in the 3D representation (figure 7.19) as seen by the apparent steep sides of the spheres.

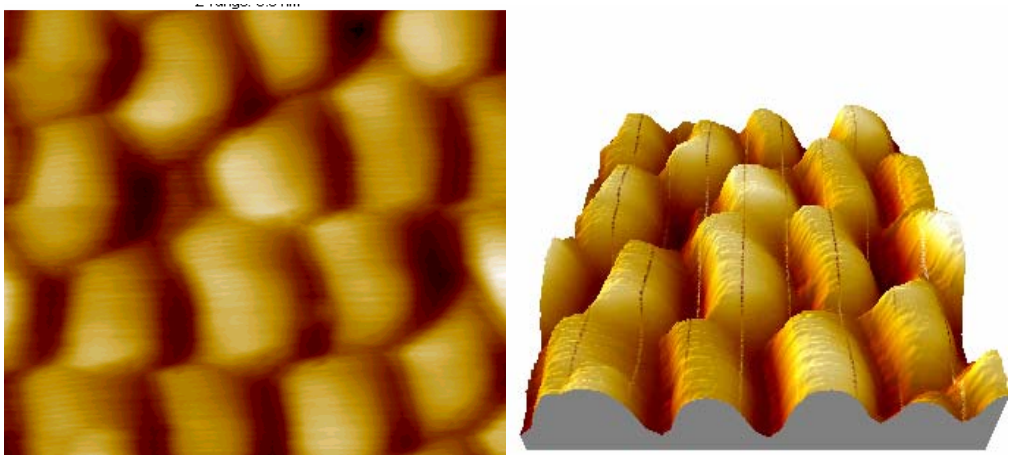

Figure 7.19: Early images of 404nm polystyrene spheres imaged in air on the cryogenic-AFM. (left) Topographic image. Scan size is 2 µm. (right) 3D representation of image

The sizes of the polystyrene spheres appear similar in the x direction but more varied in the y direction. This effect could be due to thermal drift which is more obvious in the y direction because of the AFM slower scanning rate in this direction compared to the x.

Cross sectional analysis of the polystyrene spheres in the x and y direction (figure 7.20) Reveal the average size (measured at half height) of 28 spheres is 349.8nm in the x direction (with a standard deviation of 63nm) and 525 nm in the y direction (with a standard deviation of 51nm).

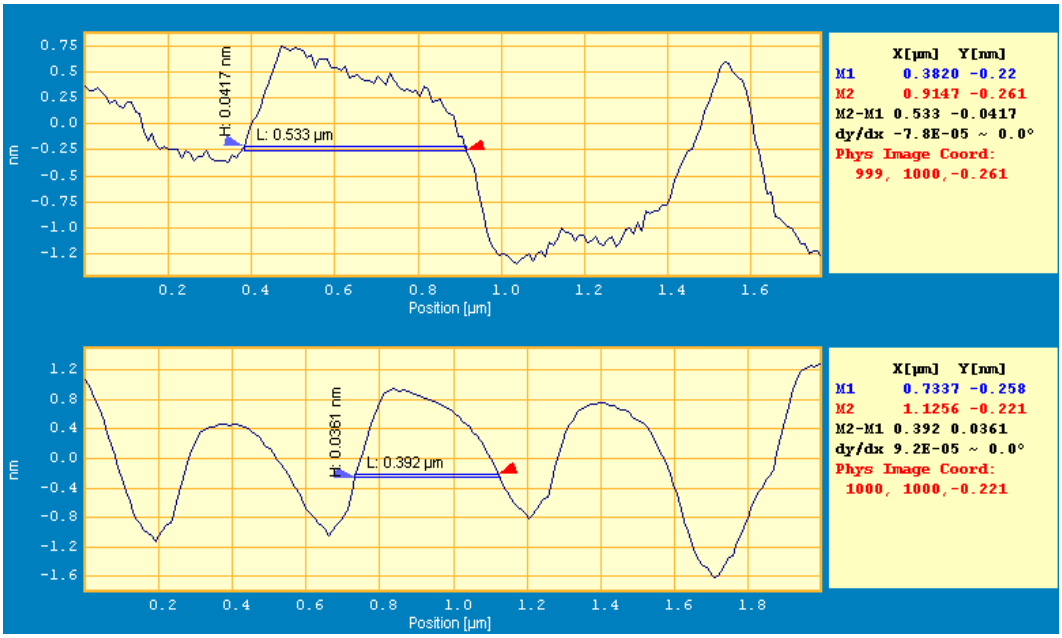

Figure 7.20: An Y (top) and X (bottom) cross section analysis of the spheres in figure x. The dimensions of one sphere are highlighted in both directions.

7.4.1.2 DI Multimode

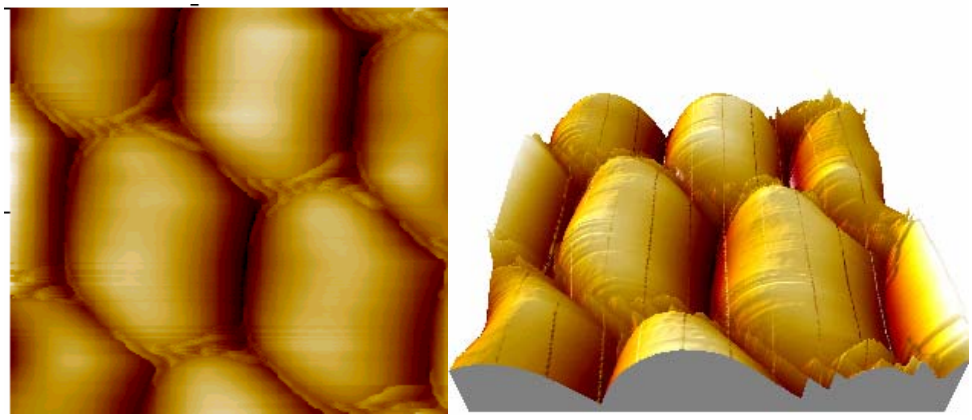

Figure 7.21: 404nm polystyrene spheres imaged in air on the DI multimode. (left) Topographic image. Scan size is 2 µm. (right) 3D representation of image

404nm polystyrene spheres imaged on the DI multimode in contact mode in air show many of the same features seen on the cryogenic-AFM (figure 7.21) the spheres appear slightly distorted due to a combination of the softness of

the spheres and convolution making to difficult to image the edges of the closely packed spheres. In addition a rippling effect can be seen which is due to excessive control loop gain, causing the probe to resonate under conditions were there is a high rate of topographic gradient change.

As seen with the cryogenic-AFM the sizes of the polystyrene spheres appears similar in the x direction but more varied in the y direction though this physical distortion is less pronounced on the DI Multimode system

Cross sectional analysis of the polystyrene spheres in the x and y direction (figure 7.22) Reveal the average size (measured at half height) of 44 spheres is 329.3nm in the x direction (with a standard deviation of 21nm) and 572.1 nm in the y direction (with a standard deviation of 23nm).

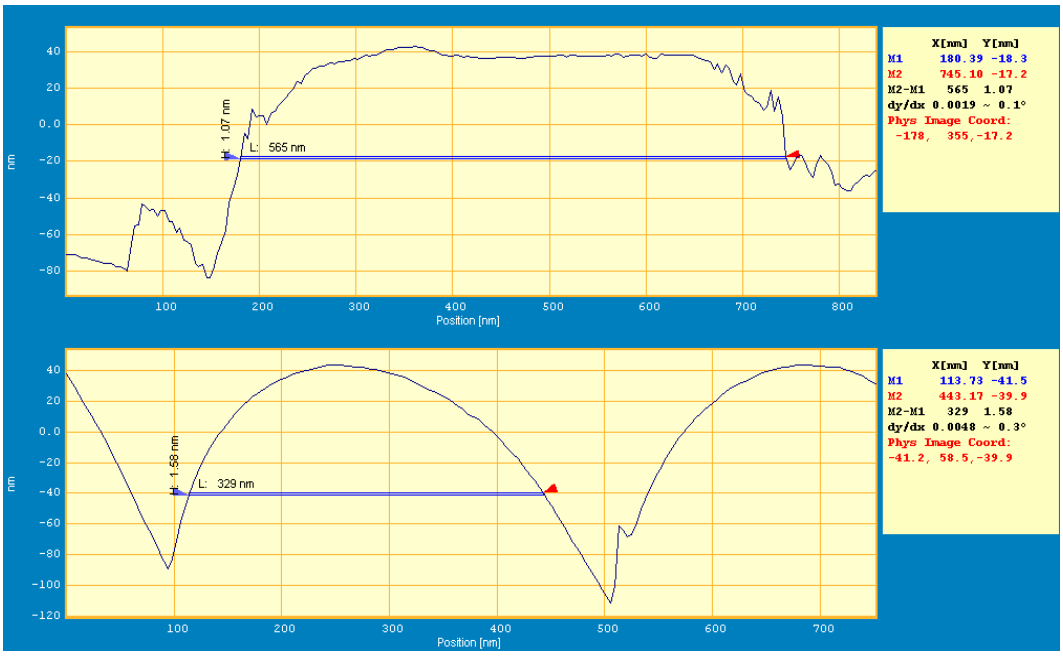

Figure 7.22: An Y (top) and X (bottom) cross section analysis of the spheres in figure x. The dimensions of one sphere are highlighted in both directions.

It has been shown by imaging 404nm spheres on the DI Multimode and cryogenic AFM that the images of a roughly comparable quality and size with some of the intrinsic features that hope to be removed by imaging at cryogenic

temperatures clearly evident. Much clearer images of polystyrene spheres exist (Tan *et al*, 2004) in many cases such images are in tapping mode. In this chapter lower quality contact mode images better highlight the intrinsic feature which cryogenic AFM is trying to remove.

7.4.2 Cryogenic Imaging

7.4.2.1 Vacuum

In order to maintain a cryogenic temperature and prevent contamination the microscope must operate under a high vacuum. An internal sensor image of polystyrene spheres imaged in vacuum, which have not been frozen in the cryogenic AFM under vacuum (figure 7.23) shows the effect of imaging the spheres in vacuum which shows a slight improvement in image quality.

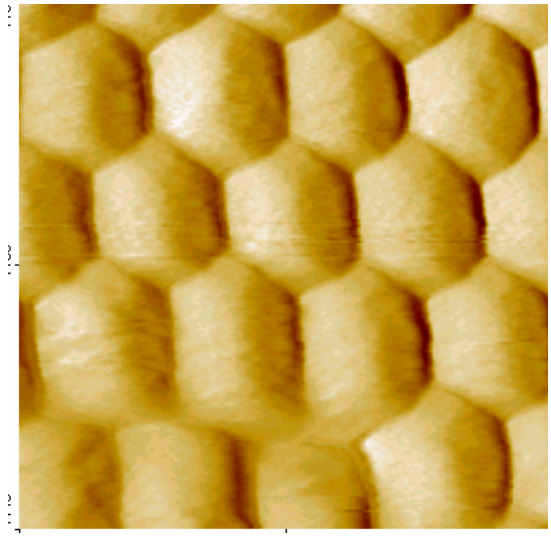

Figure 7.23: A topographic image of 404nm polystyrene spheres imaged under vacuum on the cryogenic-AFM. Scan size is 2 µm

The polystyrene spheres imaged under vacuum all appear to be uniform in size and shape though they appear hexagonal rather than spherical. This, as seen before, is probably due to the tight packing of polymer spheres making it impossible for the tip to image between the spheres leading to tip-sample convolution.

There appears to be a slight improvement in the quality of the image compared to operation in air alone (figures 7.19 and 7.21) though it is difficult to compare the topographical and internal sensor images. This could be due the time the sample was given to stabilize in the chamber, allowing reduced effects of convection currents. The spheres are still slightly elongated in the y direction and the edges of some spheres are ill defined, showing that the factors that cause these effects are not removed by imaging in vacuum.

7.4.2.2 Initial freezing

Given the large nature of the specimen the polystyrene spheres were frozen by placing them directly into the cryogenic chamber and adding liquid Nitrogen until the temperature reached –176°. Immediately post freezing at the sample was transferred to the AFM chamber and imaged (figure 7.24)

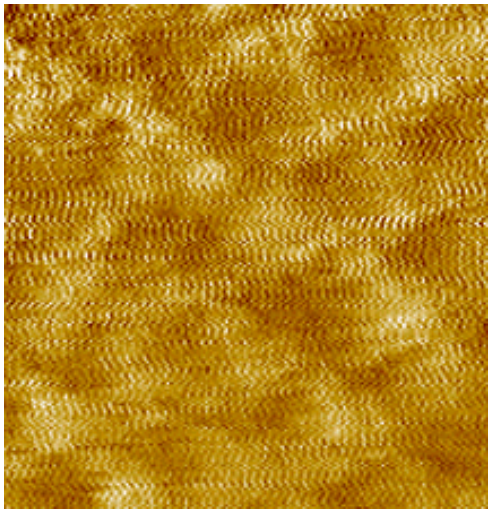

Figure 7.24: A topographical image of 404nm polystyrene spheres imaged in vacuum at -176°C on the cryogenic-AFM. Scan size is 2 µm.

The image is largely unclear due to ice on the sample surface, the outline of several polystyrene spheres are just visible beneath this layer. Little structural detail can be seen of the ice.

7.4.2.3 Gradual warming

The temperature of the cold stage was gradually raised in increments of 1°C to a temperature of -134°C in order to remove the surface ice from the sample without affecting the sample, as the polystyrene spheres were heated the cryogenic-AFM continued scanning (figure 7.25)

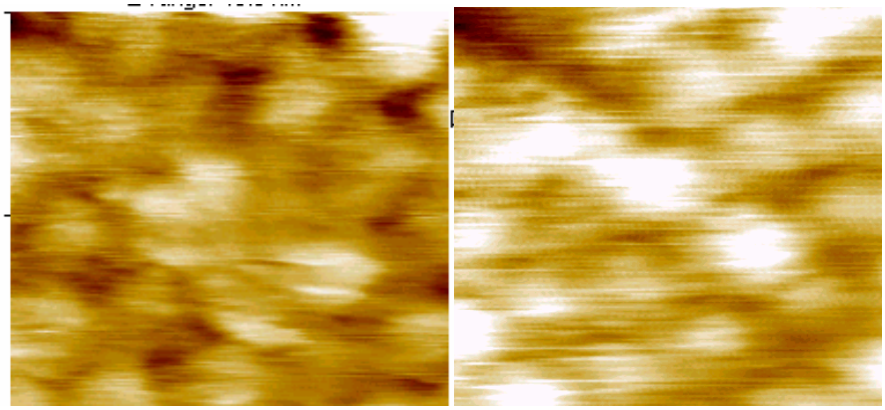

Figure 7.25: Topographically images of 404nm polystyrene spheres imaged in vacuum as the temperature is raised from -176°C to –134°C, on the cryogenic-AFM. Scan size is 2 µm.

The images from -176°C to –134°C show that as the sample is heated the layer(s) of ice covering the polystyrene spheres gradually disappears making the spheres more visible. It is possible that the laser light used to measure cantilever deflection could be having an effect on surface ice removal as it generates heat and is in close proximity to the sample this phenomenon would also happen when imaging. However the image quality didn't improve when left at this temperature, suggesting the laser temperature doesn't have an effect.

7.4.2.4 Cryogenic imaging

At a temperature of –134°C the imaging became much clearer (figure 7.26). The polystyrene spheres all appear to have a very similar spherical shape, the curved edges of the spheres are clear (as better seen by the 3D image) and the convolution effect of the tip is less pronounced. Due to being frozen, the spheres are much more rigid (have a higher Young's modulus) meaning there

is less distortion of the spheres by the force of the tip, as result the tip is able to image between the tightly packed spheres more easily. There is less evidence of the drift seen in previous air images, the spheres appear similar in the x and y directions, this is as a direct result of the cryogenic temperatures. There is some evidence of tilting of the spheres due to tip direction

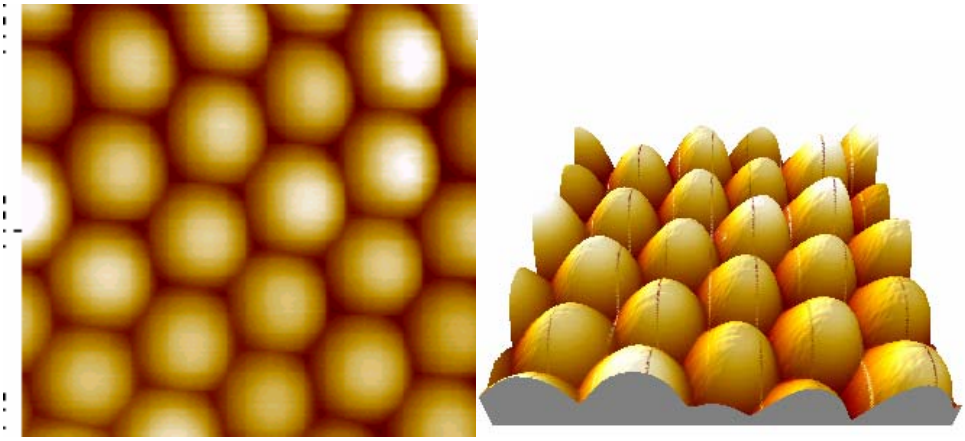

Figure 7.26: 404nm polystyrene spheres imaged in vacuum at -134°C on the cryogenic-AFM. (left) Topographic image. Scan size is 2 µm. (right) 3D representation of image

.

Cross sectional analysis of the polystyrene spheres in the x and y direction (figure 7.27) Reveal the average size (measured at half height) of 30 spheres is 398nm in the x direction (with a standard deviation of 8nm) and 409 nm in the y direction (with a standard deviation of 2nm). The cross sectional profiles highlight the good orthogonality of the scanner

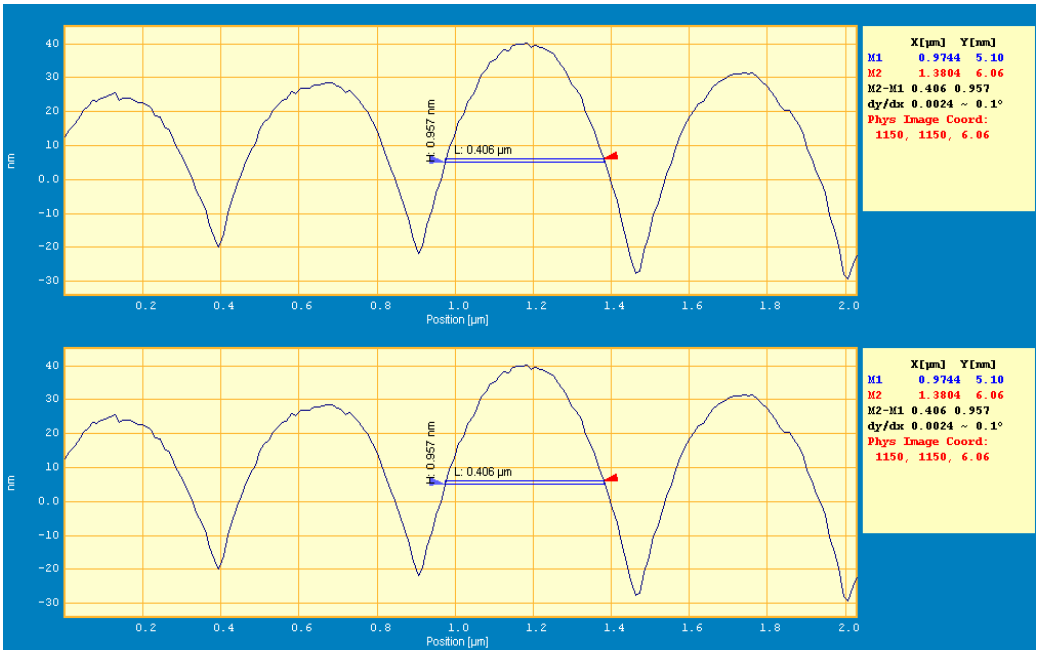

Figure 7.27: An X (top) and Y (bottom) cross section analysis of the spheres in figure 7.26. The dimensions of one sphere are highlighted in both directions.

7.5. Discussion

It is important that any advancement on currently used AFM technology such as the DI Multimode system is of comparable ability in terms of structural resolution. This is necessary so that any advance develops the instruments beyond the realms of what is already possible with current technology. The cryogenic AFM operated in air achieved a similar structural resolution to the DI MM under the same environment. The spheres imaged were measured and both systems recorded similar (though slightly inaccurate) dimensions. Similar effects and artefacts associated with AFM imaging were seen in both systems such as, the tip convolution effect, some distortion of the polymer spheres through the force of the tip and drifting of the tip caused by both thermal motion of the sample and mechanical drift of the AFM.

The spheres size of 404nm is clearly large compared to biomolecules but their robust nature and there uniform shape and size provided a good model system in which to test the cryogenic AFM. Comparison between smaller specimens and a range of biomolecules are needed before it can be said the cryogenic AFM as implemented here has a future role in bio-structural studies.

The images of the spheres obtained with the DI are quite distorted and it could be expected that a better quality image would be achieved on this system. Some of the distortion could be because the DI in this experiment was operating in contact mode so the images could be compared with the cryogenic-AFM, which operates in this mode. The DI is more commonly used in tapping mode, especially for the analysis of 'soft' biomolecules as this removes some of the distortion from the lateral tip forces and stops the samples being dragged by the tip.

Other variations such as differences in the AFM tip (sharpness, diameter etc) could account for some of the differences between the two image environments. Using AFM software, Scanning Probe Image Processor, Image Meterology (Williams *et al*, 1994)) it is possible to characterise a projected tip

profile from an AFM image. The profiles shows that the tip profile for the cryogenic images of the spheres to be apparently much sharper than that of the spheres imaged in air (figure 7.28). This does not mean that a sharper tip was used as the profile takes into account such effects as the softness of the substrate. It does indicate that the sample was more rigid and less deformation took place. Imaging with the same tip, or SEM analysis of tips would rule out any differences between the images as a result of tip variations.

Figure 7.28: Apparent tip profiles generated from AFM images of; 404nm polystyrene spheres in air (left) and at -134°C (right)

Imaging the polystyrene spheres under cryogenic conditions produced a much clearer image in which, there was less evidence of the convolution effect and sample distortion (due to the material being more rigid) and drifting effects (suppression of thermal motion). The size of the spheres could hence be much more accurately determined in the cryogenic-AFM once frozen, and measured within ± of 4nm of the manufactures stated size.

The spheres in these experiments were not frozen in the slam freezer, but frozen (relatively slowly) by placing the sample directly onto the cold stage. This resulted in a visible build of surface ice which can be seen when image with the AFM, no structural detail can be seen of the ice but given the temperature and pressure the ice formed is most likely to be hexagonal showing we could do this biomolecules. Heating the sample gradually upto a temperature of -134°C removed the ice on the sample of the surface and revealed the spheres which, appear to still be frozen. It is possible the heat of the laser on the sample contributed to the removal of ice as it is in close

proximity to the sample. This issue will have to be addressed further in future experiments.

Any ice present appears to have had a minimal effect on the structure of the spheres, this is because of their large size. When imaging smaller, fragile biomolecules the prevention of ice formation will be more critical. The rapid freezing of samples in the slam freezer should prevent most ice formation in the freezing step. Any ice which, subsequently forms in the transfer of samples into the cryogenic chamber can removed by a slight increase in the temperature as seen with the spheres. An alternative option is to use post freezing techniques such as fracturing to reveal an internal surface of the biomolecule where is surface ice will not be a problem.

Further study is needed to analyse biomolecules on a cryogenic system to test its validity as a high resolution imaging tool. An ideal candidate for analysis would be the DnaBG complex analysed in chapter 4. In this system the structural resolution was not enough in air to reveal the individual DnaG proteins bound to the DnaB in the DnaBG complexes, at cryogenic temperatures this may be possible to see.

Further studies are also needed on ice formation, its effects on biomolecules imaged by the AFM (unlike other cryomicroscopy techniques the AFM tip actually touches the surface) the temperature ranges that form imagable biomolecules and the effect of heating and removing the ice on the sample.

8. Conclusion

In this investigation a nanoscale analysis approach has been employed in a series of experiments studying the structural detail and complex interactions of a biochemical process. The bacterial primosome has been shown to be a fundamental structure forming active complexes for DNA replication at both *oric* and *priA* replication initiation sites on both bacterial chromosomal and plasmid DNA. The bacterial primosome has been well studied, many of the key components involved in its assembly have been previously characterised and their functions identified, three components of this primosomal cascade have been further studied by AFM in this thesis.

The interaction of the helicase and primase proteins is the key step in triggering the switch from primosomal mode to polymerisation mode (Patal *et al*, 2000). Previous EM studies have revealed structural details of the helicase protein in both *E.coli* and *Bacillus*, where it has been shown to predominantly exist as a hexameric ring structure, though it has been shown to adopt a trimeric structure in *Bacillus* (Patal *et al*, 2000, Yu *et al*, 1996, Haroniti *et al*, 2004). The interaction between the helicase and primase which involves 2 or 3 primase molecules per helicase hexamer has been previously studied in *Bacillus* (Bird *et al,* 2000) though little structural detail of the interaction is known. Using AFM along with a classic biochemical approach we have shown that the helicase when unbound predominately forms a hexameric ring structure. On the addition of the primase the helicase population switches to a 3-fold structure which is deduced to be a trimer of dimers with 3 primase molecules bound in some fashion across each of the three dimers, as reflected by our model. Additionally, studies revealed a small number of helicases with the trimer of dimer conformation that existed with only one or two primases molecules bound, hinting at a sequential method of primase loading.

Subsequent to this investigation the crystal structure of the p16 helicase interacting domain of the primase has been characterised (Oakeley *et al*, 2005; Syson *et al*, 2005). The structural detail revealed by this data combined with

the AFM generated model reveal an explanation for the molecular basis of the structural changes imposed on the helicase by the primase binding. This work also provides a strong link between AFM and crystallography data where the structural interactions and models identified in the AFM are subsequently supported by the crystal structures. This achievement has very rarely been achieved in AFM (Engel *et al*, 2000) and highlights the potential for AFM as a high resolution imaging tool for protein assemblies.

A protein shown to be essential in *Bacillus* primosome assembly is DnaD, this protein which has no homologue in *E.coli* has been shown by mutation studies to prevent replication in *Bacillus* when absent (Gross *et al*, 1968; Alonso *et al*, 1988). Little is known about the protein apart from that it interacts with the membrane bound DnaB protein (Rokop *et al,* 2004) and that it possibly acts to disrupt the bond between the helicase loader protein DnaI and the replicative helicase (Turner *et al*, 2004). Using the AFM and biochemical approaches it was discovered that the DnaD has a fundamental effect on the structure of DNA in a similar way to the recently reported global conformation proteins HU and H-NS.

DnaD when alone was shown to form chains and circlar structures in a concentration dependent manner. When complexed with DNA, DnaD was shown to 'open up' supercoiled regions of DNA forming a circular conformation in an event which caused the DNA to become underwound (more base pairs per turn). DnaD was show to preferentially bind to preformed complexes rather than form a new complex. These observations led to the development of a speculative model which suggests the self-recruiting of DnaD via its interaction with DnaB has a pivotal role in the opening up of the DNA and bringing the initial primosome complex to the vicinity of the membrane before the helicase and primase are loaded.

Further AFM studies investigated the link between DnaD and the global regulation proteins HU and H-NS by studying the reversibility of its action and its effect on a range of DNA substrates. The DnaD effect on DNA was shown to be universal and applicable to different types of DNA substrate. A

revised model of primosome assembly was generated using this and concurrent data showing the universal compaction role of the DnaB membrane protein (Zhang *et al*, 2005).

Structural analysis using the AFM has revealed insights into the mechanism and formation of the bacterial chromosome. In studying the helicase primase interaction the resolution of the AFM though good enough to identify the complex was not detailed enough to reveal the binding of the individual DnaG proteins to the DnaB dimers. Several instrumental and tip based factors influence the resolution of an AFM image. Two intrinsic factors that also effect resolution are the thermal motion of biomolecules at room temperature and the softness of biomolecules leading to deformation by the AFM probe.

In this a study a novel and pioneering cryogenic AFM was developed and modified. The system operates at liquid nitrogen temperatures, and aims to reduce the main intrinsic resolution reducing effects of AFM imaging by freezing samples and imaging them at sub zero temperatures. Preliminary experiments on polystyrene spheres show that these effects can be significantly reduced and show the potential for biological imaging. Further studies on biomolecules and the effects of sub zero temperatures, especially of ice formation on biomolecules structure need to be carried out before this system is routinely used for molecular imaging.

This study shows the power of AFM alongside a classical biochemical approach for the investigation of molecular structure and interactions of fundamental processes in bacterial. As well as building upon previous data the models generated by the AFM in this study have preceeded powerful techniques such as crystallography. Further more the development of a cryogenic AFM shows that advancements in the resolution of current AFM systems are possible this alongside the potential for imaging protein assemblies make AFM a more powerful tool in molecular biology.

9. Future Perspective

AFM after its introduction in 1985 has had a meteriotic rise as an imaging tool, with a number of high profile papers on a range of molecules, in the late 80's and early 90's (Hansma *et al*,1998, Marti *et al*, 1988, Drake *et al*, 1989, Lindsay *et al*, 1989, Weisenhorn *et al*, 1990, Wiegrabe *et al*, 1991, Hansma *et al*, 1991, Arawaka *et al*, 1992,). After its initial success questions started to be asked about the nature of AFM interaction with the molecules it was imaging which lead to several papers highlighting artefacts generated by AFM (Clemmer *et al*, 1991, Allen *et al*, 1992, Yang *et al*, 1993, Vesenka *et al*, 1993, Williams *et al*, 1994, Williams *et al*, 1996, Williams *et al*, 1996a). Since this period AFM has continued to be used for imaging individual biomolecules to a very high degree of resolution (Hansma *et al*, 1996, Haroniti *et al*, 2004), however, it has perhaps not built upon its early success as much as was hoped. This thesis shows for the first time that AFM can successfully be employed to image a protein assembly to a degree of resolution that is comparable to the best electron micrograph and for such assembles could be the technique of choice and suggests a possible future role of AFM in combining force sensing and dynamic studies.

References

Abdelhady, H. G., S. Allen, et al. (2003). "Direct real-time molecular scale visualisation of the degradation of condensed DNA complexes exposed to DNase I." Nucleic Acids Res 31(14): 4001-5.

Allen, S., X. Chen, et al. (1997). "Detection of antigen-antibody binding events with the atomic force microscope." Biochemistry 36(24): 7457-63.

Allen, S., J. Davies, et al. (1996). "In situ observation of streptavidin-biotin binding on an immunoassay well surface using an atomic force microscope." FEBS Lett 390(2): 161-4.

Alonso, J. C., C. A. Stiege, et al. (1988). "Functional analysis of the dna (Ts) mutants of Bacillus subtilis: plasmid pUB110 replication as a model system." Mol Gen Genet 214(3): 482-9.

Amit, R., A. B. Oppenheim, et al. (2003). "Increased bending rigidity of single DNA molecules by H-NS, a temperature and osmolarity sensor." Biophys J 84(4): 2467-73.

Amit, R., A. B. Oppenheim, et al. (2004). "Single molecule elasticity measurements: a biophysical approach to bacterial nucleoid organization." Biophys J 87(2): 1392-3.

Andrup, L., T. Atlung, et al. (1988). "Interaction of the Bacillus subtilis DnaA-like protein with the Escherichia coli DnaA protein." J Bacteriol 170(3): 1333-8.

Anselmetti, D., J. Fritz, et al. (2000). "Single molecule DNA biophysics with Atomic force microscopy." Single Mol. 1(1): 53-58.

Asakura, H., K. Kawamoto, et al. (2004). "Changes in Salmonella enterica serovar Oranienburg viability caused by NaCl-induced osmotic stress is related to DNA relaxation by the H-NS protein during host infection." Microb Pathog 36(3): 147-51.

Asklund, M. and T. Atlung (2005). "New Non-detrimental DNA-binding Mutants of the Escherichia coli Initiator Protein DnaA." J Mol Biol 345(4): 717-30.

Atlung, T. and F. G. Hansen (2002). "Effect of different concentrations of H-NS protein on chromosome replication and the cell cycle in Escherichia coli." J Bacteriol 184(7): 1843-50.

Azevedo, V., E. Alvarez, et al. (1993). "An ordered collection of Bacillus subtilis DNA segments cloned in yeast artificial chromosomes." Proc Natl Acad Sci U S A 90(13): 6047-51.

Bahloul, A., F. Boubrik, et al. (2001). "Roles of Escherichia coli histone-like protein HU in DNA replication: HU-beta suppresses the thermosensitivity of dnaA46ts." Biochimie 83(2): 219-29.

Baker, T. A. and S. P. Bell (1998). "Polymerases and the replisome: machines within machines." Cell 92(3): 295-305.

Baker, T. A. and S. H. Wickner (1992). "Genetics and enzymology of DNA replication in Escherichia coli." Annu Rev Genet 26: 447-77.

Best, R. B., D. J. Brockwell, et al. (2003). "force mode atomic force microscopy as a tool for protein folding studies." Analytica Chimica Acta 479: 87-105.

Binnig, G., K. H. Frank, et al. (1985). "Tunneling spectroscopy and inverse photoemission: Image and field states." Physical Review Letters 55(9): 991-994.

Binnig, G., N. Garcia, et al. (1985). "Conductivity sensitivity of inelastic scanning tunneling microscopy." Physical Review B. Condensed Matter 32(2): 1336-1338.

Binnig, G., C. F. Quate, et al. (1986). "Atomic force microscope." Physical Review Letters 56(9): 930-933.

Bird, L. E., H. Pan, et al. (2000). "Mapping protein-protein interactions within a stable complex of DNA primase and DnaB helicase from Bacillus stearothermophilus." Biochemistry 39(1): 171-82.

Bloch, V., Y. Yang, et al. (2003). "The H-NS dimerization domain defines a new fold contributing to DNA recognition." Nat Struct Biol 10(3): 212-8.

Bockelmann, U., P. Thomen, et al. (2004). "Dynamics of the DNA duplex formation studied by single molecule force measurements." Biophys J 87(5): 3388-96.

Bruand, C. and S. D. Ehrlich (1995). "The Bacillus subtilis dnaI gene is part of the dnaB operon." Microbiology 141 (Pt 5): 1199-200.

Bruand, C., S. D. Ehrlich, et al. (1995). "Primosome assembly site in Bacillus subtilis." Embo J 14(11): 2642-50.

Bruand, C., M. Farache, et al. (2001). "DnaB, DnaD and DnaI proteins are components of the Bacillus subtilis replication restart primosome." Mol Microbiol 42(1): 245-55.

Bruand, C., A. Sorokin, et al. (1995). "Nucleotide sequence of the Bacillus subtilis dnaD gene." Microbiology 141 (Pt 2): 321-2.

Bruand, C., M. Velten, et al. (2005). "Functional interplay between the Bacillus subtilis DnaD and DnaB proteins essential for initiation and re-initiation of DNA replication." Mol Microbiol 55(4): 1138-50.

Bujalowski, W. (2003). "Expanding the physiological role of the hexameric DnaB helicase." Trends Biochem Sci 28(3): 116-8.

Cadman, C. J. and P. McGlynn (2004). "PriA helicase and SSB interact physically and functionally." Nucleic Acids Res 32(21): 6378-87.

Cappella, B., P. Baschieri, et al. (1997). "Force-distance curves by AFM. A powerful technique for studying surface interactions." IEEE Eng Med Biol Mag 16(2): 58-65.

Christensen, B. B., T. Atlung, et al. (1999). "DnaA boxes are important elements in setting the initiation mass of Escherichia coli." J Bacteriol 181(9): 2683-8.

Clemmer, C. R. and T. P. Beebe, Jr. (1991). "Graphite: a mimic for DNA and other biomolecules in scanning tunneling microscope studies." Science 251(4994): 640-2.

Colton, R. J., D. R. Baselt, et al. (1997). "Scanning probe microscopy." Curr Opin Chem Biol 1(3): 370-7.

Czajkowsky, D. M. and Z. Shao (1998). "Submolecular resolution of single macromolecules with atomic force microscopy." FEBS Lett 430(1-2): 51-4.

Czajkowsky, D. M. and Z. Shao (2003). "Inhibition of protein adsorption to muscovite mica by monovalent cations." J Microsc 211(Pt 1): 1-7.

Dai, P., S. Wang, et al. (1993). "X-ray-diffraction and scanning-tunneling-microscopy studies of a liquid-crystal film adsorbed on single-crystal graphite." Physical Review. B. Condensed Matter. 47(12): 7401-7407.

Dame, R. T. (2005). "The role of nucleiod-associated proteins in the organisation and compaction of bacterial chromatin." In Print.

Dame, R. T. (2005). "The role of nucleiod-associated proteins in the organisation and compaction of bacterial chromatin." Molecular Microbiology.

Dame, R. T. and N. Goosen (2002). "HU: promoting or counteracting DNA compaction?" FEBS Lett 529(2-3): 151-6.

Dame, R. T., M. S. Luijsterburg, et al. (2005). "DNA bridging: a property shared among H-NS-like proteins." J Bacteriol 187(5): 1845-8.

Dame, R. T. and G. J. Wuite (2003). "On the role of H-NS in the organisation of bacterial chromatin: from bulk to single molecules and back..." Biophys J 85: 4146-4148.

Dame, R. T., C. Wyman, et al. (2000). "H-NS mediated compaction of DNA visualised by atomic force microscopy." Nucleic Acids Res 28(18): 3504-10.

Dame, R. T., C. Wyman, et al. (2001). "Structural basis for preferential binding of H-NS to curved DNA." Biochimie 83(2): 231-4.

Dame, R. T., C. Wyman, et al. (2003). "Insights into the regulation of transcription by scanning force microscopy." J Microsc 212(Pt 3): 244-53.

Dorman, C. J. (2004). "H-NS: a universal regulator for a dynamic genome." Nat Rev Microbiol 2(5): 391-400.

Dorman, C. J. and P. Deighan (2003). "Regulation of gene expression by histone-like proteins in bacteria." Curr Opin Genet Dev 13(2): 179-84.

Drake, B., C. B. Prater, et al. (1989). "Imaging crystals, polymers, and processes in water with the atomic force microscope." Science 243(4898): 1586-9.

Echlin, P. (1973). "The scanning electron microscope and its applications to research (continuation)." Microsc Acta 73(3): 189-204 contd.

Echlin, P. (1973). "The scanning electron microscope and its applications to research." Microsc Acta 73(2): 97-108 contd.

Echlin, P. (1977). "Low temperature electron microscopy." Nature 267(5609): 312-3.

Echlin, P. (1978). "Low temperature scanning electron microscopy: a review." J Microsc 112(1): 47-61.

Echlin, P. (1978). "Scanning electron microscopy." Nature 274(5666): 98.

Echlin, P. (1979). "Low temperature scanning electron microscopy and x-ray microanalysis of biological material." Mikroskopie 35(1-2): 45-9.

Echlin, P. (1991). "Ice crystal damage and radiation effects in relation to microscopy and analysis at low temperatures." J Microsc 161 (Pt 1): 159-70.

Eickbush, T. H. and E. N. Moudrianakis (1978). "The compaction of DNA helices into either continuous supercoils or folded-fiber rods and toroids." Cell 13(2): 295-306.

Ellis, J. S., H. G. Abdelhady, et al. (2004). "Direct atomic force microscopy observations of monovalent ion induced binding of DNA to mica." J Microsc 215(Pt 3): 297-301.

Erk, I., G. Nicolas, et al. (1998). "Electron microscopy of frozen biological objects: a study using cryosectioning and cryosubstitution." J Microsc 189 (Pt 3): 236-48.

Fotiadis, D., S. Scheuring, et al. (2002). "Imaging and manipulation of biological structures with the AFM." Micron 33(4): 385-97.

Fujimitsu, K. and T. Katayama (2004). "Reactivation of DnaA by DNA sequence-specific nucleotide exchange in vitro." Biochem Biophys Res Commun 322(2): 411-9.

Gajiwala, K. S. and S. K. Burley (2000). "Winged helix proteins." Curr Opin Struct Biol 10(1): 110-6.

Galletto, R., M. J. Jezewska, et al. (2004). "Unzipping mechanism of the double-stranded DNA unwinding by a hexameric helicase: the effect of the 3' arm and the stability of the dsDNA on the unwinding activity of the Escherichia coli DnaB helicase." J Mol Biol 343(1): 101-14.

Galletto, R., R. Mailard, et al. (2004). "Global conformation of the Escherichia coli replication factor DnaC protein in absence and presence of nucleotide cofactors." Biochemistry 43: 10988-11001.

Glover, B. P., A. E. Pritchard, et al. (2001). "tau binds and organizes Escherichia coli replication proteins through distinct domains: domain III, shared by gamma and tau, oligomerizes DnaX." J Biol Chem 276(38): 35842-6.

Grandbois, M., H. Clausen-Schaumann, et al. (1998). "Atomic force microscope imaging of phospholipid bilayer degradation by phospholipase A2." Biophys J 74(5): 2398-404.

Griffith, J. D. (1976). "Visualization of prokaryotic DNA in a regularly condensed chromatin-like fiber." Proc Natl Acad Sci U S A 73(2): 563-7.

Grimes, J. M., S. D. Fuller, et al. (1999). "Complementing crystallography: the role of cryo-electron microscopy in structural biology." Acta Crystallogr D Biol Crystallogr 55 (Pt 10): 1742-9.

Gross, J. D., D. Karamata, et al. (1968). "Temperature-sensitive mutants of B. subtilis defective in DNA synthesis." Cold Spring Harb Symp Quant Biol 33: 307-12.

Hansma, H. and L. Pietrasanta (1998). "Atomic force microscopy and other scanning probe microscopies." Curr Opin Chem Biol 2(6): 767.

Hansma, H. G. (2001). "Surface biology of DNA by atomic force microscopy." Annu Rev Phys Chem 52: 71-92.

Hansma, H. G., M. Bezanilla, et al. (1993). "Atomic force microscopy of DNA in aqueous solutions." Nucleic Acids Res 21(3): 505-12.

Hansma, H. G., R. Golan, et al. (1998). "DNA condensation for gene therapy as monitored by atomic force microscopy." Nucleic Acids Res 26(10): 2481-7.

Hansma, H. G. and J. H. Hoh (1994). "Biomolecular imaging with the atomic force microscope." Annu Rev Biophys Biomol Struct 23: 115-39.

Hansma, H. G. and D. E. Laney (1996). "DNA binding to mica correlates with cationic radius: assay by atomic force microscopy." Biophys J 70(4): 1933-9.

Hansma, H. G., D. E. Laney, et al. (1995). "Applications for atomic force microscopy of DNA." Biophys J 68(5): 1672-7.

Hansma, H. G., R. L. Sinsheimer, et al. (1993). "Recent advances in atomic force microscopy of DNA." Scanning 15(5): 296-9.

Hansma, P. K., J. P. Cleveland, et al. (1994). "Tapping mode atomic force microscopy in liquids." Appl. Phys. Lett 64(13): 1738-1740.

Haroniti, A., C. Anderson, et al. (2004). "The clamp-loader-helicase interaction in Bacillus. Atomic force microscopy reveals the structural organisation of the DnaB-tau complex in Bacillus." J Mol Biol 336(2): 381-93.

Harrell, L. E. and P. N. First (1999). "An ultrahigh vacuum cryogenic scanning tunneling microscope with tip and sample exchange." Review of scientific instruments 70(1): 125-132.

Helmstetter, C. E. and A. C. Leonard (1987). "Coordinate initiation of chromosome and minichromosome replication in Escherichia coli." J Bacteriol 169(8): 3489-94.
Herrick, J., M. Kohiyama, et al. (1996). "The initiation mess?" Mol Microbiol 19(4): 659-66.

Hoogeman, M. S., D. Glastra van Loon, et al. (1998). "Design and performance of a programmable-temperature scanning tunneling microscope." Review of scientific instruments 69(5): 2072-2080.

Hug, H. J., B. Stiefel, et al. (1999). "A low temperature ultrahigh vaccum scanning force microscope." Review of scientific instruments 70(9): 3625-3640.

Hui, S. W., R. Viswanathan, et al. (1995). "The structure and stability of phospholipid bilayers by atomic force microscopy." Biophys J 68(1): 171-8.

Imai, Y., N. Ogasawara, et al. (2000). "Subcellular localization of Dna-initiation proteins of Bacillus subtilis: evidence that chromosome replication begins at either edge of the nucleoids." Mol Microbiol 36(5): 1037-48.

Ishigo-Oka, D., N. Ogasawara, et al. (2001). "DnaD protein of Bacillus subtilis interacts with DnaA, the initiator protein of replication." J Bacteriol 183(6): 2148-50.

Jezewska, M. J. and W. Bujalowski (2000). "Interactions of Escherichia coli replicative helicase PriA protein with single-stranded DNA." Biochemistry 39(34): 10454-67.

Jones, S., P. van Heyningen, et al. (1999). "Protein-DNA interactions: A structural analysis." J Mol Biol 287(5): 877-96.

Kaplan, D. L. and M. O'Donnell (2002). "DnaB drives DNA branch migration and dislodges proteins while encircling two DNA strands." Mol Cell 10(3): 647-57.

Kasas, S., N. H. Thomson, et al. (1997). "Escherichia coli RNA polymerase activity observed using atomic force microscopy." Biochemistry 36(3): 461-8.

Katayama, T., T. Kubota, et al. (1998). "The initiator function of DnaA protein is negatively regulated by the sliding clamp of the E. coli chromosomal replicase." Cell 94(1): 61-71.

Kelman, Z. and M. O'Donnell (1995). "DNA polymerase III holoenzyme: structure and function of a chromosomal replicating machine." Annu Rev Biochem 64: 171-200.

Kim, J., S. H. Yoshimura, et al. (2004). "Fundamental structural units of the Escherichia coli nucleoid revealed by atomic force microscopy." Nucleic Acids Res 32(6): 1982-92.
Kirby, A. R., A. P. Gunning, et al. (1996). "Visualization of plant cell walls by atomic force microscopy." Biophys J 70(3): 1138-43.

Kirk, M. D., T. R. Albrecht, et al. (1988). "Low-temperature atomic force microscopy." Review of scientific instruments 59(6): 833-835.

Klinov, D. V., E. V. Dubrovin, et al. (1996). Probe Microscopy of DNA on Graphite. Moscow, Russia, Institute of Bioorganic Chemistry: 1-3.

Kogoma, T. (1996). "Recombination by replication." Cell 85(5): 625-7.

Kogoma, T., G. W. Cadwell, et al. (1996). "The DNA replication priming protein, PriA, is required for homologous recombination and double-strand break repair." J Bacteriol 178(5): 1258-64.

Koonin, E. V. (1992). "DnaC protein contains a modified ATP-binding motif and belongs to a novel family of ATPases including also DnaA." Nucleic Acids Res 20(8): 1997.

Krause, M., B. Ruckert, et al. (1997). "Complexes at the replication origin of Bacillus subtilis with homologous and heterologous DnaA protein." J Mol Biol 274(3): 365-80.

Lavrik, N. V., M. J. Sepaniak, et al. (2004). "Cantilever transducers as a platform for chemical and biological sensors." Review of scientific instruments 75(7): 2229-2253.

Lea, A. S., A. Pungor, et al. (1992). "Manipulation of proteins on mica by atomic force microscopy." Langmuir 8: 68-73.

Leckband, D. (2000). "Measuring the forces that control protein interactions." Annu Rev Biophys Biomol Struct 29: 1-26.

Lemon, K. P., I. Kurtser, et al. (2001). "Effects of replication termination mutants on chromosome partitioning in Bacillus subtilis." Proc Natl Acad Sci U S A 98(1): 212-7.

Lemon, K. P., S. Moriya, et al. (2002). Chromosome replication and segregation. Bacillus subtilus and its closest relatives:from genes to cells. A. L. Sonenshein. Washington, ASM Press: 73-82.

Lewis, P. J. (2004). "Bacterial subcellular architecture: recent advances and future prospects." Mol Microbiol 54(5): 1135-50.

Li, Y., K. Kurokawa, et al. (2004). "Identification of temperature-sensitive dnaD mutants of Staphylococcus aureus that are defective in chromosomal DNA replication." Mol Genet Genomics 271(4): 447-57.

Lindsay, S. M., L. A. Nagahara, et al. (1989). "STM and AFM images of nucleosome DNA under water." J Biomol Struct Dyn 7(2): 279-87.

Liu, Z., Z. Li, et al. (2005). "Imaging DNA molecules on mica surface by atomic force microscopy in air and in liquid." Microsc Res Tech 66(4): 179-85.

Lobner-Olesen, A., K. Skarstad, et al. (1989). "The DnaA protein determines the initiation mass of Escherichia coli K-12." Cell 57(5): 881-9.

Loscha, K., A. J. Oakley, et al. (2004). "Expression, purification, crystallization, and NMR studies of the helicase interaction domain of Escherichia coli DnaG primase." Protein Expr Purif 33(2): 304-10.

Lovett, S. T. and A. M. Segall (2004). "New views of the bacterial chromosome." EMBO Rep 5(9): 860-4.

Lyubchenko, Y. L. (2004). "DNA structure and dynamics: an atomic force microscopy study." Cell Biochem Biophys 41(1): 75-98.

Lyubchenko, Y. L., L. S. Shlyakhtenko, et al. (1998). "Polymerisation of the DNA binding fragment of p53 on DNA: Atomic force microscopy study." Scanning Microscopy 12(3): 455-463.

Marians, K. J. (2000). "PriA-directed replication fork restart in Escherichia coli." Trends Biochem Sci 25(4): 185-9.

Marsin, S., S. McGovern, et al. (2001). "Early steps of Bacillus subtilis primosome assembly." J Biol Chem 276(49): 45818-25.

Masai, H. and K. Arai (1996). "DnaA- and PriA-dependent primosomes: two distinct replication complexes for replication of Escherichia coli chromosome." Front Biosci 1: d48-58.

Miyata, T., T. Oyama, et al. (2004). "The clamp-loading complex for processive DNA replication." Nat Struct Mol Biol 11(7): 632-6.

Moriya, S., T. Atlung, et al. (1992). "Cloning of an autonomously replicating sequence (ars) from the Bacillus subtilis chromosome." Mol Microbiol 6(3): 309-15.

Moriya, S., Y. Imai, et al. (1999). "Regulation of initiation of Bacillus subtilis chromosome replication." Plasmid 41(1): 17-29.

Moriya, S., K. Kato, et al. (1990). "Isolation of a dnaA mutant of Bacillus subtilis defective in initiation of replication: amount of DnaA protein determines cells' initiation potential." Embo J 9(9): 2905-10.

Mou, J., D. M. Czajkowsky, et al. (1995). "High-resolution atomic-force microscopy of DNA: the pitch of the double helix." FEBS Lett 371(3): 279-82.

Muller, D. J., F. A. Schabert, et al. (1995). "Imaging purple membranes in aqueous solutions at sub-nanometer resolution by atomic force microscopy." Biophys J 68(5): 1681-6.
Muller, D. J., C. A. Schoenenberger, et al. (1996). "Immuno-atomic force microscopy of purple membrane." Biophys J 70(4): 1796-802.

Nakamoto, K., C. B. Mooney, et al. (2001). "Development of low temperature and high vacuum stomic force microscopy with freeze-fracture function." Review of scientific instruments 72(2): 1445-1448.

Nakamura, T., Y. Maeda, et al. (1999). "Atomic force microscope observations of plasmid deoxyribose nucleic acid with restriction enzyme." J. Vac. Sc. Technology. B 17(2): 288-293.

Nicholson, W. V., M. Lee, et al. (1997). "Cryo-electron microscopy of GDP-tubulin rings." Cell 90(2): 217-224.

Noirot-Gros, M. F., E. Dervyn, et al. (2002). "An expanded view of bacterial DNA replication." Proc Natl Acad Sci U S A 99(12): 8342-7.

Oakley, A. J., K. V. Loscha, et al. (2005). "Crystal and solution structures of the helicase-binding domain of Escherichia coli primase." J Biol Chem 280(12): 11495-504.

Ohnesorge, F. M., J. K. Horber, et al. (1997). "AFM review study on pox viruses and living cells." Biophys J 73(4): 2183-94.

Okamoto, K., P. Serror, et al. (1993). "Physical mapping of stable RNA genes in Bacillus subtilis using polymerase chain reaction amplification from a yeast artificial chromosome library." J Bacteriol 175(14): 4290-7.

Oussatcheva, E. A., J. Pavlicek, et al. (2004). "Influence of global DNA topology on cruciform formation in supercoiled DNA." J Mol Biol 338(4): 735-43.

Pan, H., L. E. Bird, et al. (1999). "Cloning, expression, and purification of Bacillus stearothermophilus DNA primase and crystallization of the zinc-binding domain." Biochim Biophys Acta 1444(3): 429-33.

Patel, S. S. and K. M. Picha (2000). "Structure and function of hexameric helicases." Annu Rev Biochem 69: 651-97.

Polard, P., S. Marsin, et al. (2002). "Restart of DNA replication in Gram-positive bacteria: functional characterisation of the Bacillus subtilis PriA initiator." Nucleic Acids Res 30(7): 1593-605.

Pope, L. H., M. C. Davies, et al. (2000). "Atomic force microscopy studies of intercalation-induced changes in plasmid DNA tertiary structure." J Microsc 199 (Pt 1): 68-78.

Prater, C. B. (2000). Tapping mode imaging: applications and techniques. 2000.

Prater, C. B., M. R. Wilson, et al. (1991). "Atomic force microscopy of biological samples at low temperatures." J Vac. Sci. Technol. N 9(2): 989-991.

Privalov, P. L. (1979). "Stability of proteins: small globular proteins." Adv Protein Chem 33: 167-241.

Putman, C. A. J., K. O. van der Werf, et al. (1992). "Vacuum chamber for sample attachment in atomic force microscopy." Review of scientific instruments 63(8): 4012-4013.

Reading, M., D. M. Price, et al. (2001). "Micro-thermal analysis of polymers: current capabilities and future prospects." Macromol. Symp. 167: 45-62.

Rees, W. A., R. W. Keller, et al. (1993). "Evidence of DNA bending in transcription complexes imaged by scanning force microscopy." Science 260(5114): 1646-9.

Rice, P. A., S. Yang, et al. (1996). "Crystal structure of an IHF-DNA complex: a protein-induced DNA U-turn." Cell 87(7): 1295-306.

Rimsky, S. (2004). "Structure of the histone-like protein H-NS and its role in regulation and genome superstructure." Curr Opin Microbiol 7(2): 109-14.

Rippe, K., M. Guthold, et al. (1997). "Transcriptional activation via DNA-looping: visualization of intermediates in the activation pathway of E. coli RNA polymerase x sigma 54 holoenzyme by scanning force microscopy." J Mol Biol 270(2): 125-38.

Rippe, K., N. Mucke, et al. (1997). "Molecules in motion: Imaging DNA with the scanning force microscope in aqueous solutions." Bioforum international 1: 42-44.

Roberts, C. J., P. M. Williams, et al. (1994). "Atomic force microscopy and scanning tunnelling microscopy: refining techniques for studying biomolecules." Trends Biotechnol 12(4): 127-32.

Rokop, M. E., J. M. Auchtung, et al. (2004). "Control of DNA replication initiation by recruitment of an essential initiation protein to the membrane of Bacillus subtilis." Mol Microbiol 52(6): 1757-67.

Russell, P., B. D., et al. (2001). SEM and AFM: complementary techniques for high resolution surface investigations. Santa Barbara, Digital Intruments, Veeco Metrology group: 1-11.

Sagi, D., N. Friedman, et al. (2004). "Modulation of DNA conformations through the formation of alternative high-order HU-DNA complexes." J Mol Biol 341(2): 419-28.

Sakamoto, Y., S. Nakai, et al. (1995). "The Bacillus subtilis dnaC gene encodes a protein homologous to the DnaB helicase of Escherichia coli." Microbiology 141 (Pt 3): 641-4.

Samori, B., G. Siligardi, et al. (1993). "Chirality of DNA supercoiling assigned by scanning force microscopy." Proc Natl Acad Sci U S A 90(8): 3598-601.

Sattin, B. D. and M. C. Goh (2004). "Direct Observation of the Assembly of RecA/DNA Complexes by Atomic Force Microscopy." Biophys J 87(5): 3430-6.

Scheuring, S., D. Fotiadis, et al. (2001). "single proteins observed by atomic force microscopy." Single Mol. 2(2): 59-67.

Schroder, O. and R. Wagner (2002). "The bacterial regulatory protein H-NS--a versatile modulator of nucleic acid structures." Biol Chem 383(6): 945-60.

Sekimizu, K., D. Bramhill, et al. (1987). "ATP activates dnaA protein in initiating replication of plasmids bearing the origin of the E. coli chromosome." Cell 50(2): 259-65.

Shao, Z. and Y. Zhang (1996). "Biological cryo atomic force microscopy: a brief review." Ultramicroscopy 66(3-4): 141-52.

Sherratt, D. J. (2003). "Bacterial chromosome dynamics." Science 301(5634): 780-5.

Shlyakhtenko, L. S., V. N. Potaman, et al. (1998). "Structure and dynamics of supercoil-stabilized DNA cruciforms." J Mol Biol 280(1): 61-72.

Snyder, L. and W. Champness Chapter 1. Macromolecular synthesis: Chromosome structure, replication, and segregation. Molecular Genetics of bacteria: 29-35.

Soni, R. K., P. Mehra, et al. (2005). "Helicobacter pylori DnaB helicase can bypass E. coli DnaC function in vivo." Biochem J.

Sosa, H. and R. A. Milligan (1996). "Three-dimensional structure of ncd-decorated microtubules obtained by a back-projection method." J Mol Biol 260(5): 743-55.

Soultanas, P. (2002). "A functional interaction between the putative primosomal protein DnaI and the main replicative DNA helicase DnaB in Bacillus." Nucleic Acids Res 30(4): 966-74.

Soultanas, P., M. S. Dillingham, et al. (2000). "Uncoupling DNA translocation and helicase activity in PcrA: direct evidence for an active mechanism." Embo J 19(14): 3799-810.

Soultanas, P. and D. B. Wigley (2000). "DNA helicases: 'inching forward'." Curr Opin Struct Biol 10(1): 124-8.

Swinger, K. K. and P. A. Rice (2004). "IHF and HU: flexible architects of bent DNA." Curr Opin Struct Biol 14(1): 28-35.

Syson, K., J. Thirlway, et al. (2005). "Solution structure of the helicase-interaction domain of the primase DnaG: a model for helicase activation." Structure 13: 609-616.

Takaki, R. (2004). "Physical aspect of microscopic behaviour of biomolecules." J Biosci 29(4): 385-9.

Thirlway, J., I. J. Turner, et al. (2004). "DnaG interacts with a linker region that joins the N- and C-domains of DnaB and induces the formation of 3-fold symmetric rings." Nucleic Acids Res 32(10): 2977-86.

Thomson, N. H., M. Fritz, et al. (1996). "Protein tracking and detection of protein motion using atomic force microscopy." Biophys J 70(5): 2421-31.

Todar, K. (2004). The Genus Bacillus, Todar, K. 2004.

Tougu, K. and K. J. Marians (1996). "The extreme C terminus of primase is required for interaction with DnaB at the replication fork." J Biol Chem 271(35): 21391-7.

Tougu, K. and K. J. Marians (1996). "The interaction between helicase and primase sets the replication fork clock." J Biol Chem 271(35): 21398-405.

Turner, I. J., D. J. Scott, et al. (2004). "The Bacillus subtilus DnaD protein: a putative link between DNA remodeling and intiation of DNA replication." FEBS Lett(577): 460-464.

Umemura, K., F. Nagami, et al. (2000). "AFM characterization of single strand-specific endonuclease activity on linear DNA." Nucleic Acids Res 28(9): E39.

van Noort, J., S. Verbrugge, et al. (2004). "Dual architectural roles of HU: formation of flexible hinges and rigid filaments." Proc Natl Acad Sci U S A 101(18): 6969-74.

Velankar, S. S., P. Soultanas, et al. (1999). "Crystal structures of complexes of PcrA DNA helicase with a DNA substrate indicate an inchworm mechanism." Cell 97(1): 75-84.

Vesenka, J., S. Manne, et al. (1993). "Colloidal gold particles as an incompressible atomic force microscope imaging standard for assessing the compressibility of biomolecules." Biophys J 65(3): 992-7.

Vesenka, J., S. Manne, et al. (1993). "Humidity effects on atomic force microscopy of gold-labeled DNA on mica." Scanning Microsc 7(3): 781-8.

Walther, P., E. Wehrli, et al. (1995). "Double-layer coating for high-resolution low-temperature scanning electron microscopy." J Microsc 179 (Pt 3): 229-37.

Weisenhorn, A. L., B. Drake, et al. (1990). "Immobilized proteins in buffer imaged at molecular resolution by atomic force microscopy." Biophys J 58(5): 1251-8.

White, S. W., K. S. Wilson, et al. (1999). "The high-resolution structure of DNA-binding protein HU from Bacillus stearothermophilus." Acta Crystallogr D Biol Crystallogr 55 (Pt 4): 801-9.

Wickner, S. (1977). "DNA or RNA priming of bacteriophage G4 DNA synthesis by Escherichia coli dnaG protein." Proc Natl Acad Sci U S A 74(7): 2815-9.

Wiegrabe, W., M. Nonnenmacher, et al. (1991). "Atomic force microscopy of a hydrated bacterial surface protein." J Microsc 163 (Pt 1): 79-84.

Williams, P. M., M. C. Davies, et al. (1997). "Data analysis using the Internet: the World Wide Web scanning probe microscopy data analysis system." Analyst 122(10): 1001-6.

Yang, J., J. Mou, et al. (1996). "The effect of deformation on the lateral resolution of atomic force microscopy." J Microsc 182 (Pt 2): 106-13.

Yang, J., L. K. Tamm, et al. (1993). "Promises and problems of biological atomic force microscopy." J Microsc 171 (Pt 3): 183-98.

Yang, S., X. Yu, et al. (2002). "Flexibility of the rings: structural asymmetry in the DnaB hexameric helicase." J Mol Biol 321(5): 839-49.

Yang, Y., H. Wang, et al. (2003). "Quantitative characterization of biomolecular assemblies and interactions using atomic force microscopy." Methods 29(2): 175-87.

Yu, X., M. J. Jezewska, et al. (1996). "The hexameric E. coli DnaB helicase can exist in different Quaternary states." J Mol Biol 259(1): 7-14.

Zhang, W., M. J. Carneiro, et al. (2005). "The Bacillus subtilis DnaD and DnaB proteins exhibit different DNA remodelling activities." J Mol Biol 351(1): 66-75.

Zhang, Y., Z. Shao, et al. (1997). "Cryo-atomic force microscopy of smooth muscle myosin." Biophys J 72(3): 1308-18.

Zhang, Y., S. Sheng, et al. (1996). "Imaging biological structures with the cryo atomic force microscope." Biophys J 71(4): 2168-76.

Appendix One - Control images

1) **Muscovite Mica –** Imaged in tapping mode in air as described in section. Scale bar represents 200nm

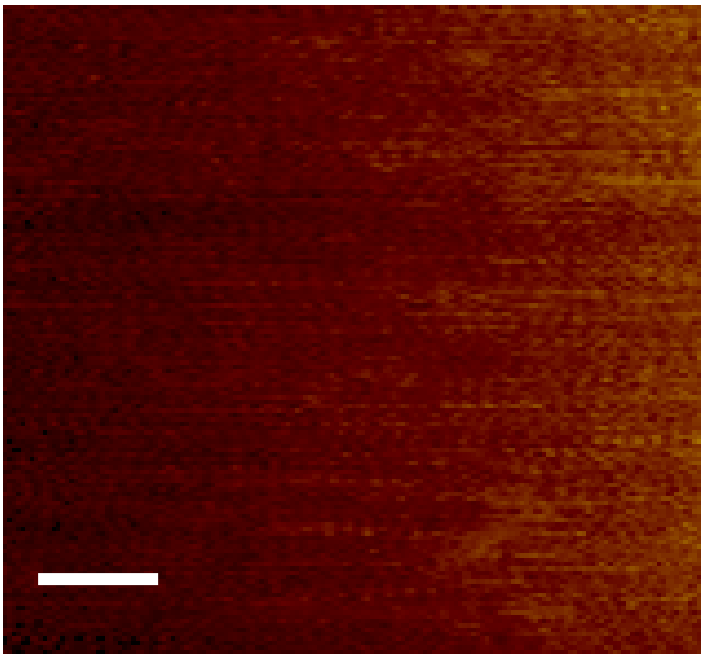

2) **Imaging Buffer -** 50nM Tris pH 7.4, 1mM EDTA 2 mM of MgCl imaged in tapping mode in air as described in section. Scale bar represnts 100nm

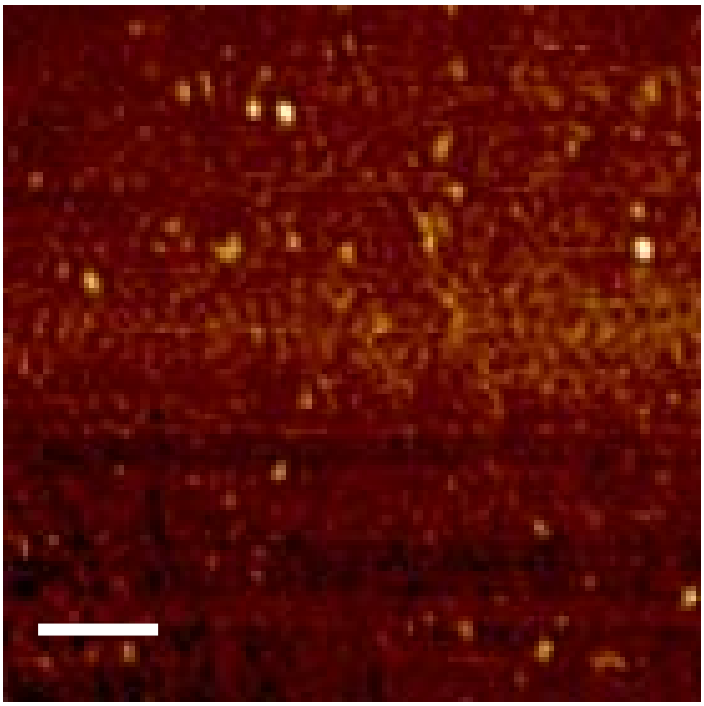

Acknowledgments

Firstly I would like to thank my supervisor Prof. Clive Roberts, for his constant support and guidance through out my time in Nottingham. His friendly and approachable nature has made my PhD an enjoyable experience.

I would like to thank the following academics in the LBSA who have assisted me with my work; Dr Stephanie Allen, Dr Phil Williams and Prof. Xinyong Chen.

Thanks goes to Dr Panos Soultanas and his lab for all the complementary work mentioned in this thesis and his enthusiastic approach to my work.

I would like to thank all the members of LBSA especially; Anne Chim, Chris Brampton, Matt Bunker, Rudesh Toofanny, Vicky Sedman, Mike Davies, Anita Pearson, Omar Wahab, James Moody and Roman Duszynski who have all helped me during the course of my PhD and become good friends.

I would like to thank the University of Nottingham and the BBRSC for funding, without which this project would not have been possible.

Finally I would like to thank Chloe Garlant, she may not remember me but she made everything seem worthwhile.